Development of Nucleic Acid Driven Peptide and Protein Sensors and Their Integration with Automated Microfluidics

by

Niamat E Khuda

A dissertation submitted to the Graduate Faculty of
Auburn University
in partial fulfillment of the
requirements for the Degree of
Doctor of Philosophy

Auburn, Alabama
December 12, 2020

Keywords: Electrochemistry, Microfluidics, Biosensor,
Analytical Chemistry

Approved by

Christopher J. Easley, C. Harry Knowles Professor of Chemistry and Biochemistry
Curtis G. Shannon, Andrew T. Hunt Professor of Chemistry and Biochemistry
Wei Zhan, Associate Professor of Chemistry and Biochemistry
Byron H. Farnum, Assistant Professor of Chemistry and Biochemistry

Abstract

Accurate detection of disease-associated biomolecules is one of the most critical steps in diagnostics in early stages of disease to provide appropriate health care and effective treatment to patients. In clinical laboratories, analysis of disease biomarkers is usually performed by standard detection methods such as Western blots and enzyme-linked immunosorbent assays (ELISA) which are expensive, laborious, and require longer time to obtain medical information. Over the years, many sensitive methods have been developed for biomarker detection aimed at point-of-care (POC) systems. These methods are specialized toward particular targets and inflexible to analyze other biomolecules of interest. However, more versatile, yet sensitive, inexpensive, and easy to use methods are required for POC settings. Nucleic acid based electrochemical sensors have proven to be ideal for this purpose as they are able to provide rapid response, can function in complex biological environment, are compatible with miniaturized devices, and are relatively inexpensive. This dissertation focuses on the development of DNA-based electrochemical sensors and their integration with automated microfluidics for quantification of biomolecules, namely small molecules, oligonucleotides, proteins, and peptides.

Chapter 1 discusses the recent developments in electrochemical DNA-based sensors and their application in clinically relevant biomolecule detection.

Chapter 2 presents a detailed study of surface hybridization kinetics. Specifically, we have explored the dependence of electrochemical signals on the relative distance of DNA binding sites from the electrode surface under different conditions and investigated the kinetics of toehold-mediated DNA strand displacement reactions near or far from the surface.

Chapter 3 describes the development of electrochemical biosensor system for the quantification of a novel analyte for electrochemistry, exendin-4, which is a widely prescribed diabetic drug. We applied our DNA nanostructure sensor architecture to directly quantify exendin-4, which has not previously been measured using direct electrochemical readout, and we show that the sensor is functional in human serum.

Chapter 4 focuses on strategies to enhance signal in nanostructure based sensor. We rationally designed two new nanostructure architectures by incorporating polyethylene glycol (PEG) and uracil (U) into selected probe strands to support molecular weight reduction, which we hypothesized would enhance the electrochemical signal and sensitivity of the sensors.

Chapter 5 highlights the integration of automated microfluidics with electrochemical detection system. We have utilized automated, valve-controlled microfluidics for electrode preparation and analyte detection in a DNA-based surface assay platform using square wave voltammetry (SWV).

Finally, Chapter 6 reviews the research contribution of this dissertation and provides an insight on future research stemming from these topics.

Table of Contents

List of Figures

List of Tables

List of Abbreviations

3D-CAD	3D computer animated design
AB	Antibody
Apt	Aptamer
ATP	Adenosine triphosphate
bp	Base pair
CV	Cyclic voltammetry
Aptasensor	Electrochemical aptamer sensor
ECPA	Electrochemical proximity assay
E-DNA	Electrochemical DNA sensor
ELISA	Enzyme-linked immunosorbent assay
f_{SWV}	Square-wave voltammetry frequency
GoG	Gold on Glass
HEPES	(4-(2-hydroxyethyl)-1-piperazineethanesulfonic acid)
HRP	Horseradish peroxidase
i_{diff}	Differential current in Square-wave voltammetry
i_f	Forward current in Square-wave voltammetry
i_p	Square-wave voltammetry peak height
i_r	reverse current in Square- wave voltammetry
LOD	Limit of detection
MB	Methylene blue

MCH	6-Mercapto-1-hexanol
nt	Nucleotide
PDMS	Polydimethylsiloxane
PLA	Polylactic acid
POC	Point-Of-Care
SAM	Self-assembled monolayer
SWV	Square-wave voltammetry
TCEP	(tris(2-carboxyethyl)phosphine)
T_m	DNA melt temperature

Chapter 1

Electrochemical Methods for Detection of Biomolecules

1.1 Analysis of Biomolecules

Biomolecules are essential building blocks of living organisms which regulate numerous biological activities of the body. The detection of biomolecular analytes is essential to understand their role in biological processes, to perform disease diagnosis, and to study therapeutic agents.[1] Clinically relevant biomolecules such as small molecules, nucleic acids, peptides, and proteins are used as biomarkers of many diseases, since irregularities in their concentration lead to a range of metabolic, genetic, and cancerous diseases.[2] Therefore, to ensure efficient treatment, regular quantification of biomarkers is required to provide truly personalized medicine, since pharmacokinetics differs between individuals.[3]

Clinically relevant endogenous small molecules include neurotransmitters, metabolites, vitamins, hormones, and amino acids. Neurotransmitters are chemical messengers that carries, enhances, and balances signals between neurons and target cells throughout the body. Diseases such as Parkinson's, Alzheimer's, schizophrenia, autism, and epilepsy are associated with abnormal levels of neurotransmitter concentrations.[4] Metabolites are the intermediates or final products of various physiological processes. Metabolites play an important role in various complex disease and their quantification is can provide better understanding of the underlying pathogenesis. Vitamins are essential bio-nutrients required in limited amounts for proper growth and development of living organisms. Hormones are signaling molecules produced by glands in the

endocrine system and travel through the bloodstream to stimulate specific cells or tissues into action.

Nucleic acids are larger biomolecules and are considered ideal molecular fingerprints, aiding identification of pathogens responsible for infectious disease. The formation and growth of cancer cells involves changes in specific nucleic acid thus can be distinguished from healthy cell by abnormalities in the structure or expression of genes. Analysis of the specific genes have been used for the detection of lung cancer[5], melanomas[6], and acute lymphoblastic leukemia[7]. Circulating cell-free nucleic acids (cfNAs) have be detected in maternal plasma and serum for early diagnosis of preterm labor[8], preeclampsia[9], fetal-maternal hemorrhage[10], and invasive placentation[11]. Analysis of cfNAs also opened a door for noninvasive diagnostic of myocardial infarction[12], renal cancer[13], bladder cancer[14], prostate cancer[15], bone allotransplantation[16], and organ transplant monitoring[17-18].

Proteins are macromolecules that regulate a wide range of biological functions such as DNA replication, catalyzing metabolism, transporting molecules, contributing to signaling pathways, etc. and are most extensively affected in diseases.[19] Clinically relevant protein markers are often used for the diagnosis of myocardial infarction, inflammatory diseases, and screening and diagnosis of cancers. Clinical assays of tumor markers such as, prostate-specific antigen[20], carcinoembryonic antigen[21], fibrinogen[22], protein kinase[23] and others have been developed for early cancer detection, classification, and progression monitoring. Troponin, myoglobin, and creatine kinase are common cardiac markers used for the diagnosis of myocardial infarction. C-reactive protein, tumor necrosis factor-α, and haptoglobin are inflammatory markers for the diagnosis of chronic inflammatory diseases such as atherosclerosis, rheumatoid arthritis, psoriasis, and inflammatory bowel disease.

All of these listed biomolecule classes are attractive targets as analytes of electrochemical sensors, and a variety of sensors have been developed for this reason. However, such sensors are typically specialized to the analyte, therefore a more generalizable technique is desirable. The research reported in this dissertation shows that our customized nucleic acid nanostructure provides improved generalizability, since it can be used for detection of small molecules and peptides, along with larger molecules.

1.2 Biorecognition Elements

Biorecognition elements are biomolecules obtained from living systems or by synthesis which recognize their target and undergo a physicochemical change in the presence of the target. These recognition elements are often highly sensitive and selective toward their targets, making them very useful for incorporation into biosensors. Molecular recognition is arguably the most important event in biosensing, and this step greatly affects the overall sensor performance. Antibodies, aptamers, nucleic acids, enzymes, and peptide nucleic acids are some of the common recognition elements used in sensors. In this dissertation, antibodies and nucleic acids are incorporated into sensors for both target recognition and structural purposes.

1.2.1 Antibodies

Antibodies are Y-shaped proteins produced by the immune system to neutralize antigen. They recognizes antigen via the fragment antigen-binding (Fab) sites by noncovalent interactions with relatively high affinity. Biosensors utilizes the sensitivity and specificity of bimolecular antibody–antigen interactions to selectively analyze targeted antigens. Antibodies can be either

polyclonal or monoclonal. Monoclonal antibodies have monovalent affinity and bind to the same epitope of an antigen, whereas polyclonal antibodies can recognize and bind to many different epitopes of a single antigen.

1.2.2 Aptamers

Aptamers are synthetic nucleic acids that bind to a target molecule and fold into highly specific three-dimensional structures through intramolecular DNA hybridization. Aptamers are isolated from a library of oligonucleotides by an in vitro selection process termed systemic evolution of ligands by exponential enrichments (SELEX).[24] Aptamers have been synthesized against a wide range of targets including proteins, small molecules, and whole cells, which makes them very useful as recognition elements. Since aptamers are synthesized, their binding affinity and selectivity can be tailored during the selection process.[25-27] Moreover, aptamers are inherently stable, so they can be stored for longer time periods and are able to withstand a wider range of temperatures and conditions than a typical antibody or protein.

1.2.3 Nucleic Acids

DNA hybridization biosensors comprise nucleic acids as the recognition element for diagnosis of genetic or infectious diseases.[28] The biorecognition process involves sequence-specific DNA hybridization between the target and the capture probe. Nucleic acids have also been used as recognition elements to develop ion sensors.[29-30] Binding of target ion hinders the flexibility of the nucleic acid, and the sensor translates that change to a measurable signal.

1.2.3 Peptide Nucleic Acids (PNAs)

PNAs are synthetic DNA analogues with a polyamide backbone instead of sugar phosphate backbone. PNAs exhibit improved chemical and enzymatic stability and higher affinity hybridization compared to nucleic acids. PNA−DNA duplexes exhibit higher thermal stability compared to DNA−DNA equivalents, which is largely due to the uncharged backbone of PNAs.

1.3 Conventional Detection Techniques

1.3.1 ELISA

Enzyme-linked immunosorbent assay (ELISA) is the most common method and considered as the current gold standard for the diagnosis of biomolecules. **Figure 1.1** depicts the commonly used heterogeneous sandwich ELISA.[31] This assay utilizes a microwell plate for the immobilization of a primary antibody, which captures the target protein with high selectivity and specificity. A secondary antibody labeled with an enzyme such as horseradish peroxidase (HRP) is then added, which binds to a second epitope of the target protein. Then the HRP substrate is introduced which reacts with the enzyme and results in a colored product. About twenty minutes later, an acidic solution is added to quench the HRP-substrate reaction, readying the assay for measurement. The absorption is measured and is proportional to the original concentration of the targeted analyte. In this rather complex workflow, multiple washing steps are needed between each step to remove unbound targets or antibodies.

ELISA can be used to quantify any target as long as the target has at least two antibodies that bind to separate epitopes on the target.[32] Enzymatic signal amplification improves detection limits, and usage of dual antibody recognition increases the specificity of the assay. Another

advantage of heterogeneous ELISA is that whole blood and serum can be accurately tested without strenuous sample cleanup.

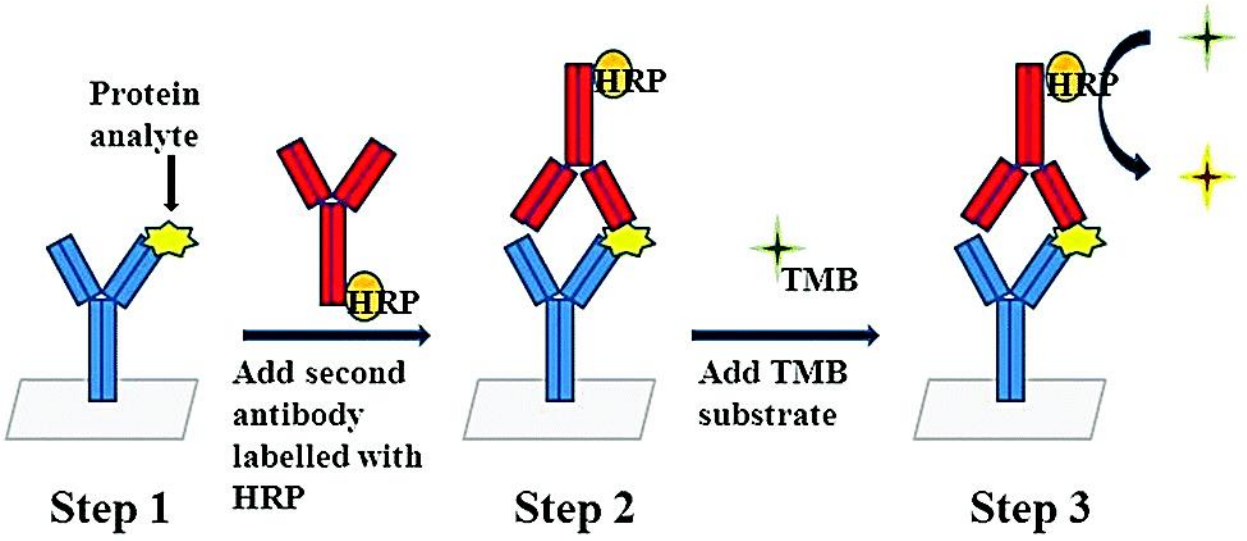

Figure 1.1. Schematic of sandwich ELISA for protein quantification. Well plate surface attached capture antibody binds the target. Detector antibodies are then added to complete the sandwich complex followed by substrate addition to generate the enzymatic color change.[31]

Even though ELISA offers many advantages, it also suffers from several drawbacks. ELISAs come in a standard 96-well format, and the reagents should be used in a single sitting. With the average cost of $500, each well represents at least $5. Duplicate or triplicate measurements are conducted to eliminate handling error, which brings the cost up to about $15 per sample. Also, the majority of the plate may go to waste when few samples are analyzed. This method is time consuming (turnaround time ~6-8 hours), laborious, and requires well-trained individuals to perform correctly. Additionally, most ELISAs require at least 10 µL of sample per

well, which can be a large volume for precious samples. Therefore, other assays need to be developed with similar characteristics as ELISA, but with lower run time, assay cost, and sample volume.

1.3.2 Digital ELISA

The sensitivity of immunoassays has been further improved by the introduction of digital ELISA to measure a variety of targets.[33-36] Walt, et al. developed a single-molecule enzyme-linked immunosorbent assay (i.e. single molecule array or "Simoa"), were the enzyme amplification is done in an micro-well of 50 fL volume.[37-40] Simoa technology is based on the high-efficiency capture of single protein molecules on magnetic beads and their detection in arrays of femtoliter-sized wells. As shown in **Figure 1.2**, this assay requires capture antibody loaded magnetic beads, biotinylated secondary antibody, and an enzyme tagged streptavidin to form a sandwich antibody complex on the beads. Then the beads are introduced into an array of ultra-small femtoliter-sized reaction wells which confines a single bead, and substrate is added to generate fluorescent signal. The bead with the target has the enzyme confined into a very small volume, thereby allowing for a single target molecule to produce a measurable signal. The percentage of beads that contain a labeled immunocomplex follows a Poisson distribution, and the concentration of the target can be calculated by simply counting the number of wells showing enzymatic activity.

Digital ELISA has a detection limit down to the zeptomolar range (10^{-21} M); it can perform in highly complex matrices such as cell culture supernatant, cerebrospinal fluid (CSF), serum, and plasma; it requires low volumes of sample and reagents; and it is 1000-fold more sensitive than

conventional ELISA.[41] However, the expensive instrumentation and assay kit costs make it less suitable for regular analysis and especially for POC analysis.

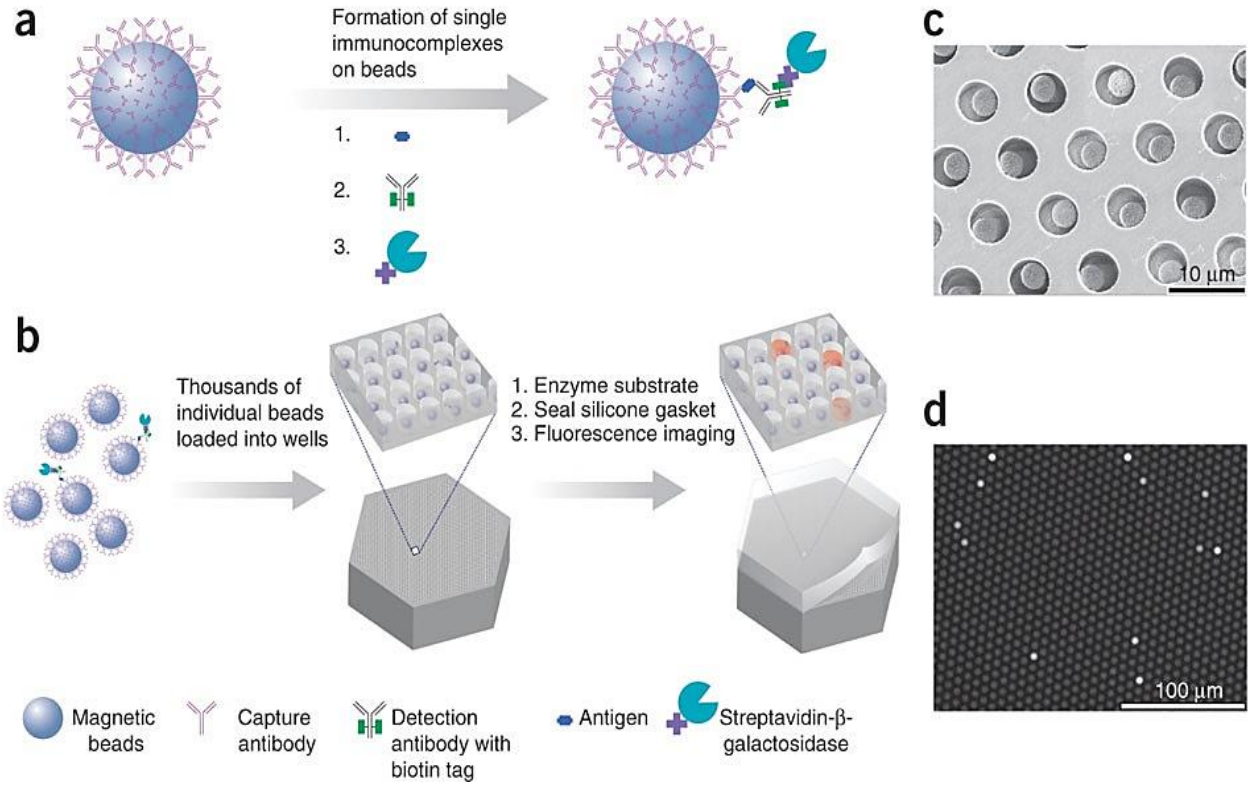

Figure 1.2. a) Sample containing a target analyte is incubated with beads coated with capture antibodies, biotinylated detection antibodies, and enzyme tagged streptavidin to form a single-enzyme–labeled immunocomplex on the bead. **b)** Beads are loaded onto femtoliter-volume well such that only one bead fits into each well, substrate is added, then the array is sealed with silicone gasket, and fluorescent images are obtained. **c)** SEM of microwell array. **d)** Fluorescence image of the array.[37]

1.3.3 AlphaLISA

AlphaLISA is a homogeneous mix-and-read assay. In this method, two beads are used. The donor bead is a photosensitizer, and the acceptor bead is a chemiluminescent. When the target is present these two beads comes into close proximity. Upon excitation of the photosensitizer at 680 nm, a flow of up to 60,000 singlet oxygen ($^1O_2$) molecule per bead per second is generated, which triggers a cascade of chemical reactions in nearby acceptor beads resulting in a chemiluminescent emission at 615 nm.[42] **Figure 1.3** illustrates the signaling mechanism of AlphaLISA.[43]

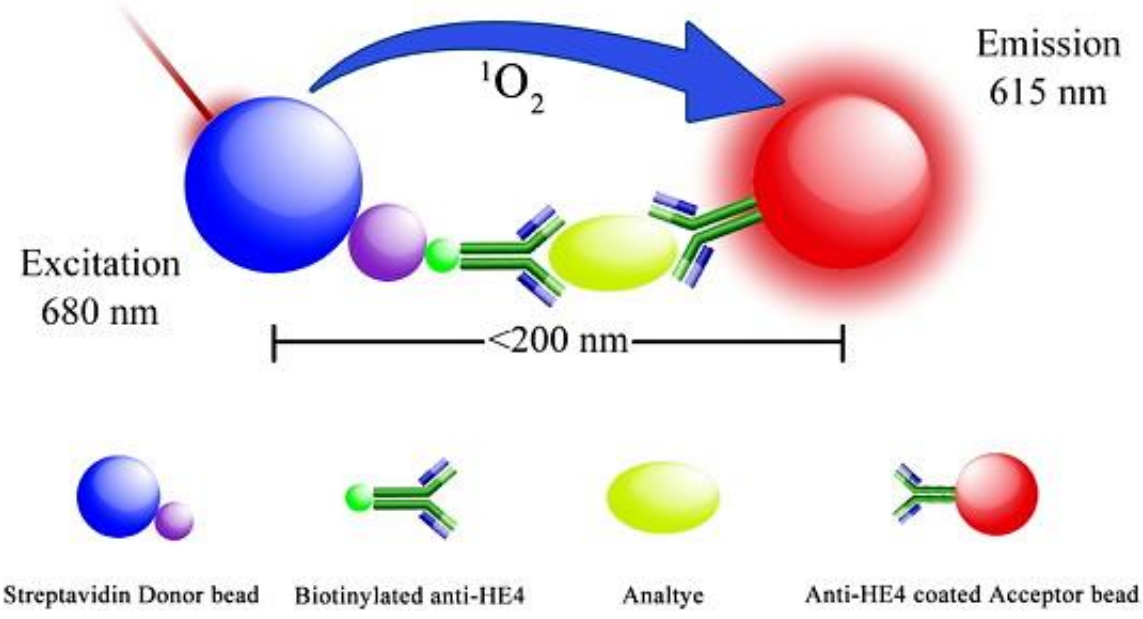

Figure 1.3. Excitation of donor bead at 680 nm generate singlet oxygen molecules, which reaches the acceptor bead in close proximity (~200 nm) and generate series of chemical reactions resulting in emission at 615 nm.[43]

The acceptor beads, which are coated with capture antibody, are incubated with sample and biotinylated secondary antibody. Then, streptavidin donor beads are introduced to form the sandwich complex enabling the acceptor and donor beads to come in close proximity, which aids in efficient $^1O_2$ transfer. AlphaLISA is a no wash, homogeneous immunoassay which is more sensitive and easily generalizable compared to ELISA. In this way, AlphaLISA has more closely approached the bioanalytical ideal of a low workflow, sensitive, generalizable assay. On the other hand, it does require special instrumentation since 680 nm excitation and 615 nm emission is irregular and is not available on typical fluorescence systems.

1.3.4 Proximity Ligation Assay (PLA)

One of the first examples of proximity immunoassays is the proximity ligation assay (PLA) designed and developed by Landegren's group for in-vitro analysis of proteins.[44-46] Similar to ELISA, PLA takes the advantage of dual-antibody binding at different epitopes on the same target protein. A pair of DNA probes, each conjugated to each of the two antibodies, are brought into close proximity upon binding of antibody to the target. The DNA probes then undergo hybridization with a connector oligo, forming the complete proximity complex (**Figure 1.4**). The two DNA probes then are enzymatically ligated by T4 DNA ligase, and various methods can then be used to amplify and detect the ligated DNA strand such as polymerase-chain-reaction (PCR).[47] The connector DNA sequences are intentionally designed in such a way that target-independent hybridization is unfavorable and does not take place in the absence of the target molecule. Through affinity binding, the local concentrations of both DNA probes greatly increases, which allows even weak hybridization interactions become strong and spontaneous at room temperature. In the

absence of protein, the proximity complex does not form, thus the ligation reaction cannot take place leaving only a weak background signal.

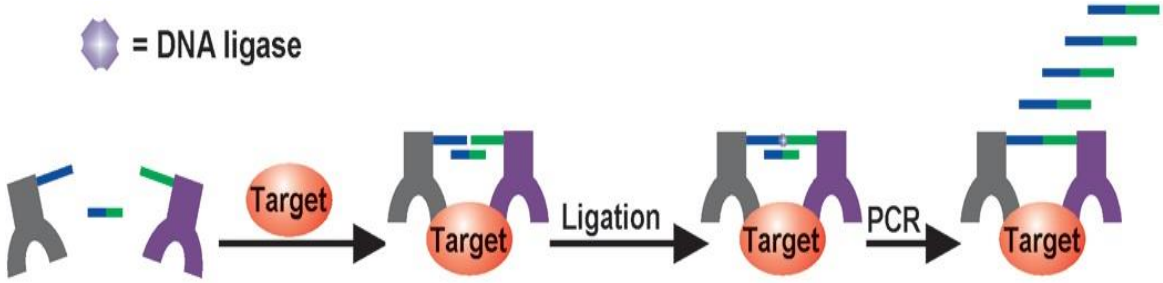

Figure 1.4. Proximity ligation assay. aTwo antibodies bind with the same target bringing the tails to close proximity, which then strongly bind with the connector. Upon enzymatic ligation of the tails a single DNA strand is formed which is subsequently amplified by PCR.[48]

1.3.5 Molecular Pincer Assay

Exploiting the same proximity effect, Heyduk et al. developed optical sensors based on fluorescence resonance energy transfer (FRET).[49-51] In this homogeneous, mix-and-read assay, the binding of a pair of affinity ligands to different epitopes of a target protein brings a pair of fluorescence acceptor and donor labeled DNA probes in close proximity. The increase in local concentration results in spontaneous DNA annealing and produces stable DNA duplexes, resulting in FRET. **Figure 1.5C** shows that emission at 670 nm takes place only in the presence of target (blue bar), while low background is observed in the absence of target (red bar).[51] With this method

a range of clinically relevant biomolecules such as insulin,[52] C-reactive protein[51], and cardiac troponin I[53] have been quantified with pM detection limits.

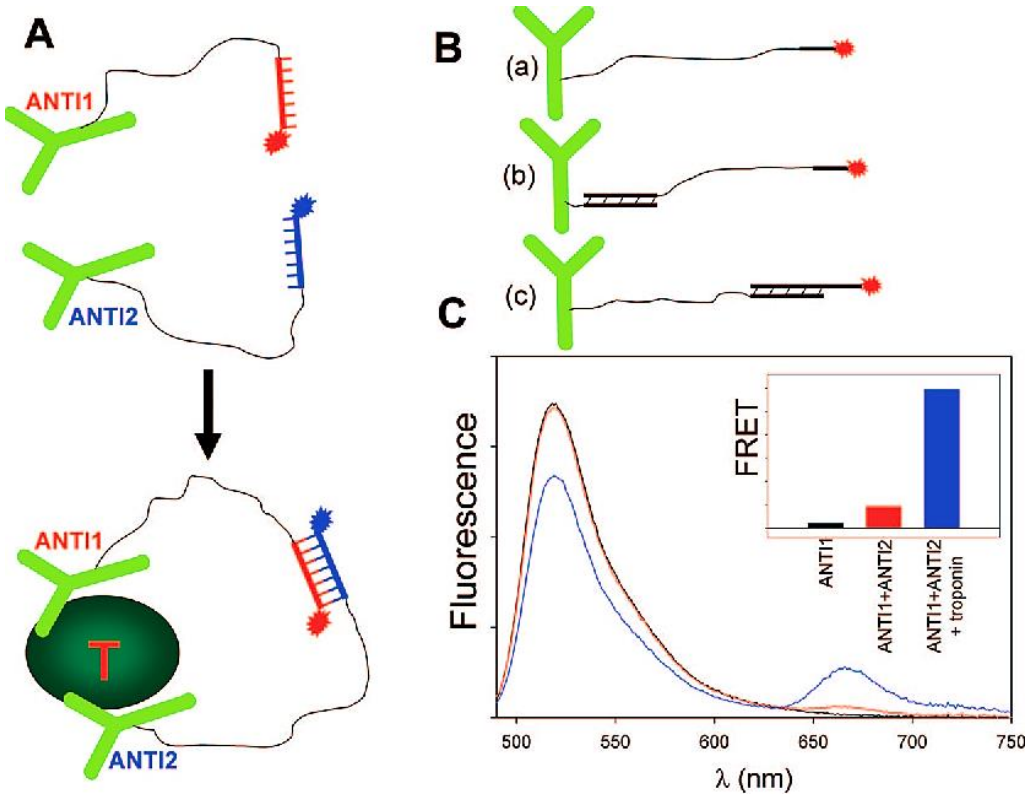

Figure 1.5. Molecular pincer assay. **A)** Target binding significantly enhances the binding energy between DNA probes due to close proximity. **B)** Antibodies modified with three variants of signaling oligonucleotides. **C)** Target binding resulted FRET signal at 670 nm.[51]

1.4 Electrochemical Biosensors

One major goal of developing biosensors is to offer new tools for the analysis of clinical samples for biomarkers of disease, enabling diagnostics to become more decentralized, less complicated, and cost effective. An electrochemical biosensor exploits a biorecognition strategy to provide analytical information using an electrochemical transducer. A vast array of electrochemical assays have been developed for the detection and quantification of clinically relevant molecules. Biosensors based on electrochemical sensing strategies have attracted much attention owing to their reliability, rapid response, low cost and portability, low sample consumption, ability to work in complex multicomponent samples, and high sensitivity.[54]

1.4.1 Commonly Used Voltammetry Techniques

Cyclic Voltammetry (CV)

The most common voltammetry used in electrochemistry is CV. In this method, current is measured as the potential is gradually varied at a working electrode in both forward and reverse directions. The voltammetry data is plotted as current versus applied voltage. Electrochemically active biomolecules such as neurotransmitters and myoglobin have been quantified by CV.[55-56] However, CV is not sensitive enough to detect lower concentrations, and non-faradic capacitive current limits the measurement sensitivity.

Square-wave Voltammetry (SWV)

SWV is a sensitive voltammetry technique for observing surface-confined reactions because it largely reduces background capacitance current and increases signal due to its differential output. The waveform and principle parameters for SWV are depicted in **Figure 1.6**. It is combination of a staircase waveform characterized by a step size (ΔE) and a square wave defined by a pulse height (E_{sw}). The time for one square wave cycle is τ, and the square wave frequency (f) in Hz is 1/τ. Current is sampled twice per cycle, forward current (i_f) at the end of the first pulse, and reverse current (i_r) at the end of the reverse pulse. The recorded data from a single SWV run usually consists of three voltammograms based on forward, reverse, and the digitally subtracted difference currents ($i_d = i_f - i_r$). SWV has several advantages, including its excellent sensitivity, ability to study faster reactions, and improved signal-to-noise ratio due to reduction of capacitive current.

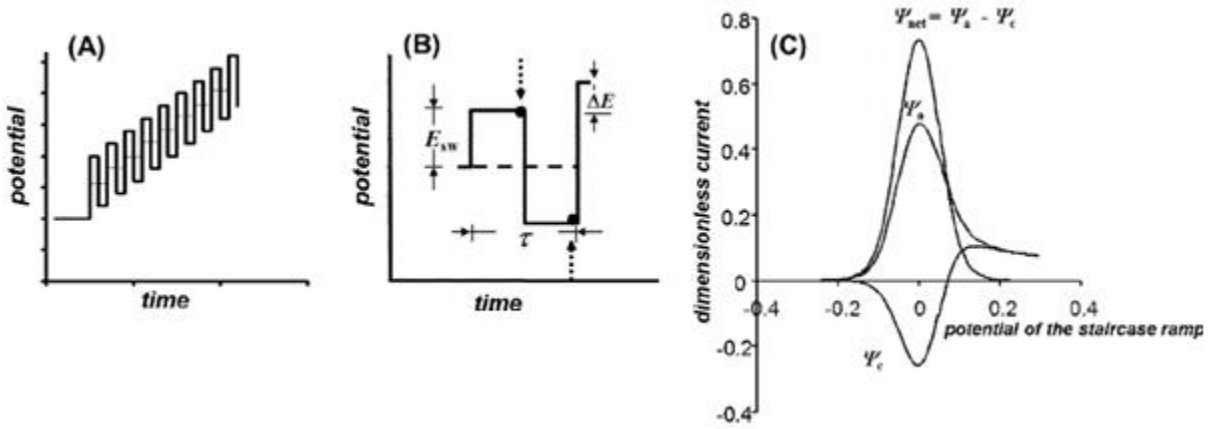

Figure 1.6. A) Potential waveform for square wave voltammetry (SWV). **B)** Single square wave cycle. **C)** Voltammogram in SWV where normalized currents Ψ_a, Ψ_c, and Ψ_{net} correspond to i_f, i_r, and i_d. [57]

1.4.2 Electrochemistry in Microfluidics

Integration of electrochemical sensing with microfluidics offers unique advantages. In comparison to analysis in bulk solution, microfluidics allow faster interaction between the recognition element and the target by reducing the distance required for interaction. Using microfluidic technologies, assays can be performed on a miniaturized chip with better control over sample flow, which reduces the amount of sample and reagents required for analysis. Microfluidic devices integrated with embedded electrodes or electrode arrays are predominantly made from elastomers such as polydimethylsiloxane (PDMS), thermoplastics such as polymethyl methacrylate (PMMA), and paper.

PDMS is one of the most widely used chip fabrication materials which is biocompatible[58], cheap, and can be molded with a resolution down to a few nanometers[59]. It is an optically transparent and gas permeable elastic polymer which enables O_2 transportation, thus it is used successfully in cellular studies[60]. The elasticity of PDMS allows stacking of multiple layers to create microfluidic designs with integrated microvalves.[61] However, nonspecific adsorption of biomolecules on PDMS surface can take place due to its hydrophobic nature which requires chemical or biochemical modification of PDMS prior to use.[62]

A few alternatives to PDMS are PMMA and paper. PMMA is gas impermeable, biocompatible, and offers better performance than PDMS under mechanical stress. PMMA-based multilayered devices can be fabricated in a few hours. Of course, the rigidity of the material make it less suitable for fabrication of low-dead-volume valves. Paper is a cellulose-based material. It is biologically compatible and can be chemically modified, can transport liquids via the capillary effect without the assistance of an external force, has high surface to volume ratio that improves the immobilization of recognition elements, it allows rapid detection, and it be used to fabricate

disposable device. Again, however, flow control is a significant limitation in paper microfluidics, and current research is underway to address these issues.

1.5 Electrochemical Assay For Biomolecules

In the past two decades, many affinity-based electrochemical biosensors have been developed which rely on the specific binding of target with a biorecognition element. In general, these modern sensors have been comprised of nucleic acid probes that contain covalently-linked redox molecules. However, the architecture of these nucleic acid based sensors depend on their sensing strategy and the target to be measured. For instance, electrochemical nucleic acid scaffold sensors employ an electrode-bound, double stranded nucleic acid, with one strand tagged with a redox molecule and another with a target recognition element.[63] Antibodies were quantified by this sensor, as they suppressed the electrochemical signal on binding with the target recognition element (**Figure 1.7**). One disadvantage of these sensors is that the labeled oligo must be separately added and can be washed away due to its non-covalent binding.

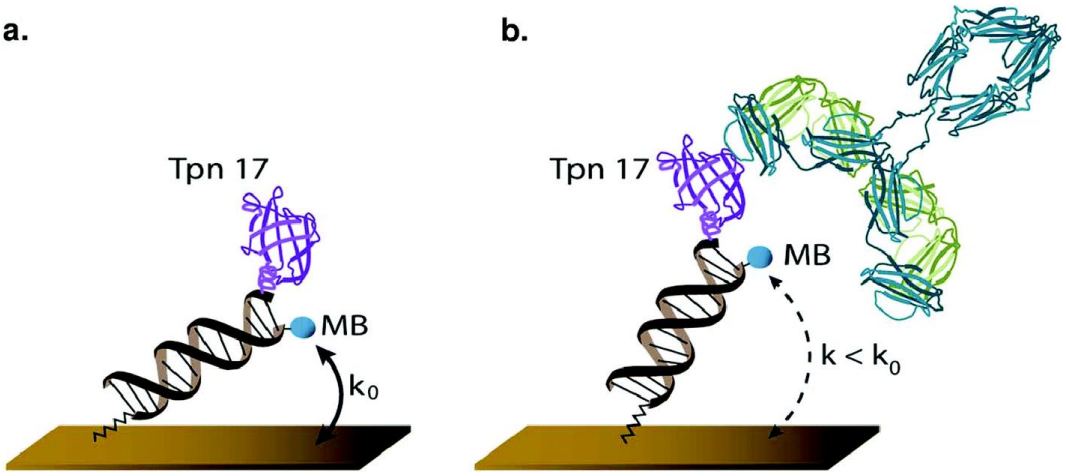

Figure 1.7. Electrochemical scaffold sensor. **a)** The distal end of the surface attached scaffold is modified with a redox reporter and antibody recognition element, Treponema pallidum TpN17. **b)** Antibody-antigen binding reduces the efficiency with which the methylene blue reporter collides with the electrode, which slows down the electron transfer rate and lower signal is observed.[63]

Reprinted with permission Copyright © 2019 Royal Society of Chemistry

Electrochemical aptamer-based sensors are comprised of surface-bound, redox-reporter-modified aptamer (**Figure 1.8**).[64] In the presence of the target molecule, a binding-induced conformational change of the aptamer alters the position of the reporter with respect to the surface, thus, changes the efficiency of electron transfer between the reporter and the electrode, resulting in a concentration-dependent change in current.

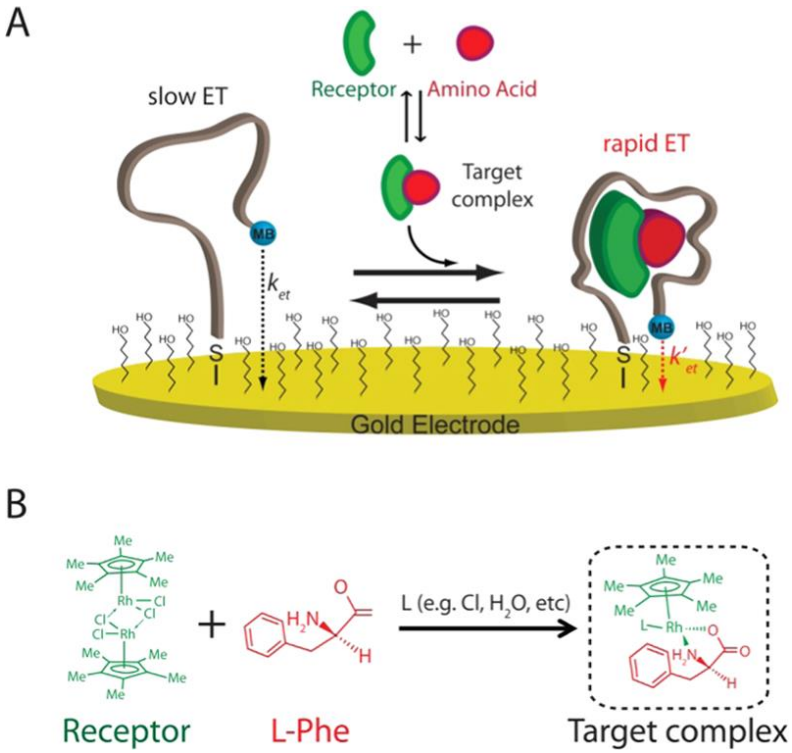

Figure 1.8. Calibration free measurement of phenylalanine. **A)** Upon binding to the target complex aptamer undergoes a conformational change which brings the distal redox reporter close to the electrode surface and higher signal is observed. **B)** Rhodium based receptor forms complex with phenylalanine (L-Phe) in presence of nucleophile which binds with the aptamer.[64]

Reprinted with permission Copyright © 2019 American Chemical Society

1.5.1 Quantification of Small Molecules

Several electrochemical aptamer-based sensors have been developed for the detection of small molecules. Yu et al. developed a reusable electrochemical aptamer sensor for rapid quantification of ampicillin in complex matrices, including serum, saliva, and milk[65-66]. Their

signaling mechanism was based on target binding-induced folding of the aptamer, resulting in an increase in the surface concentration of redox molecule, thereby increase in the signal. The same strategy was employed to quantify picomolar level platelet-derived growth factor in blood serum[67], cocaine in biological fluids[68], and tryptophan in urine[69]. Utilizing similar aptasensor, White and coworkers recently demonstrated real-time continuous monitoring of ATP secretion from astrocytes.[70] Zuo et al. developed an electrochemical aptamer switch for ATP which utilized target induced strand displacement approach.[71] The interaction between ATP and the aptamer led to displacement of a complementary sequence and folding of the aptamer, which brought redox molecules into proximity with the electrode surface.

Plaxco and Soh lab collaborated for the development of a microfluidic electrochemical detector (MEDIC) to continuously monitor concentrations of therapeutic agents in live rats.[72] The sensor utilized a target specific aptamer and acted as a signal-OFF sensor at higher frequencies (>30 Hz) and a signal-ON in lower frequencies, which gave a dual conformation of the drug concentration changes and minimized signal drifts. In their later works, a closed loop feedback control for antibiotic drug doxorubicin[3] and tobramycin[73] was developed which maintained the drug concentration in living animals with temporal resolution in the range of a few seconds; four drugs were measured with the temporal resolution of 3 seconds in the bloodstream of awake, freely moving animals[74]; and calibration-free, drift-resistant measurement of tobramycin[75] and kanamycin[76] was conducted in living animals with high temporal resolution. These recent developments illustrate that DNA-monolayer-based EC sensors could make significant impact to human health in the coming years, and the impressive results are inspiring to our work herein which aims to develop more generalizable versions of the sensing mechanism.

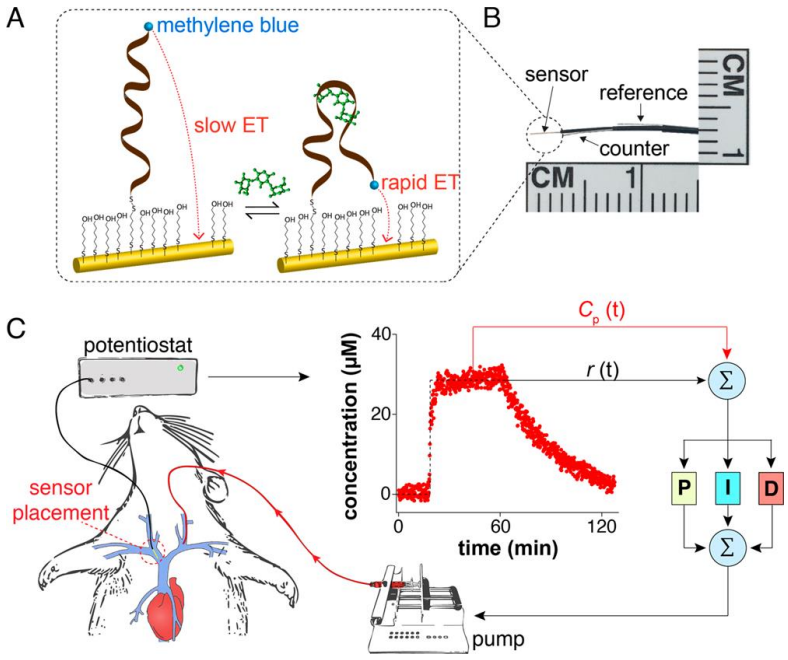

Figure 1.9. Real-time EC measurement of drugs in living animals. **A)** Target binding induced conformational change of electrode-tethered aptamer alters the electron transfer kinetics of the reporter. **B)** Miniaturized size of sensors allowed jugular placement on living rats. **C)** Drug level measurements provided by an in vivo sensor used as input to a feedback control algorithm to adjust dosing rates every 7 s via an infusion pump.[73]

1.5.2 Quantification of Nucleic Acids

Electrochemical nucleic acid sensors comprise surface-bound oligonucleotide probes and a signaling molecule to be used for target recognition. The redox reporter is either conjugated with the probe, or it can serve as a mediator for electron transfer by electrostatically interacting with the target-probe duplex. Das et al. developed a nonenzymatic electrochemical chip-based clamp assay for circulating nucleic acids using a PNA probe immobilized onto the surface of a gold

nanostructured microelectrode.[77] The sensor reads out the presence of target within 15 minutes utilizing clamp sequences that sequester closely related sequences in solution, and only the target nucleic acids hybridize to the PNA probe resulting in signal from an electrocatalytic reporter system. Mousavi et al. used integrated gene circuits with nanostructured microelectrodes for the simultaneous detection of multiple antibiotic resistance genes.[78] Their cell-free gene-circuit express reporter enzymes that cleave specific DNA sequences in solution and releases redox reporter modified DNA. The signaling DNA hybridizes with the probe DNA at the electrode surface resulting in electrochemical signal. Tavallaie et al. developed a highly sensitive sensor for direct quantification of miRNA from 10 aM to 1 nM in whole blood utilizing electrically reconfigurable network of gold coated magnetic nanoparticles.[79] The labeled nanoparticle captures the target and subsequently collects on the surface of a gold macroelectrode. The distance between the nanoparticles increases due to formation of duplex, which impedes electron tunneling through the network of nanoparticles and lower signal is observed. Since the performance of these class of sensors strongly depend on the efficiency with which the target oligonucleotide hybridizes with the surface-tethered oligonucleotide probes, thus we have carefully studied surface hybridization kinetics to improve our understanding of the process which are valuable in DNA-sensor development and optimization.

1.5.3 Quantification of Proteins

Combining the proximity assay concept with electrochemical detection, Easley et al. developed a highly sensitive sensor for femtomolar-level protein quantification.[80] The electrochemical proximity assay (ECPA) is based on target binding-induced DNA hybridization. When the surface-attached probe DNA comes in contact with the target protein and ECPA probes

(two antibody-oligo conjugates) and the redox reporter labeled DNA, the five part complex forms on the electrode surface which brings the redox molecule close enough to the surface to give electrochemical signal. In our laboratory's later work, the team strategically incorporated uracil in the DNA sequences to achieve a reusable sensor for repeated protein quantitation.[81]

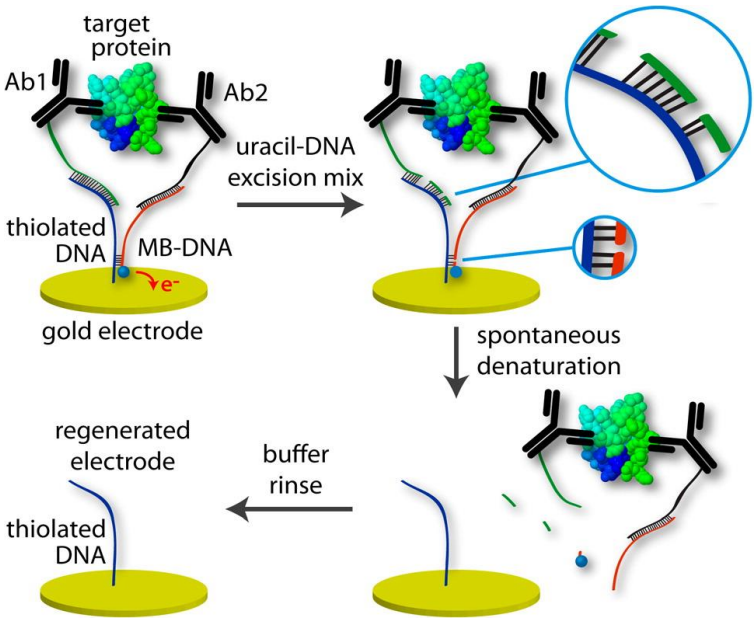

Figure 1.10. A reusable electrochemical proximity assay (ECPA). Here, uracil DNA excision mix cleaved the DNA backbone resulting shorter DNA segments that spontaneously denatured to release probe/target complex from the electrode, leaving the probe DNA on the surface for another measurement.[81]

Reprinted with permission Copyright © 2014 American Chemical Society

In other EC based protein assays, Parolo et al. developed an electrochemical nucleic acid scaffold sensor for rapid, single step detection of HIV- specific antibodies in human serum[82], and

Plaxco and coworkers developed a bioelectrochemical switch which undergoes signal suppression by antibody binding.[83] They were successful in using the sensor in whole blood. Plaxco's group has also studied protein-protein interactions on the surface, which is promising in development of various protein sensors that lack a sensitive aptamer.[84] Das et al. developed an ultrasensitive sensor for a cancer biomarker, CA-125, by using an antibody modified nanostructured gold electrode.[85] Antibody−protein interactions blocked the redox molecules ($[Fe(CN)_6]^{3-/4-}$) from reaching the surface, hence lower signal was observed. While these sensors are generalizable to proteins and highly sensitive, still require addition of signaling molecules and multiple conjugation steps, making probe preparation laborious and expensive. Therefore, more generalizable sensors with simple workflow and without complex, noncovalent structures are still needed.

1.5.4 Generalizable Electrochemical Sensor

To date, aptamers have been evolved against a wide variety of targets, and aptamer-based sensors were even successful in real time monitoring of analytes in living animals.[3, 73-74, 76] However, most electrochemical aptamer-based sensors require a target-induced structure switching aptamer, which limits the generalizability of these sensors. To address this problem, Mahshid et al. did not use aptamers but instead developed an electrochemical steric-hindrance hybridization assay which utilized steric hindrance effects for the detection of large macromolecules such as proteins or antibodies (**Figure 1.11A**).[86] The target protein in the bound state with a signaling DNA strand sterically hindered the hybridization to a surface-attached complementary DNA strand and subsequently reduced the current response. In the absence of target, more signal was generated because it was unhindered. This sensor was able to detect macromolecules with size ranging from 50 to 150 kDa and multiple proteins in whole blood. This

method was also extended for indirect quantification of small molecules[87] (**Figure 1.11B**), and sensitivity was improved by utilizing nanostructured electrodes.[88] This work has recently been followed by an application of detecting signaling factors in stem cell cultures[89] and HIV-1 antibodies in patient specimens.[90] In general, such assay systems are highly sensitive and successful in quantifying multiple proteins and small molecules. However, steric hindrance assays require sample processing and multiple components in the buffer to generate signal, thus they cannot yet provide direct readout upon target addition. Therefore, the demand for a more versatile biosensor still remains.

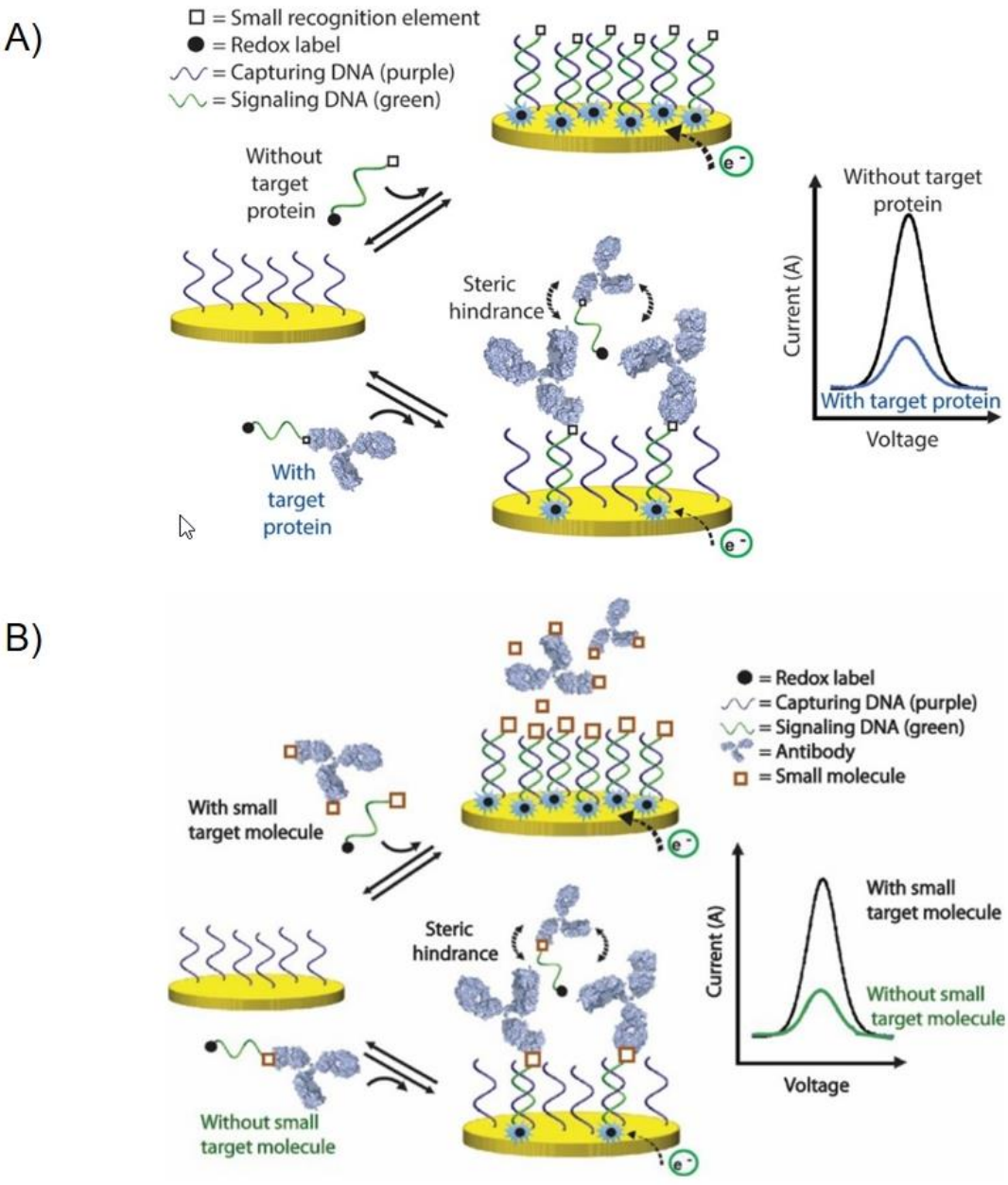

Figure 1.11. Steric hindrance assay. **A)** Target protein binds with the recognition element on the signaling DNA and sterically hinder surface hybridization resulting lower signal.[86] **B)** Target small molecule binds with the protein which leaves the signaling DNA available for surface hybridization resulting higher signal.[87]

Recently, Easley and Somasundaram designed a novel nucleic acid nanostructure-based electrochemical sensor for the quantification of a broad range of analytes which does not require sample preparation, signaling substrate addition (using direct assay format), or enzymatic signal amplification, therefore providing direct readout that should be suitable for point-of-care detection.[91]

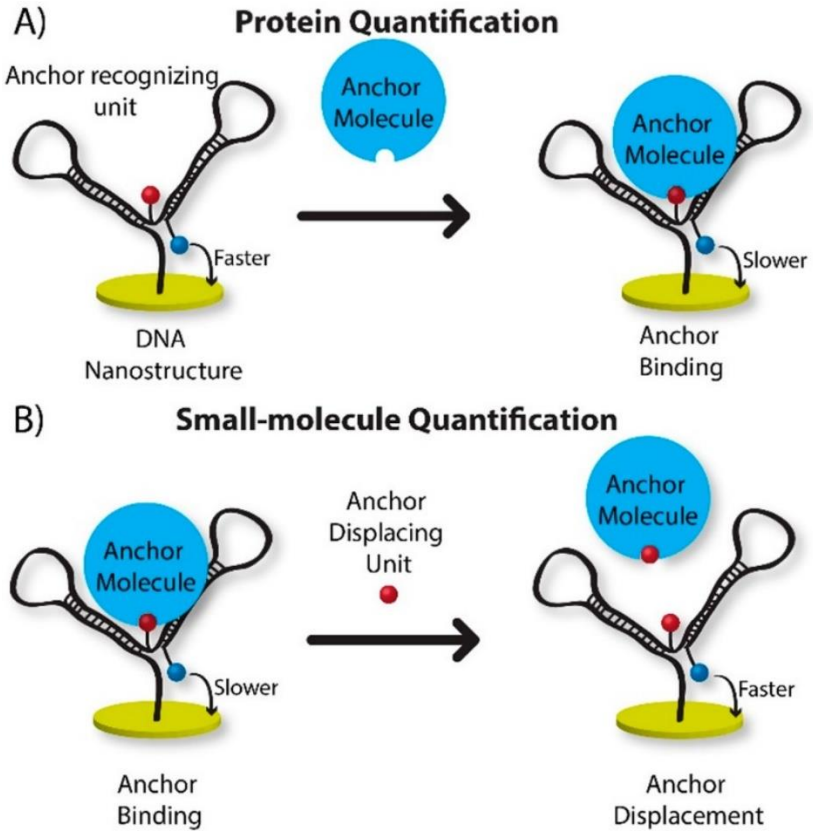

Figure 1.12. Nucleic acid nanostructure sensor. **A)** The faster tethered diffusion of the DNA nanostructure slows down by protein binding resulting lower signal. **B)** In indirect assay format, the mall molecule analyte displaces pre-bound anchor molecule form the nanostructure which promotes faster diffusion, resulting in higher signal.[91]

As shown in **Figure 1.12**, the rational design of the DNA nanostructure holds the redox reporter and the anchor recognizing unit (i.e. target-binding unit) in close proximity and in predictable positions. This ensures effective alteration of the tethered diffusion of the redox tag upon either attachment or displacement of an anchor molecule to the anchor recognition unit, and it helps improve the generalizability of the assay. Target protein binding slows the tethered diffusion of the nanostructure due to the increased molecular weight of the complex, reducing electrochemical signal proportional to anchor concentration. The same DNA nanostructure can also be deployed to detect small molecules in solution. Small-molecules can be quantified through amplification of the signal by displacing the anchor molecule. The sensor was able to quantify a widely prescribed immunosuppressant drug, tacrolimus, directly with electrochemistry for the first time. This methodology, along with its optimization and further development, are discussed in Chapters 3 and 4.

1.6 Concluding Remarks

One of the major goals of biosensor research and development is to provide noninvasive methods for assessing health conditions, monitoring disease onset and progression, and evaluate treatment outcomes. Working toward these goals, researchers have focused on devising innovative strategies for detection of biomolecules. EC sensing strategies have the potential to provide rapid, sensitive, selective, and quantitative information about biomolecular analytes. To date, a variety of electrochemical assays have been developed utilizing aptamers which can bind to a range of analytes with high specificity. With these sensors, real-time monitoring of therapeutic agents in living animals has been accomplished. However, the requirement of structure-switching aptamers limits the generalizability of these class of sensors. To generalize, electrochemical steric hindrance

assays have been developed for both large proteins and small molecules. The drawback of this method is the requirement of sample processing and multiple components in the solution which hinders direct readout. Our recently developed DNA nanostructure based sensors exhibited unprecedented generalizability by quantifying analytes ranging from small molecules to antibodies with minimal workflow. While the nanostructure sensors show great promise, there remains significant work to be done to validate their generalizability and to permit single-step detection of small molecules (using the indirect format in **Figure 1.12B**).

The main goal of this dissertation is to further develop our DNA-based electrochemical sensors for biomolecule quantification and to engineer an electrode-coupled microfluidic device for automated electrode preparation and nucleic acid quantification. Chapter 2 focuses on the understanding of surface hybridization kinetics and toehold-mediated DNA strand displacement reactions. Chapter 3 describes the development of a peptide sensor, where we have expanded the DNA nanostructure based sensor platform to quantify exendin-4, a prescription medication for diabetics. Chapter 4 presents our efforts toward optimization of the nanostructure based sensor to enhance the sensitivity of the system. We compared two strategies to reduce the molecular weight of the DNA nanostructure for signal enhancement. Chapter 5 describes the integration of electrochemical sensors with an automated microfluidic device. We have shown that the automated, valve-controlled device is useful for electrode preparation and nucleic acid detection using square wave voltammetry (SWV). Finally, Chapter 6 provides a view on the conclusions and future directions based on this dissertation work.

1.7 References

1. Hood, L.; Heath, J. R.; Phelps, M. E.; Lin, B., Systems biology and new technologies enable predictive and preventative medicine. *Science (New York, N.Y.)* **2004,** *306* (5696), 640-3.

2. Labib, M.; Sargent, E. H.; Kelley, S. O., Electrochemical Methods for the Analysis of Clinically Relevant Biomolecules. *Chemical Reviews* **2016,** *116* (16), 9001-9090.

3. Mage, P. L.; Ferguson, B. S.; Maliniak, D.; Ploense, K. L.; Kippin, T. E.; Soh, H. T., Closed-loop control of circulating drug levels in live animals. *Nature Biomedical Engineering* **2017,** *1* (5), 0070.

4. García-Cazorla, À.; Artuch, R., Chapter 63 - Neurotransmitter Disorders. In *Rosenberg's Molecular and Genetic Basis of Neurological and Psychiatric Disease (Fifth Edition)*, Rosenberg, R. N.; Pascual, J. M., Eds. Academic Press: Boston, 2015; pp 703-712.

5. Fan, Y.-S., Companion diagnostic testing for targeted cancer therapies: an overview. *Genet Test Mol Biomarkers* **2013,** *17* (7), 515-523.

6. Lovly, C. M.; Dahlman, K. B.; Fohn, L. E.; Su, Z.; Dias-Santagata, D.; Hicks, D. J.; Hucks, D.; Berry, E.; Terry, C.; Duke, M.; Su, Y.; Sobolik-Delmaire, T.; Richmond, A.; Kelley, M. C.; Vnencak-Jones, C. L.; Iafrate, A. J.; Sosman, J.; Pao, W., Routine multiplex mutational profiling of melanomas enables enrollment in genotype-driven therapeutic trials. *PloS one* **2012,** *7* (4), e35309.

7. Alonso, C. N.; Gallego, M. S.; Rossi, J. G.; Medina, A.; Rubio, P. L.; Bernasconi, A. R.; Zubizarreta, P. A.; Felice, M. S., RT-PCR diagnosis of recurrent rearrangements in pediatric acute lymphoblastic leukemia in Argentina. *Leukemia research* **2012,** *36* (6), 704-8.

8. Leung, T. N.; Zhang, J.; Lau, T. K.; Hjelm, N. M.; Lo, Y. M., Maternal plasma fetal DNA as a marker for preterm labour. *Lancet (London, England)* **1998,** *352* (9144), 1904-5.

9. Sekizawa, A.; Jimbo, M.; Saito, H.; Iwasaki, M.; Matsuoka, R.; Okai, T.; Farina, A., Cell-free fetal DNA in the plasma of pregnant women with severe fetal growth restriction. *American Journal of Obstetrics and Gynecology* **2003,** *188* (2), 480-484.

10. Lau, T. K.; Lo, K. W. K.; Chan, L. Y. S.; Leung, T. Y.; Lo, Y. M. D., Cell-free fetal deoxyribonucleic acid in maternal circulation as a marker of fetal-maternal hemorrhage in patients undergoing external cephalic version near term. *American Journal of Obstetrics and Gynecology* **2000,** *183* (3), 712-716.

11. Sekizawa, A.; Jimbo, M.; Saito, H.; Iwasaki, M.; Sugito, Y.; Yukimoto, Y.; Otsuka, J.; Okai, T., Increased Cell-free Fetal DNA in Plasma of Two Women with Invasive Placenta. *Clinical Chemistry* **2002,** *48* (2), 353-354.

12. Chang, C. P.; Chia, R. H.; Wu, T. L.; Tsao, K. C.; Sun, C. F.; Wu, J. T., Elevated cell-free serum DNA detected in patients with myocardial infarction. *Clinica chimica acta; international journal of clinical chemistry* **2003,** *327* (1-2), 95-101.

13. Eisenberger, C. F.; Schoenberg, M.; Enger, C.; Hortopan, S.; Shah, S.; Chow, N.-H.; Marshall, F. F.; Sidransky, D., Diagnosis of Renal Cancer by Molecular Urinalysis. *JNCI: Journal of the National Cancer Institute* **1999,** *91* (23), 2028-2032.

14. Utting, M.; Werner, W.; Dahse, R.; Schubert, J.; Junker, K., Microsatellite analysis of free tumor DNA in urine, serum, and plasma of patients: a minimally invasive method for the detection of bladder cancer. *Clinical cancer research : an official journal of the American Association for Cancer Research* **2002,** *8* (1), 35-40.

15. Jerónimo, C.; Usadel, H.; Henrique, R.; Silva, C.; Oliveira, J.; Lopes, C.; Sidransky, D., Quantitative GSTP1 hypermethylation in bodily fluids of patients with prostate cancer. *Urology* **2002,** *60* (6), 1131-5.

16. Partsalis, T.; Chan, L. Y.; Hurworth, M.; Willers, C.; Pavlos, N.; Kumta, N.; Wood, D.; Xu, J.; Kumta, S.; Lo, Y. M.; Zheng, M. H., Evidence of circulating donor genetic material in bone allotransplantation. *International journal of molecular medicine* **2006,** *17* (6), 1151-5.

17. Lo, Y. M.; Tein, M. S.; Pang, C. C.; Yeung, C. K.; Tong, K. L.; Hjelm, N. M., Presence of donor-specific DNA in plasma of kidney and liver-transplant recipients. *Lancet (London, England)* **1998,** *351* (9112), 1329-30.

18. Zhong, X. Y.; Hahn, D.; Troeger, C.; Klemm, A.; Stein, G.; Thomson, P.; Holzgreve, W.; Hahn, S., Cell-free DNA in urine: a marker for kidney graft rejection, but not for prenatal diagnosis? *Annals of the New York Academy of Sciences* **2001,** *945*, 250-7.

19. Anderson, N. L.; Anderson, N. G., The human plasma proteome: history, character, and diagnostic prospects. *Molecular & cellular proteomics : MCP* **2002,** *1* (11), 845-67.

20. Ertürk, G.; Hedström, M.; Tümer, M. A.; Denizli, A.; Mattiasson, B., Real-time prostate-specific antigen detection with prostate-specific antigen imprinted capacitive biosensors. *Analytica chimica acta* **2015,** *891*, 120-9.

21. Jeong, B.; Akter, R.; Han, O. H.; Rhee, C. K.; Rahman, M. A., Increased Electrocatalyzed Performance through Dendrimer-Encapsulated Gold Nanoparticles and Carbon Nanotube-Assisted Multiple Bienzymatic Labels: Highly Sensitive Electrochemical Immunosensor for Protein Detection. *Analytical Chemistry* **2013,** *85* (3), 1784-1791.

22. Ojeda, I.; Garcinuño, B.; Moreno-Guzmán, M.; González-Cortés, A.; Yudasaka, M.; Iijima, S.; Langa, F.; Yáñez-Sedeño, P.; Pingarrón, J. M., Carbon Nanohorns as a Scaffold for the Construction of Disposable Electrochemical Immunosensing Platforms. Application to the Determination of Fibrinogen in Human Plasma and Urine. *Analytical Chemistry* **2014,** *86* (15), 7749-7756.

23. Wang, Z.; Sun, N.; He, Y.; Liu, Y.; Li, J., DNA Assembled Gold Nanoparticles Polymeric Network Blocks Modular Highly Sensitive Electrochemical Biosensors for Protein Kinase Activity Analysis and Inhibition. *Analytical Chemistry* **2014,** *86* (12), 6153-6159.

24. Ellington, A. D.; Szostak, J. W., In vitro selection of RNA molecules that bind specific ligands. *Nature* **1990,** *346* (6287), 818-822.

25. Labib, M.; Zamay, A. S.; Muharemagic, D.; Chechik, A. V.; Bell, J. C.; Berezovski, M. V., Aptamer-Based Viability Impedimetric Sensor for Viruses. *Analytical Chemistry* **2012,** *84* (4), 1813-1816.

26. Labib, M.; Zamay, A. S.; Kolovskaya, O. S.; Reshetneva, I. T.; Zamay, G. S.; Kibbee, R. J.; Sattar, S. A.; Zamay, T. N.; Berezovski, M. V., Aptamer-Based Viability Impedimetric Sensor for Bacteria. *Analytical Chemistry* **2012,** *84* (21), 8966-8969.

27. Wehbe, M.; Labib, M.; Muharemagic, D.; Zamay, A. S.; Berezovski, M. V., Switchable aptamers for biosensing and bioseparation of viruses (SwAps-V). *Biosensors and Bioelectronics* **2015,** *67*, 280-286.

28. Huang, Y.; Xu, J.; Liu, J.; Wang, X.; Chen, B., Disease-Related Detection with Electrochemical Biosensors: A Review. *Sensors (Basel)* **2017,** *17* (10), 2375.

29. Guerreiro, G. V.; Zaitouna, A. J.; Lai, R. Y., Characterization of an electrochemical mercury sensor using alternating current, cyclic, square wave and differential pulse voltammetry. *Analytica chimica acta* **2014,** *810*, 79-85.

30. Wu, Y.; Lai, R. Y., Electrochemical Gold(III) Sensor with High Sensitivity and Tunable Dynamic Range. *Analytical Chemistry* **2016,** *88* (4), 2227-2233.

31. Zhang, S.; Garcia-D'Angeli, A.; Brennan, J. P.; Huo, Q., Predicting detection limits of enzyme-linked immunosorbent assay (ELISA) and bioanalytical techniques in general. *Analyst* **2014,** *139* (2), 439-445.

32. Hsieh, Y. H. P.; Rao, Q., Immunoassays. In *Food Analysis*, Nielsen, S. S., Ed. Springer International Publishing: Cham, 2017; pp 487-502.

33. Yelleswarapu, V.; Buser, J. R.; Haber, M.; Baron, J.; Inapuri, E.; Issadore, D., Mobile platform for rapid sub–picogram-per-milliliter, multiplexed, digital droplet detection of proteins. *Proceedings of the National Academy of Sciences* **2019,** *116* (10), 4489-4495.

34. Akama, K.; Shirai, K.; Suzuki, S., Highly sensitive multiplex protein detection by droplet-free digital ELISA. *Electronics and Communications in Japan* **2019,** *102* (2), 43-47.

35. Pérez-Ruiz, E.; Decrop, D.; Ven, K.; Tripodi, L.; Leirs, K.; Rosseels, J.; van de Wouwer, M.; Geukens, N.; De Vos, A.; Vanmechelen, E.; Winderickx, J.; Lammertyn, J.; Spasic, D., Digital ELISA for the quantification of attomolar concentrations of Alzheimer's disease biomarker protein Tau in biological samples. *Analytica chimica acta* **2018,** *1015*, 74-81.

36. Song, L.; Zhao, M.; Duffy, D. C.; Hansen, J.; Shields, K.; Wungjiranirun, M.; Chen, X.; Xu, H.; Leffler, D. A.; Sambol, S. P.; Gerding, D. N.; Kelly, C. P.; Pollock, N. R., Development and Validation of Digital Enzyme-Linked Immunosorbent Assays for Ultrasensitive Detection and Quantification of Clostridium difficile Toxins in Stool. *Journal of Clinical Microbiology* **2015,** *53* (10), 3204-3212.

37. Rissin, D. M.; Kan, C. W.; Campbell, T. G.; Howes, S. C.; Fournier, D. R.; Song, L.; Piech, T.; Patel, P. P.; Chang, L.; Rivnak, A. J.; Ferrell, E. P.; Randall, J. D.; Provuncher, G. K.; Walt, D.

R.; Duffy, D. C., Single-molecule enzyme-linked immunosorbent assay detects serum proteins at subfemtomolar concentrations. *Nature Biotechnology* **2010,** *28* (6), 595-599.

38. Rissin, D. M.; Walt, D. R., Digital Concentration Readout of Single Enzyme Molecules Using Femtoliter Arrays and Poisson Statistics. *Nano Letters* **2006,** *6* (3), 520-523.

39. Rissin, D. M.; Walt, D. R., Digital Readout of Target Binding with Attomole Detection Limits via Enzyme Amplification in Femtoliter Arrays. *Journal of the American Chemical Society* **2006,** *128* (19), 6286-6287.

40. Rissin, D. M.; Gorris, H. H.; Walt, D. R., Distinct and Long-Lived Activity States of Single Enzyme Molecules. *Journal of the American Chemical Society* **2008,** *130* (15), 5349-5353.

41. Cohen, L.; Walt, D. R., Single-Molecule Arrays for Protein and Nucleic Acid Analysis. *Annual Review of Analytical Chemistry* **2017,** *10* (1), 345-363.

42. Peppard, J.; Glickman, F.; He, Y.; Hu, S. I.; Doughty, J.; Goldberg, R., Development of a high-throughput screening assay for inhibitors of aggrecan cleavage using luminescent oxygen channeling (AlphaScreen). *Journal of biomolecular screening* **2003,** *8* (2), 149-56.

43. Zhao, H.; Lin, G.; Liu, T.; Liang, J.; Ren, Z.; Liang, R.; Chen, B.; Huang, W.; Wu, Y., Rapid quantitation of human epididymis protein 4 in human serum by amplified luminescent proximity homogeneous immunoassay (AlphaLISA). *Journal of Immunological Methods* **2016,** *437*, 64-69.

44. Fredriksson, S.; Gullberg, M.; Jarvius, J.; Olsson, C.; Pietras, K.; Gústafsdóttir, S. M.; Ostman, A.; Landegren, U., Protein detection using proximity-dependent DNA ligation assays. *Nat Biotechnol* **2002,** *20* (5), 473-7.

45. Greenwood, C.; Ruff, D.; Kirvell, S.; Johnson, G.; Dhillon, H. S.; Bustin, S. A., Proximity assays for sensitive quantification of proteins. *Biomol Detect Quantif* **2015,** *4*, 10-16.

46. Gullberg, M.; Fredriksson, S.; Taussig, M.; Jarvius, J.; Gustafsdottir, S.; Landegren, U., A sense of closeness: protein detection by proximity ligation. *Current Opinion in Biotechnology* **2003,** *14* (1), 82-86.

47. Conze, T.; Shetye, A.; Tanaka, Y.; Gu, J.; Larsson, C.; Göransson, J.; Tavoosidana, G.; Söderberg, O.; Nilsson, M.; Landegren, U., Analysis of Genes, Transcripts, and Proteins via DNA Ligation. *Annual Review of Analytical Chemistry* **2009,** *2* (1), 215-239.

48. Zhang, H.; Li, F.; Dever, B.; Wang, C.; Li, X.-F.; Le, X. C., Assembling DNA through Affinity Binding to Achieve Ultrasensitive Protein Detection. *Angewandte Chemie International Edition* **2013,** *52* (41), 10698-10705.

49. Heyduk, E.; Heyduk, T., Nucleic Acid-Based Fluorescence Sensors for Detecting Proteins. *Analytical Chemistry* **2005,** *77* (4), 1147-1156.

50. Heyduk, T., Practical biophysics: Sensors for rapid detection of biological targets utilizing target-induced oligonucleotide annealing. *Biophys Chem* **2010,** *151* (3), 91-95.

51. Heyduk, E.; Dummit, B.; Chang, Y.-H.; Heyduk, T., Molecular Pincers: Antibody-Based Homogeneous Protein Sensors. *Analytical Chemistry* **2008,** *80* (13), 5152-5159.

52. Heyduk, E.; Moxley, M. M.; Salvatori, A.; Corbett, J. A.; Heyduk, T., Homogeneous Insulin and C-Peptide Sensors for Rapid Assessment of Insulin and C-Peptide Secretion by the Islets. *Diabetes* **2010,** *59* (10), 2360-2365.

53. Tian, L.; Heyduk, T., Antigen Peptide-Based Immunosensors for Rapid Detection of Antibodies and Antigens. *Analytical Chemistry* **2009,** *81* (13), 5218-5225.

54. Hianik, T.; Wang, J., Electrochemical Aptasensors – Recent Achievements and Perspectives. *Electroanalysis* **2009,** *21* (11), 1223-1235.

55. Bucher, E. S.; Wightman, R. M., Electrochemical Analysis of Neurotransmitters. *Annu Rev Anal Chem (Palo Alto Calif)* **2015,** *8*, 239-261.

56. Niu, Y.; Xie, H.; Luo, G.; Weng, W.; Ruan, C.; Li, G.; Sun, W., Electrochemical performance of myoglobin based on TiO2-doped carbon nanofiber decorated electrode and its applications in biosensing. *RSC Advances* **2019,** *9* (8), 4480-4487.

57. Mirceski, V.; Guziejewski, D.; Lisichkov, K., Electrode kinetic measurements with square-wave voltammetry at a constant scan rate. *Electrochimica Acta* **2013,** *114*, 667.

58. Peterson, S. L.; McDonald, A.; Gourley, P. L.; Sasaki, D. Y., Poly(dimethylsiloxane) thin films as biocompatible coatings for microfluidic devices: cell culture and flow studies with glial cells. *Journal of biomedical materials research. Part A* **2005,** *72* (1), 10-8.

59. Sun, Y.; Rogers, J. A., Fabricating Semiconductor Nano/Microwires and Transfer Printing Ordered Arrays of Them onto Plastic Substrates. *Nano Letters* **2004,** *4* (10), 1953-1959.

60. Tanyeri, M.; Tay, S., Viable cell culture in PDMS-based microfluidic devices. *Methods in cell biology* **2018,** *148*, 3-33.

61. Araci, I. E.; Quake, S. R., Microfluidic very large scale integration (mVLSI) with integrated micromechanical valves. *Lab on a chip* **2012,** *12* (16), 2803-6.

62. Roman, G. T.; Hlaus, T.; Bass, K. J.; Seelhammer, T. G.; Culbertson, C. T., Sol−Gel Modified Poly(dimethylsiloxane) Microfluidic Devices with High Electroosmotic Mobilities and Hydrophilic Channel Wall Characteristics. *Analytical Chemistry* **2005,** *77* (5), 1414-1422.

63. Ogden, N. E.; Kurnik, M.; Parolo, C.; Plaxco, K. W., An electrochemical scaffold sensor for rapid syphilis diagnosis. *Analyst* **2019,** *144* (17), 5277-5283.

64. Idili, A.; Parolo, C.; Ortega, G.; Plaxco, K. W., Calibration-Free Measurement of Phenylalanine Levels in the Blood Using an Electrochemical Aptamer-Based Sensor Suitable for Point-of-Care Applications. *ACS sensors* **2019,** *4* (12), 3227-3233.

65. Yu, Z.-g.; Sutlief, A. L.; Lai, R. Y., Towards the development of a sensitive and selective electrochemical aptamer-based ampicillin sensor. *Sensors and Actuators B: Chemical* **2018,** *258*, 722-729.

66. Yu, Z.-g.; Lai, R. Y., A reagentless and reusable electrochemical aptamer-based sensor for rapid detection of ampicillin in complex samples. *Talanta* **2018,** *176*, 619-624.

67. Lai, R. Y.; Plaxco, K. W.; Heeger, A. J., Aptamer-Based Electrochemical Detection of Picomolar Platelet-Derived Growth Factor Directly in Blood Serum. *Analytical Chemistry* **2007,** *79* (1), 229-233.

68. Baker, B. R.; Lai, R. Y.; Wood, M. S.; Doctor, E. H.; Heeger, A. J.; Plaxco, K. W., An Electronic, Aptamer-Based Small-Molecule Sensor for the Rapid, Label-Free Detection of Cocaine in Adulterated Samples and Biological Fluids. *Journal of the American Chemical Society* **2006,** *128* (10), 3138-3139.

69. Idili, A.; Gerson, J.; Parolo, C.; Kippin, T.; Plaxco, K. W., An electrochemical aptamer-based sensor for the rapid and convenient measurement of L-tryptophan. *Analytical and bioanalytical chemistry* **2019,** *411* (19), 4629-4635.

70. Santos-Cancel, M.; Simpson, L. W.; Leach, J. B.; White, R. J., Direct, Real-Time Detection of Adenosine Triphosphate Release from Astrocytes in Three-Dimensional Culture Using an Integrated Electrochemical Aptamer-Based Sensor. *ACS chemical neuroscience* **2019,** *10* (4), 2070-2079.

71. Zuo, X.; Song, S.; Zhang, J.; Pan, D.; Wang, L.; Fan, C., A Target-Responsive Electrochemical Aptamer Switch (TREAS) for Reagentless Detection of Nanomolar ATP. *Journal of the American Chemical Society* **2007,** *129* (5), 1042-1043.

72. Ferguson, B. S.; Hoggarth, D. A.; Maliniak, D.; Ploense, K.; White, R. J.; Woodward, N.; Hsieh, K.; Bonham, A. J.; Eisenstein, M.; Kippin, T. E.; Plaxco, K. W.; Soh, H. T., Real-Time, Aptamer-Based Tracking of Circulating Therapeutic Agents in Living Animals. *Science Translational Medicine* **2013,** *5* (213), 213ra165-213ra165.

73. Arroyo-Currás, N.; Ortega, G.; Copp, D. A.; Ploense, K. L.; Plaxco, Z. A.; Kippin, T. E.; Hespanha, J. P.; Plaxco, K. W., High-Precision Control of Plasma Drug Levels Using Feedback-Controlled Dosing. *ACS Pharmacology & Translational Science* **2018,** *1* (2), 110-118.

74. Arroyo-Currás, N.; Somerson, J.; Vieira, P. A.; Ploense, K. L.; Kippin, T. E.; Plaxco, K. W., Real-time measurement of small molecules directly in awake, ambulatory animals. *Proceedings of the National Academy of Sciences* **2017,** *114* (4), 645-650.

75. Arroyo-Currás, N.; Dauphin-Ducharme, P.; Ortega, G.; Ploense, K. L.; Kippin, T. E.; Plaxco, K. W., Subsecond-Resolved Molecular Measurements in the Living Body Using Chronoamperometrically Interrogated Aptamer-Based Sensors. *ACS sensors* **2018,** *3* (2), 360-366.

76. Li, H.; Li, S.; Dai, J.; Li, C.; Zhu, M.; Li, H.; Lou, X.; Xia, F.; Plaxco, K. W., High frequency, calibration-free molecular measurements in situ in the living body. *Chemical Science* **2019,** *10*, 10843-10848.

77. Das, J.; Ivanov, I.; Montermini, L.; Rak, J.; Sargent, E. H.; Kelley, S. O., An electrochemical clamp assay for direct, rapid analysis of circulating nucleic acids in serum. *Nature Chemistry* **2015,** *7* (7), 569-575.

78. Sadat Mousavi, P.; Smith, S. J.; Chen, J. B.; Karlikow, M.; Tinafar, A.; Robinson, C.; Liu, W.; Ma, D.; Green, A. A.; Kelley, S. O.; Pardee, K., A multiplexed, electrochemical interface for gene-circuit-based sensors. *Nature Chemistry* **2020,** *12* (1), 48-55.

79. Tavallaie, R.; McCarroll, J.; Le Grand, M.; Ariotti, N.; Schuhmann, W.; Bakker, E.; Tilley, R. D.; Hibbert, D. B.; Kavallaris, M.; Gooding, J. J., Nucleic acid hybridization on an electrically reconfigurable network of gold-coated magnetic nanoparticles enables microRNA detection in blood. *Nature Nanotechnology* **2018,** *13* (11), 1066-1071.

80. Hu, J.; Wang, T.; Kim, J.; Shannon, C.; Easley, C. J., Quantitation of Femtomolar Protein Levels via Direct Readout with the Electrochemical Proximity Assay. *Journal of the American Chemical Society* **2012,** *134* (16), 7066-7072.

81. Hu, J.; Yu, Y.; Brooks, J. C.; Godwin, L. A.; Somasundaram, S.; Torabinejad, F.; Kim, J.; Shannon, C.; Easley, C. J., A Reusable Electrochemical Proximity Assay for Highly Selective, Real-Time Protein Quantitation in Biological Matrices. *Journal of the American Chemical Society* **2014,** *136* (23), 8467-8474.

82. Parolo, C.; Greenwood, A. S.; Ogden, N. E.; Kang, D.; Hawes, C.; Ortega, G.; Arroyo-Currás, N.; Plaxco, K. W., E-DNA scaffold sensors and the reagentless, single-step, measurement of HIV-diagnostic antibodies in human serum. *Microsystems & Nanoengineering* **2020,** *6* (1), 13.

83. Vallée-Bélisle, A.; Ricci, F.; Uzawa, T.; Xia, F.; Plaxco, K. W., Bioelectrochemical Switches for the Quantitative Detection of Antibodies Directly in Whole Blood. *Journal of the American Chemical Society* **2012,** *134* (37), 15197-15200.

84. Kang, D.; Sun, S.; Kurnik, M.; Morales, D.; Dahlquist, F. W.; Plaxco, K. W., New Architecture for Reagentless, Protein-Based Electrochemical Biosensors. *Journal of the American Chemical Society* **2017,** *139* (35), 12113-12116.

85. Das, J.; Kelley, S. O., Protein Detection Using Arrayed Microsensor Chips: Tuning Sensor Footprint to Achieve Ultrasensitive Readout of CA-125 in Serum and Whole Blood. *Analytical Chemistry* **2011,** *83* (4), 1167-1172.

86. Mahshid, S. S.; Camiré, S.; Ricci, F.; Vallée-Bélisle, A., A Highly Selective Electrochemical DNA-Based Sensor That Employs Steric Hindrance Effects to Detect Proteins Directly in Whole Blood. *Journal of the American Chemical Society* **2015,** *137* (50), 15596-15599.

87. Mahshid, S. S.; Ricci, F.; Kelley, S. O.; Vallée-Bélisle, A., Electrochemical DNA-Based Immunoassay That Employs Steric Hindrance To Detect Small Molecules Directly in Whole Blood. *ACS sensors* **2017,** *2* (6), 718-723.

88. Mahshid, S. S.; Vallée-Bélisle, A.; Kelley, S. O., Biomolecular Steric Hindrance Effects Are Enhanced on Nanostructured Microelectrodes. *Analytical Chemistry* **2017,** *89* (18), 9751-9757.

89. Zhou, W.; Mahshid, S. S.; Wang, W.; Vallée-Bélisle, A.; Zandstra, P. W.; Sargent, E. H.; Kelley, S. O., Steric Hindrance Assay for Secreted Factors in Stem Cell Culture. *ACS sensors* **2017,** *2* (4), 495-500.

90. Mahshid, S. S.; Mahshid, S.; Vallée-Bélisle, A.; Kelley, S. O., Peptide-Mediated Electrochemical Steric Hindrance Assay for One-Step Detection of HIV Antibodies. *Analytical Chemistry* **2019,** *91* (8), 4943-4947.

91. Somasundaram, S.; Easley, C. J., A Nucleic Acid Nanostructure Built through On-Electrode Ligation for Electrochemical Detection of a Broad Range of Analytes. *Journal of the American Chemical Society* **2019,** *141* (29), 11721-11726.

Chapter 2

Double-layer Effects on Nucleic Acid Hybridization Kinetics at Self-assembled DNA Monolayers Studied by Square-wave Voltammetry

2.1 Introduction

Development of DNA-based sensors for highly sensitive, sequence-specific quantification has become crucial due to their extensive applications in clinical diagnosis, pathogen detection, gene expression studies, and environmental monitoring.[1-4] To date, numerous analytical techniques have been established for oligonucleotide detection, such as electrochemistry, fluorescence, surface plasmon resonance, chemiluminiscence, and quartz crystal microbalance.[5-6] Among these methods, electrochemical (EC) DNA sensors have attracted much attention owing to their reliability, rapid response, low cost and portability, low sample consumption, ability to work in complex/multicomponent samples, and remarkably high sensitivity and selectivity.[7-11] Many nucleic-acid based EC methods use structure switching of a probe for target-dependent signal change[12], and some of these sensors have recently made the impressive leap into real-time measurements directly in the blood of living animals.[13-16] To address generalizability, other sensor architectures based on steric hindrance[8, 17-18] or tethered diffusion of surface DNA probes have been developed more recently.[19-20] Within this field, targeted analytes have been greatly expanded[21] from the original sensors of nucleic acids to other molecular categories such as small drug molecules, small hormones, and larger proteins (e.g. antibodies).

Regardless of the analyte class, the common theme in these sensors is a foundation made with a mixed, self-assembled monolayer (SAM) of the signaling nucleic acids and passivating

alkanethiols on the electrode.[22] Along with complementary base-pair hybridization between long oligonucleotides for DNA detection, several DNA-based sensors targeting nucleic acids or other analytes employ short oligonucleotides (≤10 base pair) toward this goal.[23-27] Plaxco and co-workers constructed a clever bioelectrochemical switch for direct quantification of antibodies directly in blood samples, in which the target distorted the 5 base pair (bp) stem-loop conformation of the probe DNA on the surface, resulting in analyte-dependent electrochemical signal change.[25] In our previous work, we reported a highly sensitive and selective protein assay, the electrochemical proximity assay (ECPA), where target-induced DNA hybridization (5, 7, or 10 bp) on the surface recruited redox-tagged DNA close to the sensor surface for electrochemical readout.[23-24] Several research groups have studied the performance of similar EC biosensors by investigating the effects of immobilized probe structure[28] and probe surface density[29], the nature of the co-adsorbates used to form the SAM[30], the redox reporter used[31], the use of reversible cation-induced collapse [32], and even by modifying square-wave voltammetric (SWV) frequency.[33]

However, the dependence of EC signals on the relative distance of DNA binding sites from the electrode surface has not been explored in this context. As solution-to-surface hybridization is distinct from solution-phase hybridization in terms of kinetics and thermodynamics[34-35], sensor performance may be sensitive to the location of the redox reporter and/or DNA binding site. The surface charge will likely alter the hybridization rate of negatively charged DNA[36], thereby altering the signaling properties of the EC sensor. Especially for short hybridization sequences (≤10 bp) near the electrode surface, this effect may lead to distinctive consequences such as low binding energy, degrading the assay performance. Here, we describe our detailed study in which we varied the site of DNA hybridization relative to the electrode under different conditions. As shown below, the surface hybridization kinetics of short DNA strands depend strongly upon the distance between

the electrode and the binding site, and the ionic strength dependence suggests that this effect is driven by the electric double-layer. Lastly, the importance of this effect is demonstrated using toehold-mediated DNA strand displacement reactions at the electrodes, where more rapid and efficient sensing is achieved by distancing the binding site away from the electrode by about 12.5 nm. Ultimately, this study suggests that the nucleic acid hybridization site relative to the electrode should be carefully controlled in conjunction with the ionic strength when developing DNA-based EC sensors.

2.2 Reagents and Materials

All solutions were prepared with deionized, ultrafiltered water (Fisher Scientific). The following reagents were used as received: 4-(2-hydroxyethyl)-1-piperazineethanesulfonic acid (HEPES) (99.5%), tris-(2-carboxyethyl) phosphine hydrochloride (TCEP), (Sigma-Aldrich, St. Louis, MO). HPLC-purified, methylene blue-conjugated DNA (MB-DNA) was purchased from Biosearch Technologies (Novato, CA). Oligonucleotides were obtained from Integrated DNA Technologies (IDT; Coralville, Iowa), with purity and yield confirmed by mass spectrometry and HPLC, respectively. Sequences of ssDNAs used in the experiment are given in **Table 2.1**. These sequences were designed using the nucleic acid package web server (NUPACK).[37]

Table 2.1: Single-Stranded DNA Sequences Used in Hybridization Kinetics Study

Sequence Name	DNA sequence, listed 5′ to 3′
0A-DNA	/**5ThioMC6-D**/GCA TGG TGA CAT TTT TCG TTC GTT AGG GTT CAA ATC CGC G
1A-DNA	**/5ThioMC6-D /A**GC ATG GTG ACA TTT TTC GTT CGT TAG GGT TCA AAT CCG C
2A-DNA	**/5ThioMC6-D /AA**G CAT GGT GAC ATT TTT CGT TCG TTA GGG TTC AAA TCC G
3A-DNA	**/5ThioMC6-D /AAA** GCA TGG TGA CAT TTT TCG TTC GTT AGG GTT CAA ATC C
4A-DNA	**/5ThioMC6-D /AAA A**GC ATG GTG ACA TTT TTC GTT CGT TAG GGT TCA AAT C
5A-DNA	**/5ThioMC6-D /AAA AA**G CAT GGT GAC ATT TTT CGT TCG TTA GGG TTC AAA T
6A-DNA	**/5ThioMC6-D /AAA AAA** GCA TGG TGA CAT TTT TCG TTC GTT AGG GTT CAA A
7A-DNA	**/5ThioMC6-D / AAA AAA A**GC ATG GTG ACA TTT TTC GTT CGT TAG GGT TCA A
M10	CCA CCC TCC TCC TTT TCC TAT CTC TCC CTC GTC ACC ATG C/**MB-C7**/
M40	CGC GGA TTT GAA CCC TAA CGA ACG AAA AAT GTC ACC ATG C/**MB-C7/**
C-33-LTH	CGC GGA TTT GAA CCC TAA CGA ACG AAA AAT GTC
C-33-UTH	TTG AAC CCT AAC GAA CGA AAA ATG TCA CCA TGC

Abbreviations: /5ThioMC6-D/ = disulfide bond flanked by two six-carbon spacers (IDT), /MB-C7/ = methylene blue modification (Biosearch).

2.3 Experimental Methods

2.3.1 Preparation of the Electrode

Electrochemical sensors for the kinetics study were prepared using a gold working electrode (2 mm diameter, CH Instruments, Inc., Austin, TX). Electrodes were polished using a previously reported protocol,[23] with slight modification. Briefly, electrodes were cleaned with freshly prepared piranha solution (H_2SO_4/H_2O_2, 3:1) for 5 min, and rinsed with deionized water. (Caution: piranha solution is dangerous to human health and should be used with extreme caution and handled only in small quantities). The electrode was then polished carefully with an aqueous alumina slurry with particle size of 0.05 μm (Buehler, Lake Bluff, IL) for 3 min on polishing pad followed by sonication in ethanol/water (1:1) for 5 min. Subsequently, the gold electrode was rinsed with deionized water and electrochemically polished by means of cyclic voltammetry (CV) in 0.5 M H_2SO_4 by applying the potential from −0.35 to +1.5 V vs Ag|AgCl(s) (3 M KCl) at a scan rate of 0.1 V s^{-1} for 5 cycles. The cleaned gold electrode was thoroughly rinsed with D. I. water and dried under flowing nitrogen.

2.3.2 DNA Self-assembled Monolayer Formation

Typical experiments herein included preparation of three electrodes in parallel, as follows. Thiolated DNA (thio-DNA), with a dithiol group at its 5' terminus, was used for monolayer assembly. To effectively form the self-assembled monolayer (SAM), first the dithiol was reduced to a monothiol with TCEP. A 6 μL portion (2 μL per electrode) of 200 μM thiolated DNA was mixed with 18 μL (6 μL per electrode) of 10 mM TCEP and incubated for 1 h at room temperature

(~21 °C) in the dark for reduction of disulfide bonds in the thiolated DNA. The solution was then diluted to a total volume of 300 μL in HEPES/$NaClO_4$ buffer (10 mM HEPES and 0.5 M $NaClO_4$, pH 7.0)[23] to a final concentration of 1.25 μM. Unless otherwise noted, all solutions used in the experiments to follow were carried out at pH 7.0 and 0.5 M salt concentration. Immobilization of DNA was carried out by directly transferring freshly cleaned electrode to the reduced thiolated DNA solution and incubated for 1 h at room temperature in the dark. Following the self-assembled monolayer (SAM) formation, the electrodes were thoroughly rinsed with deionized water (~ 20 s) to remove any excess thiolated-DNA physically adsorbed on the electrode surface. To prevent nonspecific binding, immediately the SAM modified electrode was transferred to 3 mM 6-mercaptohexanol (MCH) solution and incubated for 1 h at room temperature in the dark[38] followed by rinsing with deionized water (~ 40 s) to remove any excess MCH physically adsorbed on the sensor surface. The electrode was then placed into a glass container with HEPES/$NaClO_4$ buffer.

2.3.3 Electrochemical Measurements

Electrochemical measurements were performed using a GAMRY Reference 600 electrochemistry workstation with a standard three-electrode system, composed of a Ag|AgCl(s) (3 M KCl) reference electrode (Bioanalytical Systems), platinum wire counter electrode, and a Au working electrode (diameter = 2 mm). All potentials are reported relative to Ag|AgCl (3 M KCl) reference electrode. Electrochemical measurements were performed at 25 °C in HEPES/$NaClO_4$ buffer using square wave voltammetry (SWV) with a step size of 1 mV, a pulse height of 25 mV, and a frequency of 100 Hz over the potential range from −0.45 to 0.00 V.

For the hybridization kinetics measurement, a voltammetric trace was recorded upon immersion of the electrode into the sample ($t \approx 0$ min), and the voltammetric scan was carried out every 5 min for a total of 125 min. For the calibration experiment, the sensor was allowed to equilibrate in 500 µL of HEPES/$NaClO_4$ buffer with various concentrations of MB10-DNA for 30 min at 25 °C. Subsequently the counter and reference electrodes were introduced, and SWV measurement was initiated.

2.3.4 Hybridization Kinetics

To study the signal of a short DNA analyte, immediately before starting the measurement, the sensor was immersed in a glass electrochemical cell containing 100 nM MB conjugated DNA sequences (MB-10 DNA) in 500 µL of HEPES/$NaClO_4$ buffer.

Strategy 1: *Varying Salt Concentration.* Four different salt concentrations, 0.125 M, 0.25 M, 0.5 M, and 1.0 M $NaClO_4$ were used to prepare the buffer in strategy 1. By varying the salt concentration, double layer thickness was adjusted. For comparison, we also used the MB-40 DNA strand (M40) to increase the number of complementary bases, in order to increase binding affinity; 0.5 M salt concentration was used with this system.

Strategy 2: *Use of a Long DNA Competitor.* Two competitor DNA sequences, C-33-LTH and C-33-UTH, were used (**Table 2.1**). The sensor was allowed to equilibrate with 500 nM of competitors in 300 µL HEPES/$NaClO_4$ buffer for 24 h at room temperature (~21 °C) in the dark. Following the duplex formation of competitor and thio-DNA, the electrodes were rinsed with HEPES/$NaClO_4$ buffer (~ 5 s) to remove any excess physically adsorbed competitor on the sensor surface. To study

the effects of hybridization site, immediately before starting the measurement, the sensor was immersed in a glass electrochemical cell containing 100 nM MB conjugated DNA sequences (MB-40 DNA) in 500 µL of HEPES/$NaClO_4$ buffer.

2.3.5 Data Analyses

Peak Height

Each set of raw SWV data (including V_{step} and I_{diff} data) was transferred to Microsoft Excel, and a third-order polynomial baseline was calculated near the redox potential of MB-DNA. To do so, the "Linest" function in Excel was used, and data points from −0.450 to −0.360 V and −0.12 to −0.001 V were selected for baseline fitting. The resultant baseline function was subtracted from the raw data to get a baseline corrected SWV voltammagram. The maximum current from this graph was used as the peak height of each particular run.

Hybridization Kinetics

The DNA−DNA hybridization on the electrode surface is a reversible process which can be described by a Langmuir kinetic model[39],

$$\frac{d\theta}{dt} = k_{on} c\,(1-\theta) - k_{off}\theta$$

where θ is the fraction of hybridized target DNA on the surface, c is the concentration of target ssDNA in solution, and k_{on} and k_{off} are the association and dissociation rate constant, respectively. The solution of the first order differential equation is,

$$\theta = \frac{Kc}{1+Kc}\left(1 - e^{-(t/\tau)}\right) \quad (1)$$

which describes the adsorption kinetics, where $K_C = k_{on} / k_{off}$ is the equilibrium constant. Eq. (1) was used to fit the kinetic data and to estimate the hybridization time constant, τ, which measures the time for the hybridization reaction to reach the equilibrium.

$$\tau = \frac{1}{k_{on}c+k_{off}}$$

The hybridization data was analyzed in GraphPad Prism 7.03. For all the cases, the average of three measurements is reported. Error bars represent standard deviation.

2.4 Results and Discussion

2.4.1 Hybridization of Short DNA Strands Near the Electrode Surface

Electrochemical assays based on DNA hybridization have been expanded by successfully quantifying a wide range of analytes in the past decade [5, 11, 19, 21, 25]. The flexibility to control the specific site of hybridization and to attach a redox label in the desired position supports this trend. Nonetheless, there is a shortage in the understanding of the surface based hybridization. In this work, we have evaluated sensors with a single DNA hybridization site, in which a redox-labeled ssDNA analyte in solution hybridizes to a SAM of complementary ssDNA on the surface of the

electrode. By this hybridization, the redox molecule was place at various distances from the electrode surface. For ease of understanding, we use distance units of equivalent nucleotides (nt). Here we designed eight different 40 nt thio-DNA (0A-thiol to 7A-thiol), which places the binding site at varying distances (in units of nt) relative to the sensor surface by tuning the length of the spacer, a series of adenines (A) at the 5'-end of thio-DNA. To keep the length of all eight thio-DNAs at 40 nt, in order to permit equal flexibility, we removed nucleotides from the 3'-end accordingly.

The strategy employed to prepare a DNA sensor surface and to study the kinetics of DNA hybridization is shown in **Figure 2.1**. Through binding equilibria, hybridization of the thio-DNA (blue) and MB-DNA (red) brings the MB label close enough to the gold electrode surface to enable transfer of electrons, which leads to an electrochemical signal during the potential scan.

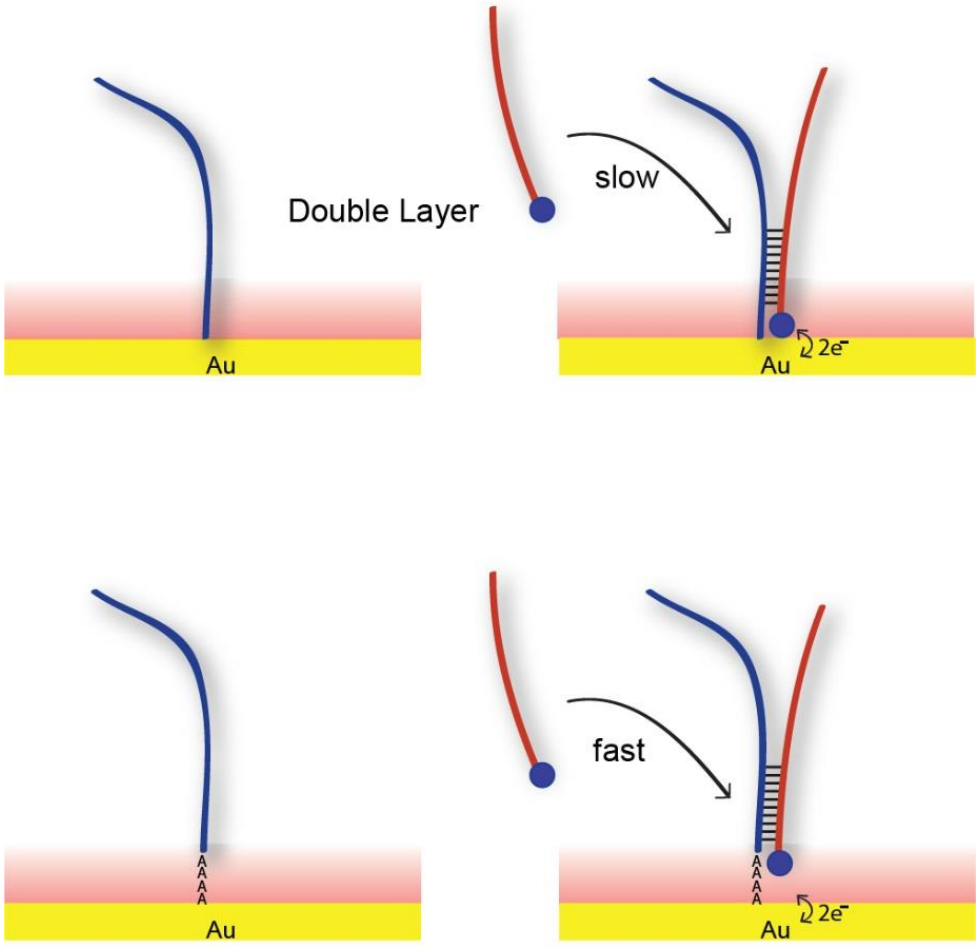

Figure 2.1. Schematic representation of the sensor surface. Poly adenine (A) spacer pushes short hybridization sequence away from the solid surface resulting improvement in the hybridization kinetics.

We observed the signal change upon addition of target DNA (M10) hybridization, and peak currents and kinetic data were used to determine the lifetimes for DNA hybridization at different spacings and salt concentrations. In these experiments, methylene blue labeled DNA (M10) was used, which binds with the thiolated DNAs via 10 base pairs. Since the hybridization energy is the same, one possibility would be that the concentration of MB-DNA hybridized on the surface

should be about the same in all the cases, with a decrease in signal magnitude as the MB label is moved further from the electrode. However, a different effect was observed, where signal gradually increased as the label was moved further from the electrode, up to about 5 nt, then it started to decrease (**Figure 2-2**). Since this effect is not observed with long, stable DNA hybridizations, we hypothesized that electric double layer or charge repulsion effects (shaded in red) played a significant role in the decreased signal close to the electrode.

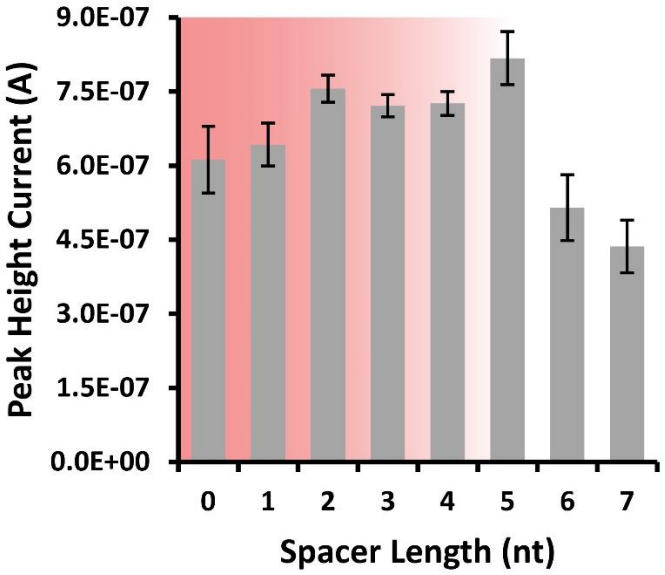

Figure 2.2. After equilibrating MB-labeled DNA (M10 DNA; 10 base pairs) with the electrode, peak currents were observed to counterintuitively increase from about 600 nA to 800 nA as the MB label was placed further from the electrode, from zero to about 5 nt spacing. Beyond 5 nt spacing, the expected decrease in peak current was observed. These effects were hypothesized to be a result of the electric double layer or charge repulsion (shaded in red). The salt concentration ($NaClO_4$) was kept at 0.5 M, and error bars represent the standard deviations from replicate experiments with three different electrodes.

Surface dependent effects were also observed in the kinetic data, shown in **Figure 2.3**. With binding occurring closest to the surface (0A-DNA, green), the hybridization kinetics were significantly slower, and peak current was slightly lower than that of the moderately spaced 4A-DNA (blue). With further spacing (7A-DNA, orange), the kinetics were relatively fast, but the peak current was significantly lower, as expected.

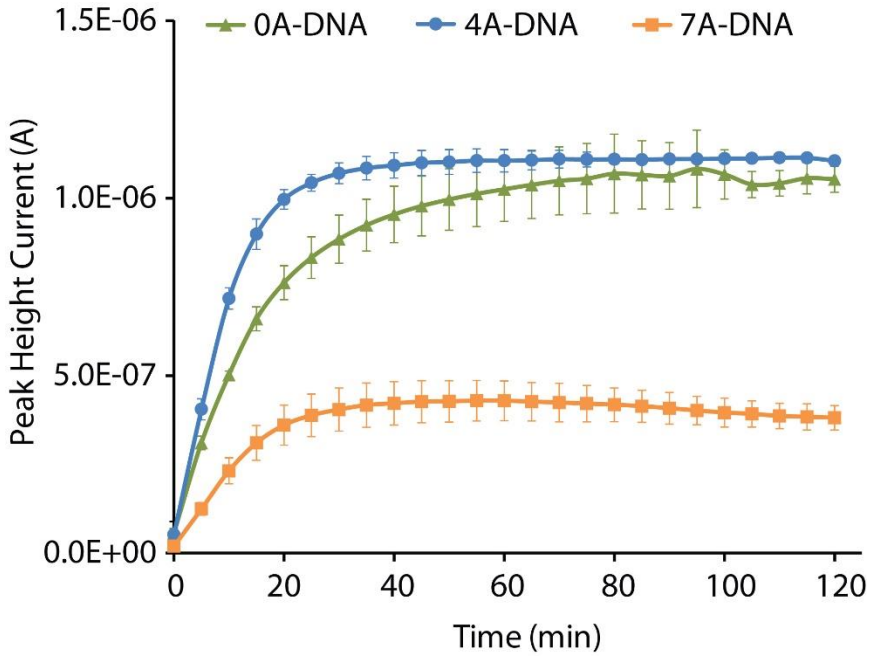

Figure 2.3. Example traces used to determine effects of hybridization kinetics of M10 DNA at the surface as a function of distance from the surface. The salt concentration ($NaClO_4$) was kept at 0.5 M, and error bars represent the standard deviations from replicate experiments with three different electrodes.

2.4.2 The Role of the Electric Double Layer in DNA Hybridization Kinetics

From these initial results, our *hypothesis* was that double layer repulsion effects at the electrode surface will hinder hybridization of short DNA sequences at locations very close to the electrode. To test our hypothesis, we employed two strategies: 1) change the electric double layer thickness by changing the salt concentration; 2) study toehold-mediated strand displacement of DNA where the toehold regions are inside and outside of the double layer.

An electric double layer consisting of random ions appears on a surface when it is exposed to fluids, and this may hinder the access of MB-DNA to the surface and slow down the hybridization rate. The thickness of the double layer depends on the electrolyte concentration and its thickness is approximately $1.5\kappa^{-1}$, where κ^{-1} is the Debye-Hückel length.[40]

$$\kappa^{-1} = \left(\frac{\varepsilon\varepsilon_0 kT}{2c^0 z_i^2 e_0^2}\right)^{1/2}$$

here ε is the relative permittivity of the solvent, ε_0 is the vacuum permittivity, k is the Boltzmann constant, T is the temperature, c^0 is the bulk electrolyte concentration, z_i is the ion charge, and e_0 is the elementary charge. We used three different salt concentrations to gradually increase double layer thickness. The approximate double layer thickness calculated for $NaClO_4$ concentrations of 1.0 M, 0.5 M, 0.25 M, and 0.125 M were 0.46 nm, 0.65 nm, 0.91 nm, and 1.29 nm respectively.

Similar to the kinetic experiments shown in **Figure 2.3**, more kinetic experiments were carried out as a function of both spacer length and salt concentration, where "salt" is meant to refer to $NaClO_4$. These data were fit to Equation (1), and resultant hybridization lifetimes are shown in **Figure 2.4** on a logarithmic y-axis.

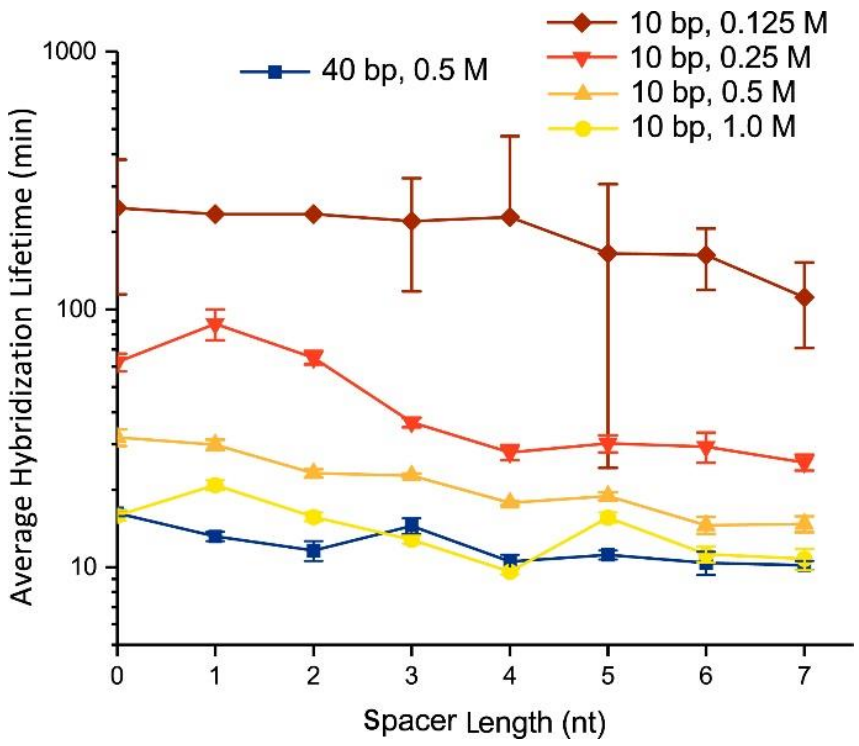

Figure 2.4. DNA hybridization lifetimes were determined as a function of spacer length and salt concentration. Generally, it was shown that the double layer interference effects could be mitigated by increasing salt concentration or by positioning the DNA binding site further from the surface.

As expected from our hypothesis, at higher salt concentration (1.0 M) all spacer lengths resulted in relatively short hybridization lifetimes (~10 – 20 min), and at lower salt concentration (0.125 M) all spacer lengths exhibited very long hybridization lifetimes (2 – 3 h). The observed enhancement in hybridization speed with increasing salt concentration indicated that double layer repulsion could be reduced experimentally, in turn facilitating more efficient hybridization of complementary DNA close to the sensor surface. The kinetic data at the middle range of salt concentrations (0.25 and 0.5 M) provided even more evidence for double-layer or charge repulsion effects, where increasing the distance from the electrode (from 0 to 7 nt spacers) facilitated faster

kinetics in both cases. Finally, as a control, strands with much more stable hybridization energy (40 bp) were evaluated at higher salt concentration (blue data in **Figure 2.4**). This essentially provided a limit on the speed of hybridization (~10 – 15 min lifetime), and as expected the 10-bp binding at the highest salt concentration (1.0 M; yellow data) was very similar to this control.

If we consider as an example the single-molecule random walk model[41] developed by Huang and White, an electrode surface-tethered redox molecule is confined to a hemispherical volume above the surface and is allowed to randomly move inside the hemisphere, and the maximum radius is determined by the flexible tether length. From this viewpoint, since the DNA hybridization site in our sensors with short spacer lengths is very close to the surface, there is a much higher chance for double-layer interference in the hybridization process. For example, the complementary sequence in our 0A-DNA strand is positioned at 1.26 nm away from the surface at its *maximum* tether length, meaning that the majority of time the position will be closer to the surface (<1.26 nm). At low salt concentration (0.125 M), where the double layer thickness is approximately 1.29 nm, there is a high probability that the closely positioned binding region encounters the double layer and thus hybridization kinetics is affected to a greater extent.

2.4.3 Double Layer Effects on Maximum Sensor Currents

We also investigated the effects of spacer length and salt concentration on the maximum current achieved in these sensors (**Figure 2.5**). It should be noted that with increasing salt concentration, DNA binding energy increases, where 10 bp at 0.5 M has ΔG = -19.4 kcal/mol, while 10 bp at 1.0 M has ΔG = -20.5 kcal/mol). This could be a cause of an increase in maximum current, although the effect should be the same for all eight spacer lengths tested. However we

found that the 10-bp binding at both 6A-DNA and 7A-DNA spacers gave statistically the same current response ($p>0.6$) with 0.5 M and 1.0 M salt, whereas shorter spacer lengths gave distinct current response ($p<0.05$), which indicates not the increased binding energy but attenuation of the double layer is responsible for the improved current response for 0 to 5 nt spacers in 0.5 M $NaClO_4$ (**Figure 2.5**).

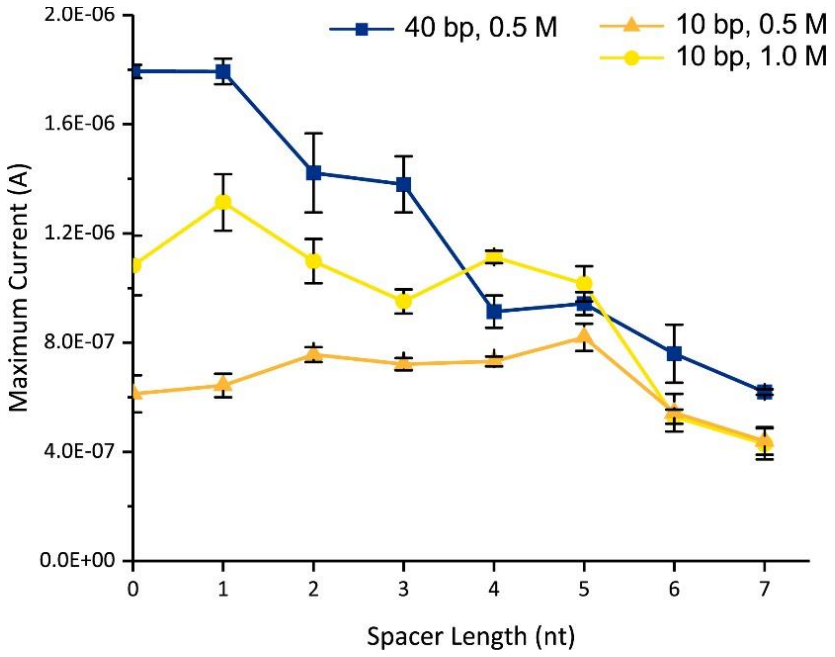

Figure 2.5. Maximum current responses from SWV sensing of DNA were determined as a function of spacer length and salt concentration. These data confirm that double-layer screening effects were the main driving force behind the differences in hybridization efficiencies near the electrode.

Again, the 40 bp strand at 0.5 M salt (blue data in **Figure 2.5**) was used to control for any hybridization energy effects. In this case, the fact that current continued to increase as the MB label was positioned closer to the electrode suggests that the very strong hybridization (ΔG = -62.2

kcal/mol) was able to overcome any double layer repulsion effects, and the expected increasing SWV current response was observed as the MB label was moved closer to the surface.

2.4.4 Toehold-mediated Strand Displacement Near Electrode Surfaces

To further test our hypothesis of double layer repulsion on DNA hybridization, our second strategy was to investigate the kinetics of toehold-mediated strand displacement reactions. Here, we utilized 40 bp MB-DNA as an analyte (M40) which displaces a 33 bp competitor hybridized with two spacer lengths, 0A-DNA and 4A-DNA. Upon hybridization with the toehold region, the M40 DNA strand can attach to one end of the thio-DNA and displace the complementary competitor strand of the DNA duplex, a mechanism referred to as toehold-mediated strand displacement[42-43]. We designed two competitor DNA sequences, C-33-LTH and C-33-UTH in such a way that C-33-LTH binds with the top part of the thio-DNA, leaving a 7 nt toehold at the 5′-terminus of the thio-DNA which is closer to the surface (LTH stands for “lower toe hold”). In the case of C-33-UTH, the 7 nt toehold is left on the 3′-terminus of the strand, away from the surface (UTH, “upper toe hold”). **Figure 2.6** shows a schematic that conveys our hypothesized result, where the kinetics of binding to a lower toe hold (LTH) would be significantly slower than that binding to an upper toe hold (UTH). In both the cases, the analyte DNA binding energies are equal (both 40 bp), and the seven nucleotide toehold will be formed first then push the competitor away due to the higher stability of that complex compared to the competitor.

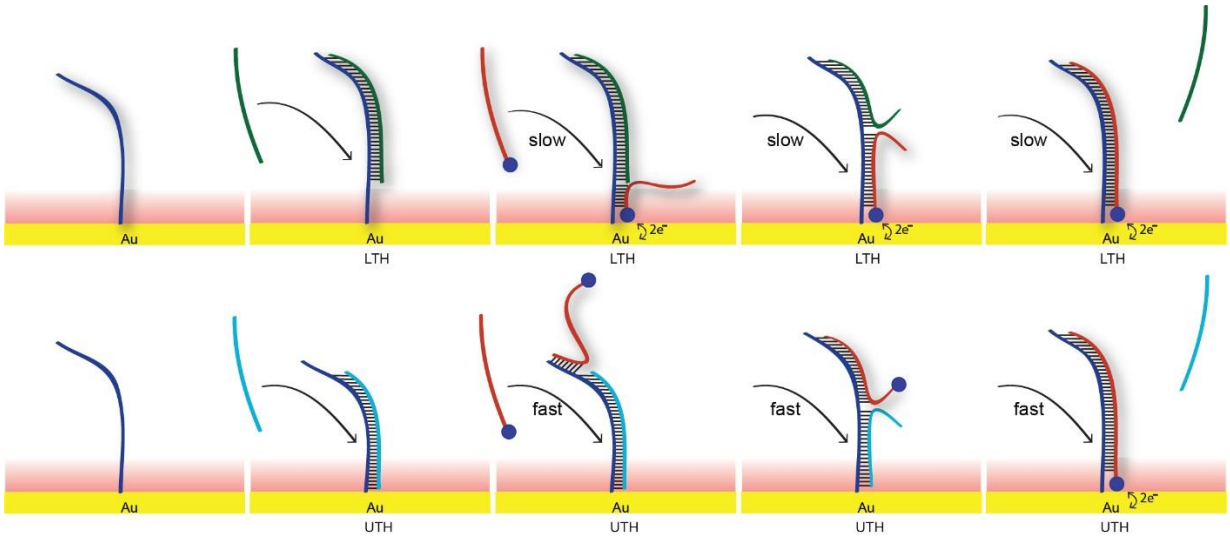

Figure 2.6. Schematic of toehold mediated DNA strand displacement that occurs near the electrode (top row; LTH = "lower toe hold") or far from the electrode (lower row; UTH = "upper toe hold").

According to our hypothesis, M40 DNA would readily displace the competitor using the UTH with faster kinetics. But with a LTH, strand displacement kinetics should slow down as the double layer repulsion is now perturbing hybridization of MB-DNA with the toehold and displacement of the competitor. **Figure 2.7** shows the measured kinetic profiles for these systems.

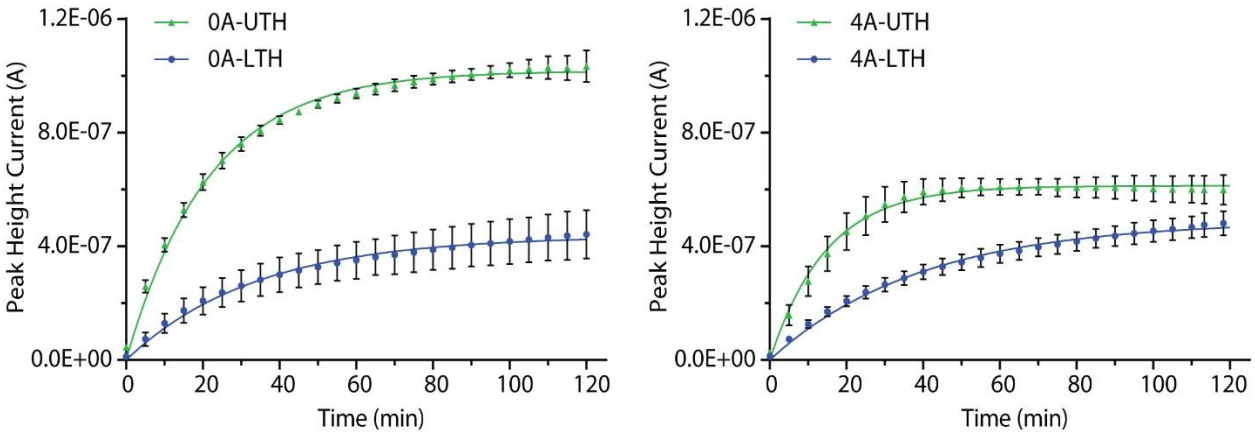

Figure 2.7. Toehold-mediated DNA strand displacement kinetics. With no poly-A spacer (0A, leftmost data), a drastic difference in both kinetics and final current were observed between the lower toehold (blue, 0A-LTH) and upper tohold (green, 0A-UTH). When a 4 nt spacer was added (4A, rightmost data), the difference between the UTH and LTH was diminished, where kinetics were slower with the LTH (blue) but the final currents were similar.

As hypothesized, in 0A-DNA, the upper toehold (0A-UTH) promotes much faster and higher yield of hybridization compared to the lower toehold (0A-LTH) displacement reaction (**Figure 2.7**). The displacement with a lower toehold did not reach an equivalent peak height compared to the upper toehold, and these results confirm our hypothesis that double layer repulsion is responsible for the slower kinetics and suppressed current response. By including a 4 nt spacer (4A-DNA), in which the lower toehold is spaced further from the double layer effects, while lower toehold (4A-LTH) reaction followed a slower kinetics than upper toehold (4A-UTH), both the displacement reactions ultimately reached a similar peak height. This indicates that double layer repulsion still has an influence on the displacement kinetics of 4A-DNA but that the effects were diminished by spacing it further from the electrode. Therefore, any similar surface confined

toehold mediated sensors may show improved response with the toehold positioned away from the surface.

These toehold-mediated strand displacement reaction data support our hypothesis that the effect of the double layer is less prominent at longer distance, and similar support is provided by the hybridization kinetics. **Figure 2.8** shows the average hybridization lifetimes of the 40 bp MB-DNA hybridization with 0 nt and 4 nt spacers in the presence of competitor strands leaving upper (UTH) and lower (LTH) toeholds. Data without a competitor is also shown (M-40). The 4A-DNA system exhibited shorter hybridization lifetimes (faster hybridization kinetics) without the competitor (M-40) and with the upper toehold competitor (UTH). With the 0A-DNA system using the lower toehold, the reaction exhibited a similarly slowed rate to that of 4A-DNA, but the overall peak height did not reach that of the upper toehold displacement reaction.

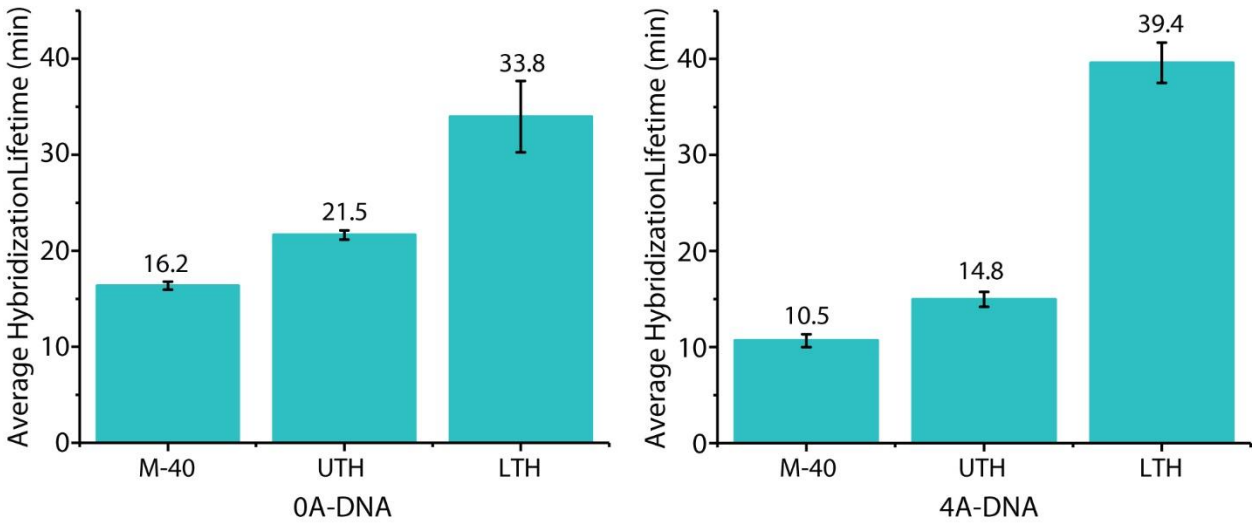

Figure 2.8. Hybridization lifetimes of toehold-mediated DNA strand displacement reactions as a function of spacer length.

2.4.5 Calibration Curves of E-DNA Sensors: Double-Layer Effects

To further illustrate the importance of double-layer effects on shorter hybridization regions, we designed an E-DNA sensor[44] with both favorable and unfavorable conditions based solely on salt concentration and hybridization site positioning relative to the electrode. The peak height current plot of different MB-10 DNA concentrations ranging from 1 nM to 160 nM is presented in **Figure 2.9**. It was observed that for a 4 nt spacer (4A-DNA) with 1.0 M salt, the peak height current increased in proportion to the concentration of MB-DNA, resulting in a curve that fist well to a Langmuir isotherm (blue curve). Data at low concentrations show good linearity (inset) in the range of 1 to 40 nM (R^2=0.979); the sensitivity (slope of best fit linear equation) was 14.0 nA nM^{-1}, and the 3σ LOD for MB-DNA was 300 pM.. By contrast, with no spacer (0A-DNA) and using 0.125M salt concentration, the sensitivity of the E-DNA sensor was only 0.0719 nA nM^{-1}, and the LOD was much worse at 40 nM. The sensitivity improvement of 4A-DNA at high salt over 0A-DNA at low salt was about 190-fold, and the LOD was improved by ~130-fold. These results, with drastically improved LOD and sensitivity, indicate that salt concentration and hybridization sites are important parameters that can be used to engineer better E-DNA sensors.

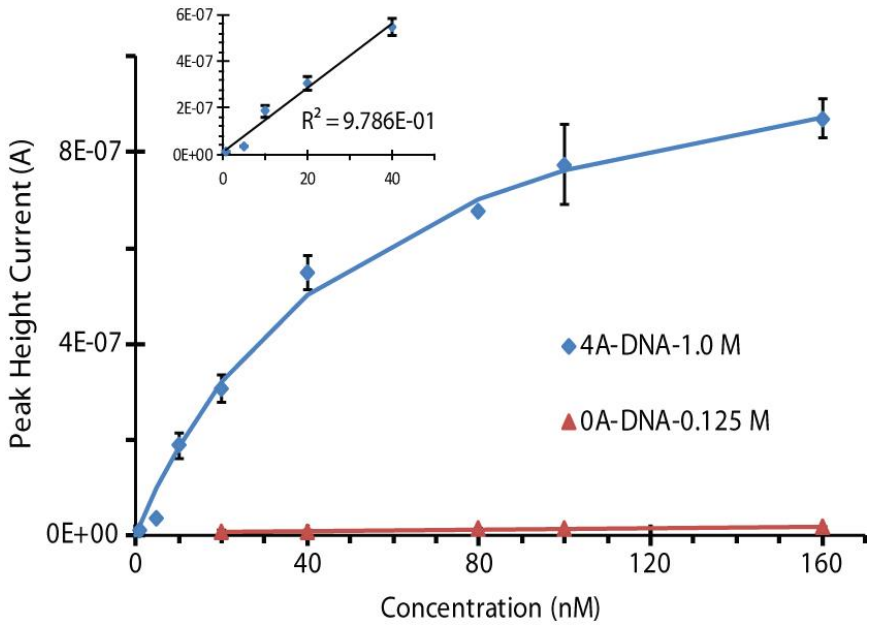

Figure 2.9. Calibration of sensors under ideal conditions (blue) with high salt and a spacer for hybridization compared to non-ideal conditions with low salt and no spacer (red). The sensitivity improvement of 4A-DNA at high salt (blue) over 0A-DNA at low salt (red) was about 190-fold, with an LOD improvement of ~130-fold. The LOD of the idealized sensor was 0.3 nM, while that under non-ideal conditions was 40 nM.

2.5 Conclusions

Since DNA plays a vital role in the E-DNA class of biosensors[44] and in various other modern electrochemical sensors [16, 19-20, 23-24, 33], an improved understanding of the kinetics of DNA hybridization at the electrode surface is crucial. In this work, we studied these kinetics using square-wave voltammetry (SWV). A 40-nucleotide (nt) thiolated-DNA was immobilized as a monolayer on a gold electrode surface, and the hybridization of a methylene blue tagged complementary target (MB-DNA) with 10 common base pairs was quantified at 5-min intervals.

Unlike in solution-based hybridization, we found surface kinetics to depend strongly on the distance between the electrode and on the binding site. As the site was positioned closer to the surface, decreases in kinetics were observed, implicating the electric double-layer as interfering with hybridization. Indeed, reduction of double-layer thickness with high ionic strength increased kinetics near the surface, and lower salt concentrations decreased kinetics, even at more distant sites. Strategically designed DNA strand displacement reactions at electrodes further validated our findings. Using toehold sites close to the electrode diminished the reaction yield, while sites further from the electrode—with the same number of base pairs—showed faster and more efficient binding. This work has important implications in DNA-based biosensors, showing that the positions of nucleic acid hybridization sites and the salt concentration should be carefully chosen.

2.6 References

1. Xiong, E.; Zhang, X.; Liu, Y.; Zhou, J.; Yu, P.; Li, X.; Chen, J., Ultrasensitive electrochemical detection of nucleic acids based on the dual-signaling electrochemical ratiometric method and exonuclease III-assisted target recycling amplification strategy. *Analytical Chemistry* **2015,** *87* (14), 7291-7296.

2. Liu, J.; Cao, Z.; Lu, Y., Functional Nucleic Acid Sensors. *Chemical Reviews* **2009,** *109* (5), 1948-1998.

3. Lu, C. H.; Yang, H. H.; Zhu, C. L.; Chen, X.; Chen, G. N., A graphene platform for sensing biomolecules. *Angewandte Chemie* **2009,** *121* (26), 4879-4881.

4. Sawyers, C. L., The cancer biomarker problem. *Nature* **2008,** *452* (7187), 548-552.

5. Smith, S. J.; Nemr, C. R.; Kelley, S. O., Chemistry-Driven Approaches to Ultrasensitive Nucleic Acid Detection. *Journal of the American Chemical Society* **2016**.

6. Sassolas, A.; Leca-Bouvier, B. D.; Blum, L. J., DNA biosensors and microarrays. *Chemical reviews* **2008,** *108* (1), 109-139.

7. Wang, H.; Wang, Y.; Liu, S.; Yu, J.; Guo, Y.; Xu, Y.; Huang, J., Signal-on electrochemical detection of antibiotics based on exonuclease III-assisted autocatalytic DNA biosensing platform. *RSC Advances* **2016,** *6* (49), 43501-43508.

8. Mahshid, S. S.; Camiré, S. b.; Ricci, F.; Vallée-Bélisle, A., A highly selective electrochemical DNA-based sensor that employs steric hindrance effects to detect proteins directly in whole blood. *Journal of the American Chemical Society* **2015,** *137* (50), 15596-15599.

9. Lubin, A. A.; Plaxco, K. W., Folding-based electrochemical biosensors: the case for responsive nucleic acid architectures. *Accounts of chemical research* **2010,** *43* (4), 496-505.

10. Hianik, T.; Wang, J., Electrochemical aptasensors–recent achievements and perspectives. *Electroanalysis* **2009,** *21* (11), 1223-1235.

11. Pellitero, M. A.; Shaver, A.; Arroyo-Currás, N., Critical Review—Approaches for the Electrochemical Interrogation of DNA-Based Sensors: A Critical Review. *Journal of The Electrochemical Society* **2020,** *167* (3), 037529.

12. Schoukroun-Barnes, L. R.; Macazo, F. C.; Gutierrez, B.; Lottermoser, J.; Liu, J.; White, R. J., Reagentless, Structure-Switching, Electrochemical Aptamer-Based Sensors. *Annual review of analytical chemistry (Palo Alto, Calif.)* **2016,** *9* (1), 163-81.

13. Arroyo-Currás, N.; Somerson, J.; Vieira, P. A.; Ploense, K. L.; Kippin, T. E.; Plaxco, K. W., Real-time measurement of small molecules directly in awake, ambulatory animals. *Proceedings of the National Academy of Sciences* **2017,** *114* (4), 645-650.

14. Li, H.; Li, S.; Dai, J.; Li, C.; Zhu, M.; Li, H.; Lou, X.; Xia, F.; Plaxco, Kevin W., High frequency, calibration-free molecular measurements in situ in the living body. *Chemical Science* **2019,** *10* (47), 10843-10848.

15. Scida, K.; Plaxco, K. W.; Jamieson, B. G., High frequency, real-time neurochemical and neuropharmacological measurements in situ in the living body. *Translational Research* **2019,** *213*, 50-66.

16. Arroyo-Currás, N.; Dauphin-Ducharme, P.; Scida, K.; Chávez, J. L., From the beaker to the body: translational challenges for electrochemical, aptamer-based sensors. *Analytical Methods* **2020,** *12* (10), 1288-1310.

17. Mahshid, S. S.; Vallée-Bélisle, A.; Kelley, S. O., Biomolecular Steric Hindrance Effects Are Enhanced on Nanostructured Microelectrodes. *Analytical Chemistry* **2017,** *89* (18), 9751-9757.

18. Zhou, W.; Mahshid, S. S.; Wang, W.; Vallée-Bélisle, A.; Zandstra, P. W.; Sargent, E. H.; Kelley, S. O., Steric Hindrance Assay for Secreted Factors in Stem Cell Culture. *ACS sensors* **2017,** *2* (4), 495-500.

19. Somasundaram, S.; Easley, C. J., A Nucleic Acid Nanostructure Built through On-Electrode Ligation for Electrochemical Detection of a Broad Range of Analytes. *Journal of the American Chemical Society* **2019,** *141* (29), 11721-11726.

20. Das, J.; Gomis, S.; Chen, J. B.; Yousefi, H.; Ahmed, S.; Mahmud, A.; Zhou, W.; Sargent, E. H.; Kelley, S. O., Reagentless Biomolecular Analysis Using a Nanoscale Molecular Pendulum. *bioRxiv* **2020**, 2020.04.02.020453.

21. Parolo, C.; Idili, A.; Ortega, G.; Csordas, A.; Hsu, A.; Arroyo-Currás, N.; Yang, Q.; Ferguson, B. S.; Wang, J.; Plaxco, K. W., Real-Time Monitoring of a Protein Biomarker. *ACS Sensors* **2020,** *5* (7), 1877-1881.

22. Shaver, A.; Curtis, S. D.; Arroyo-Currás, N., Alkanethiol Monolayer End Groups Affect the Long-Term Operational Stability and Signaling of Electrochemical, Aptamer-Based Sensors in Biological Fluids. *ACS Applied Materials & Interfaces* **2020,** *12* (9), 11214-11223.

23. Hu, J.; Wang, T.; Kim, J.; Shannon, C.; Easley, C. J., Quantitation of Femtomolar Protein Levels via Direct Readout with the Electrochemical Proximity Assay. *Journal of the American Chemical Society* **2012,** *134* (16), 7066-7072.

24. Hu, J.; Yu, Y.; Brooks, J. C.; Godwin, L. A.; Somasundaram, S.; Torabinejad, F.; Kim, J.; Shannon, C.; Easley, C. J., A reusable electrochemical proximity assay for highly selective, real-time protein quantitation in biological matrices. *Journal of the American Chemical Society* **2014,** *136* (23), 8467-8474.

25. Vallée-Bélisle, A.; Ricci, F.; Uzawa, T.; Xia, F.; Plaxco, K. W., Bioelectrochemical switches for the quantitative detection of antibodies directly in whole blood. *Journal of the American Chemical Society* **2012,** *134* (37), 15197-15200.

26. Zhang, H.; Li, X.-F.; Le, X. C., Binding-induced DNA assembly and its application to yoctomole detection of proteins. *Analytical chemistry* **2011,** *84* (2), 877-884.

27. Liu, S.; Fang, L.; Wang, Y.; Wang, L., Universal Dynamic DNA Assembly-Programmed Surface Hybridization Effect for Single-step, Reusable, and Amplified Electrochemical Nucleic Acid Biosensing. *Analytical Chemistry* **2017**.

28. White, R. J.; Plaxco, K. W., Engineering New Aptamer Geometries for Electrochemical Aptamer-Based Sensors. *Proceedings of SPIE--the International Society for Optical Engineering* **2009,** *7321*, 732105.

29. White, R. J.; Phares, N.; Lubin, A. A.; Xiao, Y.; Plaxco, K. W., Optimization of Electrochemical Aptamer-Based Sensors via Optimization of Probe Packing Density and Surface Chemistry. *Langmuir : the ACS journal of surfaces and colloids* **2008,** *24* (18), 10513-10518.

30. Ricci, F.; Zari, N.; Caprio, F.; Recine, S.; Amine, A.; Moscone, D.; Palleschi, G.; Plaxco, K. W., Surface chemistry effects on the performance of an electrochemical DNA sensor. *Bioelectrochemistry (Amsterdam, Netherlands)* **2009,** *76* (0), 10.1016/j.bioelechem.2009.03.007.

31. Kang, D.; Ricci, F.; White, R. J.; Plaxco, K. W., Survey of Redox-Active Moieties for Application in Multiplexed Electrochemical Biosensors. *Analytical Chemistry* **2016,** *88* (21), 10452-10458.

32. Sykes, K. S.; Oliveira, L. F. L.; Stan, G.; White, R. J., Electrochemical Studies of Cation Condensation-Induced Collapse of Surface-Bound DNA. *Langmuir* **2019,** *35* (40), 12962-12970.

33. Dauphin-Ducharme, P.; Plaxco, K. W., Maximizing the Signal Gain of Electrochemical-DNA Sensors. *Analytical Chemistry* **2016,** *88* (23), 11654-11662.

34. Gao, Y.; Wolf, L. K.; Georgiadis, R. M., Secondary structure effects on DNA hybridization kinetics: a solution versus surface comparison. *Nucleic acids research* **2006,** *34* (11), 3370-3377.

35. Fish, D. J.; Horne, M. T.; Brewood, G. P.; Goodarzi, J. P.; Alemayehu, S.; Bhandiwad, A.; Searles, R. P.; Benight, A. S., DNA multiplex hybridization on microarrays and thermodynamic stability in solution: a direct comparison. *Nucleic Acids Research* **2007,** *35* (21), 7197-7208.

36. Vainrub, A.; Montgomery Pettitt, B., Surface electrostatic effects in oligonucleotide microarrays: control and optimization of binding thermodynamics. *Biopolymers* **2003,** *68* (2), 265-270.

37. Zadeh, J. N.; Steenberg, C. D.; Bois, J. S.; Wolfe, B. R.; Pierce, M. B.; Khan, A. R.; Dirks, R. M.; Pierce, N. A., NUPACK: analysis and design of nucleic acid systems. *Journal of computational chemistry* **2011,** *32* (1), 170-173.

38. Xiao, Y.; Lai, R. Y.; Plaxco, K. W., Preparation of electrode-immobilized, redox-modified oligonucleotides for electrochemical DNA and aptamer-based sensing. *Nature protocols* **2007,** *2* (11), 2875-2880.

39. Fiche, J. B.; Buhot, A.; Calemczuk, R.; Livache, T., Temperature Effects on DNA Chip Experiments from Surface Plasmon Resonance Imaging: Isotherms and Melting Curves. *Biophysical Journal* **2007,** *92* (3), 935-946.

40. Stojek, Z., The electrical double layer and its structure. In *Electroanalytical methods*, Springer: 2010; pp 3-9.

41. Huang, K.-C.; White, R. J., Random walk on a leash: a simple single-molecule diffusion model for surface-tethered redox molecules with flexible linkers. *Journal of the American Chemical Society* **2013,** *135* (34), 12808-12817.

42. Zhang, D. Y.; Winfree, E., Control of DNA Strand Displacement Kinetics Using Toehold Exchange. *Journal of the American Chemical Society* **2009,** *131* (47), 17303-17314.

43. Li, F.; Tang, Y.; Traynor, S. M.; Li, X.-F.; Le, X. C., Kinetics of Proximity-Induced Intramolecular DNA Strand Displacement. *Analytical Chemistry* **2016,** *88* (16), 8152-8157.

44. Ricci, F.; Plaxco, K. W., E-DNA sensors for convenient, label-free electrochemical detection of hybridization. *Microchimica Acta* **2008,** *163* (3), 149-155.

Chapter 3

A Nucleic Acid Nanostructure Based Electrochemical Sensor for Quantifying the Peptide Drug, Exendin-4

3.1 Introduction

Peptides play significant roles as selective and efficient signaling molecules by binding to specific cell surface receptors and triggering intracellular effects.[1] In recent years, use of peptides as therapeutic agents has increased substantially owing to their high potency and selectivity, tolerability, and safety profiles in humans.[2-4] Also, secretion of endogenous peptides such as peptide hormones and cytokines are monitored for diagnostic purposes.[5-7] It is therefore essential to have a sensitive, specific, and accurate method for the determination and quantification of peptide therapeutics and cell secreted bioactive peptides. To date, various methods have been developed for the quantification of peptides, such as chromatographic assays (HPLC/MS/MS), electrophoretic immunoassays, radioimmunoassays (RIA), and enzyme linked immunosorbent assay (ELISA).[8-12] However, sophisticated instrumentation and high cost limit the application of chromatographic or electrophoretic methods in routine analysis. While ELISA is the classical analytical approach due to its high sensitivity and throughput capacity, it often suffers from poor repeatability and specificity, as well as interferences from endogenous substances[13], and the ELISA workflow is prohibitive for certain applications.[14] RIA has similar issues and also requires radioactively labeled antigens which introduce a radiation hazard. Moreover, these methods are expensive, time consuming, and requires professional personnel, therefore, hinders them from being point-of-care assays.

Diabetes is a complex endocrine metabolic disease and considered to be a global health care problem.[15] Diabetes arises due to insulin deficiency (type 1 diabetes) or insulin resistance (type 2 diabetes), and it is associated with impaired secretion of peptides from islets.[16] Exendin-4 is a human glucagon-like peptide-1 (GLP-1) agonist with a molecular weight of 4.2 kDa, and it was originally isolated from the venom of *Heloderma suspectum* gila monster.[17] Exenatide, a synthetic version of exendin-4 was approved by the U.S. Food and Drug Administration in 2005 for the adjunctive treatment of patients with type 2 diabetes.[18] Exenatide regulates glucose metabolism and insulin secretion by increasing glucose-dependent insulin secretion and suppressing elevated postprandial glucagon secretion.[19] Due to the narrow therapeutic range (0.1 to 24 nM), monitoring the blood concentration of exendin-4 is crucial for formulation optimization in order to achieve its efficacy and to assess disease progression. Development of an electrochemical (EC) biosensor for exendin-4 quantification could therefore make an immediate impact on human health monitoring.

In our recent work, we reported a highly sensitive and versatile DNA nanostructure probe for the quantification of a wide range of analytes including small molecules and large antibodies.[20] While the novel DNA nanostructure-based assay format is theoretically suitable for the detection and quantification of a variety of peptides, this version of the sensor has yet to be demonstrated. In principle, this sensor should be able to directly quantify any peptide, provided that the relevant peptide can be conjugated to the DNA nanostructure and that it has a large enough binding partner. In this work, we applied our DNA nanostructure sensor architecture[20] to directly quantify exendin-4, which has not previously been measured using direct electrochemical readout, and we show that the sensor is functional in human serum.

3.2 Reagents and Materials

All solutions were prepared with deionized, ultra-filtered water (Fisher Scientific). The following reagents were used as received: 4-(2-hydroxyethyl)-1-piperazineethanesulfonic acid (HEPES), magnesium chloride hexahydrate from OmniPur, sodium chloride from BDH. Tris-(2-carboxyethyl) phosphine hydrochloride (TCEP), mercaptohexanol (MCH), gold etchant, and chromium etchant were from Sigma-Aldrich. Gold-sputtered on glass (GoG) (Au 100 nm with Cr adhesion layer 5 nm) was purchased from Deposition Research Lab, Inc (St. Charles, MO) with dimensions of 25.4 mm x 76.2 mm x 1.1 mm. AZ 40XT (positive thick photoresist) and AZ 300 MIF developer were obtained from Microchemicals, polydimethylsiloxane (PDMS) from Dow Corning, and dimethyl sulfoxide (DMSO) from Anachemia. Exendin-4 was purchased from LifeTein, Anti-Exendin-4 antibody from Abcam, protein-oligo conjugation kit from Solulink, and 2kD molecular weight cut off (MWCO) Vivacon® 500 centrifugal concentrators from Vwr. Custom, methylene blue-conjugated DNA (MB-DNA) was purchased from Biosearch Technologies (Novato, CA), purified by RP-HPLC. Thiolated DNA was obtained from Integrated DNA Technologies (IDT; Coralville, Iowa), with purity confirmed by mass spectroscopy. T4 DNA ligase (400,000 units) and adenosine triphosphate (ATP, 10 mM) were from New England Biolabs. Prescreened human serum samples were acquired from BioreclamationIVT. Sequences of DNAs used in this work are listed in **Table 3.1**.

Table 3.1: Single-Stranded DNA Sequences Used in Nanostructure Construction

Sequence Name	Abbreviation	DNA sequence, listed 5′ to 3′
Thiolated DNA	thio-DNA	**/5Phos/** CTG TGC AAG AAC TCA CAG CCT CAC CTC TTC CTA AAA A **/3ThioMC3-D/**
Anchor connector DNA	anchor-DNA	**/5Phos/** GAG ACA CTG TGT CGT CTC CGG TTG AAG TGG AGA **/iAmMC6/** TAG GAA GAG GTG AGG
Methylene Blue DNA	MB-DNA	**/dT MB/** CTC CAC TTC AAC CG

Abbreviations: /5phos/ = Phosphorylation (IDT), /3ThioMC3-D/ = Dithiol attachment (IDT), /iAmMC6/ = Intermediate Amine (IDT), /dT MB/ = Methylene Blue modification (Biosearch).

3.3 Experimental Methods

3.3.1 Preparation of Gold Electrodes

The photomask of electrode design used in the experiment was designed in Adobe Illustrator, and files were sent to Fineline Imaging (Colorado Springs, Colorado) for printing a positive photomask. **Figure 3.1A** shows the mask design. In total, eighteen independent 2-mm diameter gold working electrodes were prepared in one microscope slide using this mask. Using AZ 40XT photoresist, standard photolithographic procedure was followed to make the photoresist pattern on the gold-on-glass slide (GoG). Then the GoG was introduced into gold enchant followed by chromium etchant for 30 s and 15 s, respectively. In this way, gold and chromium which was not blocked by AZ photoresist was removed, resulting in gold electrodes defined by the mask design. Heating this electrode patterned GoG in DMSO at 110 °C for 30 min removed the positive photoresist layer from the gold. The GoG electrodes were rinsed with deionized water followed by ethanol and dried with nitrogen.

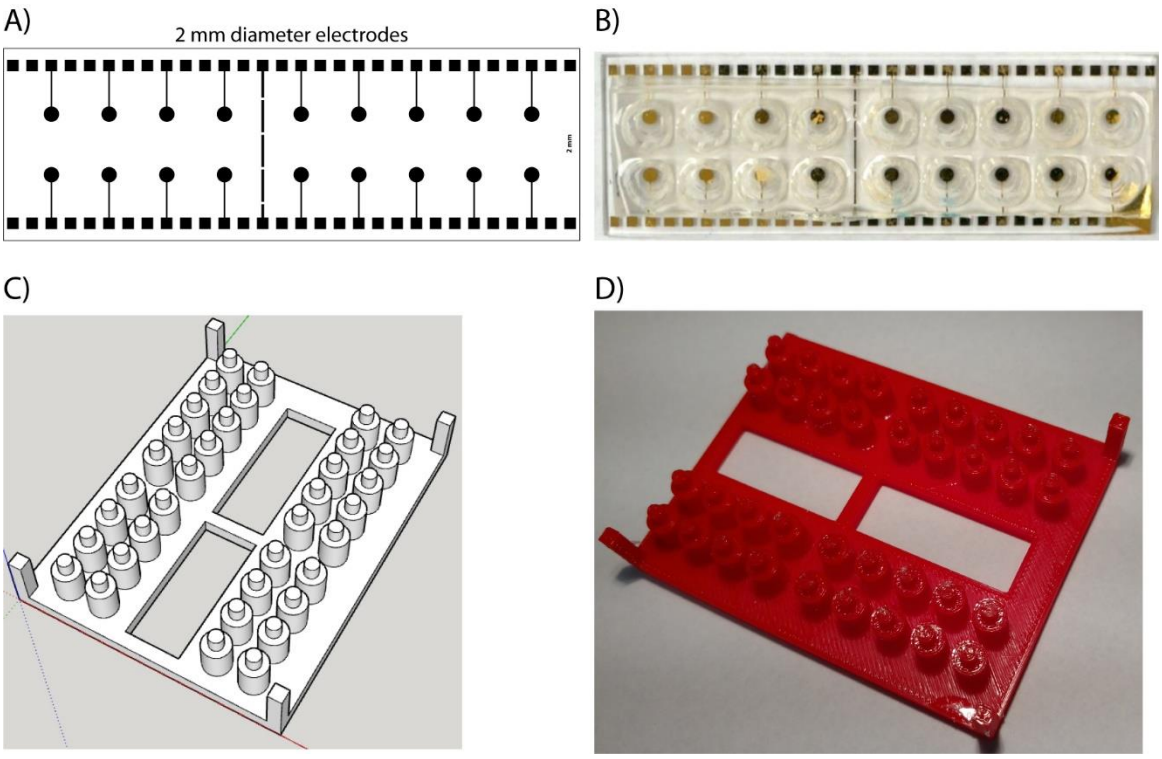

Figure 3.1. A) Photomask design used for gold-on-glass (GoG) preparation. There are in total eighteen 2 mm diameter electrodes in one microscope slide. **B)** Photo of assembled device. **C)** 3D CAD of the master to prepare electrochemical cells. **D)** 3D-printed PLA used for molding PDMS electrochemical cells

3.3.2 Preparation of PDMS Electrochemical Cells

To form the electrochemical cell, custom PDMS reservoirs were bonded to the GoG slide. A 3D computer animated design (CAD) file was designed in Sketchup© (Trimble Navigation Limited), and a Makerbot Replicator 2 (200 µm layer resolution in the z-direction) with Hatchbox's polylactic acid filament (PLA, 1.75 mm diameter) was used to print the 3D mold. The 3D CAD depiction and an example of a printed template is shown in **Figure 3.1B** and **3.1C**. The PDMS and curing agent were mixed in the standard 10:1 ratio and poured onto a silicon wafer,

and this assembly was placed of on flat surface for overnight curing at 60 °C with the 3D-printed template in place (care must be taken to keep below the glass transition temperature of PLA, which is 60 – 65 °C). With one template, 36 electrochemical cells could be made in one cycle, and a single template could be used multiple times. Once the curing process was complete, the template was removed, and the template PDMS was sliced to the desired shape, sonicated in methanol for 20 min to quench any leftover curing agent, and placed in an oven at 100 °C for a minimum of two hours. This PDMS was irreversibly bonded by plasma oxidation to the GoG slide to form the electrochemical cell. Each electrode was placed in an individual electrochemical cell of ~100 µL volume. Therefore, with one microscopic slide, eighteen different samples could be tested.

3.3.3 DNA Monolayer Assembly

Electrodes were cleaned with piranha solution prior to plasma oxidation of the electrochemical cell. The piranha solution (H_2SO_4:H_2O_2, 3:1) was freshly prepared and dropped onto the surface of the electrode for 1 minute, and later the electrodes was rinsed with deionized water. Since IDT recommended to reduce the dithiol bond prior to usage, the thio-DNA was reduced by adding a reducing agent, TCEP. To reduce 1 µL of 200 µM thio-DNA, 3 µL of 10 mM TCEP was mixed and incubated at room temperature in the dark for 1 hour. The solution was then diluted to a final thio-DNA concentration of 30 nM using buffer solution (10 mM HEPES with 10 mM $MgCl_2$ at pH 7). To form the initial DNA monolayer, 100 µL of thio-DNA was introduced into each electrochemical cell and incubated for 2 hours at room temperature. Then electrode was then rinsed, and 3 mM MCH in buffer was introduced into electrochemical cell and incubated for 1 hour. Then the electrochemical cell was filled with buffer including 0.1 % BSA (for PDMS

surface passivation) and incubated for 1 hour at room temperature. After this step, the electrode could be rinsed and stored at 4 °C in buffer for up to a week before use.

3.3.4 Bioconjugation of Exendin-4 and Anchor-DNA

Amino Oligo Modification With Succinimidyl 4-Formylbenzoate (S-4FB)

The oligo desalting spin column was prepared by using 0.5 mL 7kD molecular weight cut off Zeba desalting column with 1x modification buffer. Briefly, the spin column was placed in a 2.0 mL microcentrifuge collection tube and centrifuged at 1,500*g* for 1 minute to remove storage solution. Later, 300 µL of 1x modification buffer was added to the center of the resin bed and centrifuged at 1,500*g* for 1 minute to prepare the oligo desalting spin column. 100 µL of 21 µM oligo solution was then added slowly into the center of the resin bed and centrifuged at 1,500*g* for 2 minutes to collect the desalted oligo. 30 µL of DMF and 20.5 µL of S-4FB reagent (Solulink kit) was then added to 60 µL of the desalted oligo and vigorously vortexed to mix. This oligo-modification reaction mixture was incubated at room temperature for 2 hours followed by centrifugation at 15,000*g* for 2 minutes to pellet any insoluble reaction by-products. In order to remove excess S-4FB from the modified oligo solution, the reaction mixture was centrifuged at 1,500*g* for 2 minutes using a 0.5 mL Zeba column with 1x conjugation buffer.

Exendin-4 Modification With Succinimidyl 6-hydrazinonicotinate acetone hydrazone (S-HyNic)

The peptide desalting spin column was prepared by using a 2kD molecular weight cut off filtration spin column with 1x modification buffer. 90 µL of 1.6 mM exendin-4 was centrifuged at 14,000*g* for 15 minutes followed by a reverse spin at 2,500*g* to collect the concentrated peptide. 70 µL of 1x modification buffer and 5 µL of S-HyNic reagent Solulink) was then added to 20 µL of the concentrated peptide and incubated at room temperature in the dark for 3 hours. Later, the HyNic-modified peptide was desalted using a Zeba column with 1x conjugation buffer.

On-electrode Surface Bioconjugation

HyNic-modified exendin-4 was diluted to final concentration of 8 µM with 1x conjugation buffer and 10x turboLink catalyst buffer. The DNA nanostructure was then constructed on the electrode surface following the protocol in Section 3.3.5 (below), with 100 nM of S-4FB-modified anchor-DNA. Later, 20 µL of 8 µM HyNic-modified exendin-4 was introduced into each electrochemical cell and incubated for 3 hours at room temperature. Then the electrode was rinsed and incubated with measurement buffer (10 mM HEPES with 0.5 M NaCl at pH 7, including 0.1 % BSA) for at least 30 minutes.

Solution Bioconjugation

The peptide-oligo conjugate was alternatively prepared in free solution by mixing 1.5 µL of 10 µM S-4FB-modified anchor-DNA, 2 µL of 160 µM HyNic-modified exendin-4, 4.5 µL of

1x conjugation buffer, and 2 µL of 10x turboLink catalyst buffer. The mixture was incubated overnight at 4 °C. Later, the DNA nanostructure was constructed on the electrode surface following the protocol in Section 3.3.5 (below), with 100 nM exendin-4 conjugated anchor-DNA.

3.3.5 DNA Nanostructure Construction by On-Electrode Enzymatic Ligation

Once the electrode was ready for construction, a mixture containing 100 nM of anchor-DNA (from Section 3.3.4 above), 100 nM MB-DNA, 1.0 mM ATP, and 1.0 µL of 400,000 U T4 DNA ligase was prepared in HEPES buffer (10 mM HEPES with 10 mM $MgCl_2$ at pH 7). 100 µL of this mixture was introduced into the electrochemical cell, wrapped in parafilm, and incubated for 6 hours at room temperature. Then the electrode was rinsed with deionized water to remove enzymes and excess DNAs. Later, the electrode was incubated with the measurement buffer (10 mM HEPES with 0.5 M NaCl at pH 7, including 0.1 % BSA) for at least 30 minutes.

3.3.6 Electrochemical Measurements

Electrochemical measurements were performed using a Gamry Reference 600 potentiostat. Once the electrode was ready to measure, the silver/silver chloride (3 M KCl) reference electrode (BASi) and platinum counter electrode (CH instruments) were introduced into the electrochemical cell. Square-wave voltammagrams were measured from -0.425 to 0 V (versus reference electrode) with a step size of 1 mV, a pulse height of 25 mV, and a SWV frequency of 100 Hz.

3.3.7 Anti-exendin-4 Antibody Detection

Once the DNA nanostructure was constructed with the exendin-4-DNA conjugate as theanchor recognition unit, the electrode was ready for initial SWV measurement in measurement buffer of 100 µL volume. 100 nM of anti-exendin-4 (antibody) was prepared in measurement buffer. The electrochemical cell was emptied, and 20 µL of anti-exendin-4 was introduced into the cell and incubated at room temperature for 1 hour. Then the sample was removed, and a final measurement was done in 100 µL of the same buffer.

3.3.8 Optimization of Anti-exendin-4 Antibody Concentration

SWV measurement was made in 100 µL measurement buffer every 10 min for 30 min. Later, the buffer was removed, 5 nM of 100 µL anti-exendin-4 antibody was added, and the measurements were continued for another 30 min. At the 60 min time point, antibody solution was removed, and 100 µL of 10 nM of antibody was added. In this manner, titration was continued with 25, 50, 75, and 100 nM antibody solution for total of 210 min. Signal suppression was compared with respect to signal at the 10 min measurement point.

3.3.9 Exendin-4 Quantification

Once the DNA nanostructure was constructed, initial SWV measurement was made in 100 µL measurement buffer. Exendin-4 was quantified by a two-step process, where anti-exendin-4 antibody was pre-incubated with target followed by dropping the mixture onto the sensor surface. 10 nM antibody was mixed with varying exendin-4 analyte concentrations (total volume was 100

μL) and incubated at 37 °C for 30 min. To have a better understanding of the binding kinetics, SWV was conducted every 3 minutes. At 15 min, the buffer was removed, target antibody mixture (100 μL) was added, and the measurements were continued every 3 min for a total of 75 min.

3.3.10 Measurement in Human Serum

Small volumes of exendin-4 and anti-exendin-4 antibody were spiked into human serum resulting in 98% serum with analyte. For a negative control (serum without exendin-4) only anti-exendin-4 antibody was spiked, giving 99% serum. Any of these samples to be measured were incubated at 37 °C for 30 min. The initial SWV protocol was carried out, followed by addition of pre-incubated mixtures (100 μL) into the cell, then incubation for 60 min. Finally, the serum mixture was removed, measurement buffer was introduced, and a final measurement was done. The same SWV parameters were used as mentioned above.

3.3.11 Data Analyses

Peak Height

SWV raw data (including V_{step} and I_{diff}) was transferred to Microsoft Excel, and a 9-point moving average was applied. To remove capacitance current, a third-order polynomial baseline was calculated using the "Linest" function in EXCEL. Data points from -0.421 to -0.358 V and -0.140 to -0.005 V were used in this calculation. The calculated baseline was subtracted from the raw data. An example was shown in **Figure 3.2**. The maximum current from the difference graph (not shown) was used as the peak height.

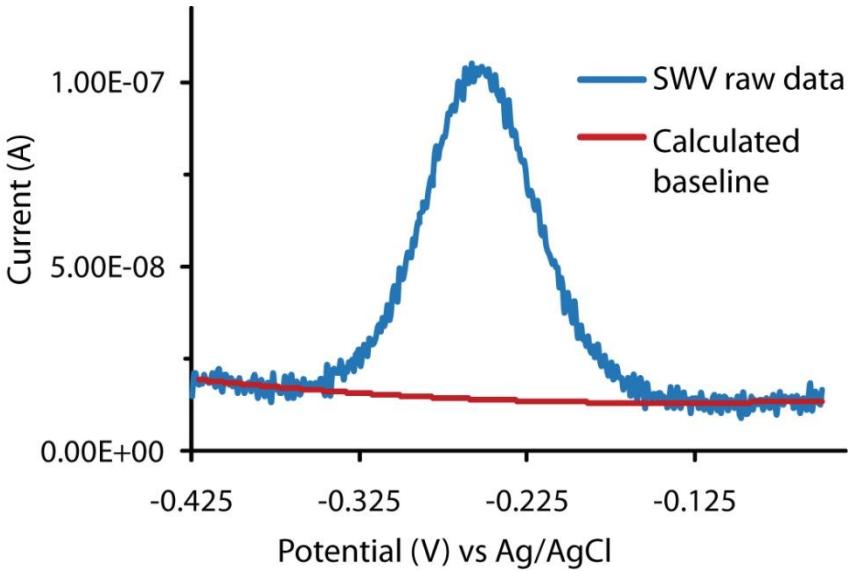

Figure 3.2. Example MB-DNA redox current sampled during SWV (raw data) along with the calculated baseline curve used for Faradaic current extraction. The maximum current from the difference curve (not shown here) was used as the peak height of each individual measurement.

Average Distance Between Nanostructures

The number of moles of nanostructure, N_{tot}, was determined using a previously established relationship[21-22] using the following relationship,

$$i_p = 2nfFN_{tot} \times \frac{sinh\left(\frac{nFE}{RT}\right)}{cosh\left(\frac{nFE}{RT}\right) + 1}$$

where i_p is the peak height of the current measurement, n is the number of electrons transferred per redox event (with MB label, n = 2), F is the Faraday constant, R is the universal gas constant, T is the temperature, E is the applied voltage amplitude, and f is the SWV frequency. We assumed that electron transfer only takes place between MB and the electrode surface upon formation of the nanostructure, based on earlier results that show the MB to be washed away without correct

formation.[20] The number of nanostructure moles was divided by the electrode surface area to obtain the nanostructure surface density in units of mol cm^{-2}. By reversing the value of density (strands cm^{-2}), a circular area around each DNA-nanostructure was estimated, and the distance between nanostructures was then calculated from the diameter of this circle.

Signal Suppression

The following equation was used to calculate signal suppression, where i_p *(initial)* is the peak height of the initial current measurement (before target incubation) and i_p *(final)* is the peak height of the final current measurement (after target incubation).

$$\boldsymbol{Signal\ Suppression}\ (\%) = -\mathbf{100} \times \frac{\boldsymbol{i_p\ (final)} - \boldsymbol{i_p\ (initial)}}{\boldsymbol{i_p\ (initial)}}$$

3.4 Results and Discussion

In our previous work, a DNA-based assembly was enzymatically constructing directly onto the electrode surface, resulting in a versatile electrochemical biosensor system.[20] The nanostructure, a single DNA molecule that includes both an electrochemical label and a binding moiety, is stabilized with both labels at a fixed distance from the surface. Our current understanding suggests that the nanostructure undergoes a change in mass upon target binding, possibly with some added steric hindrance of movement, both of which will alter the tethered-diffusion[23] of the MB label that is reported as a signal change at specific SWV frequencies. In this work, the novel DNA nanostructure-based assay format is applied for the detection and quantification of exendin-4. The peptide itself serves as the anchor-binding moiety in the anchor-DNA strands, facilitated by the

synthesis of novel exendin-4-nanostructure conjugates (peptide-DNA conjugates). As shown by the schematic in **Figure 3.3**, initially the DNA nanostructure modified with exendin-4 has faster tethered diffusion, which slows by binding of exendin-4 antibodies, resulting in higher signal suppression. This effect can be blocked through a competitive assay workflow, where preincubation of the antibodies with exendin-4 (analyte) in solution leads to reduction in concentration of antibody-nanostructure complex on the surface, and less signal suppression is observed in proportion to the analyte concentration.

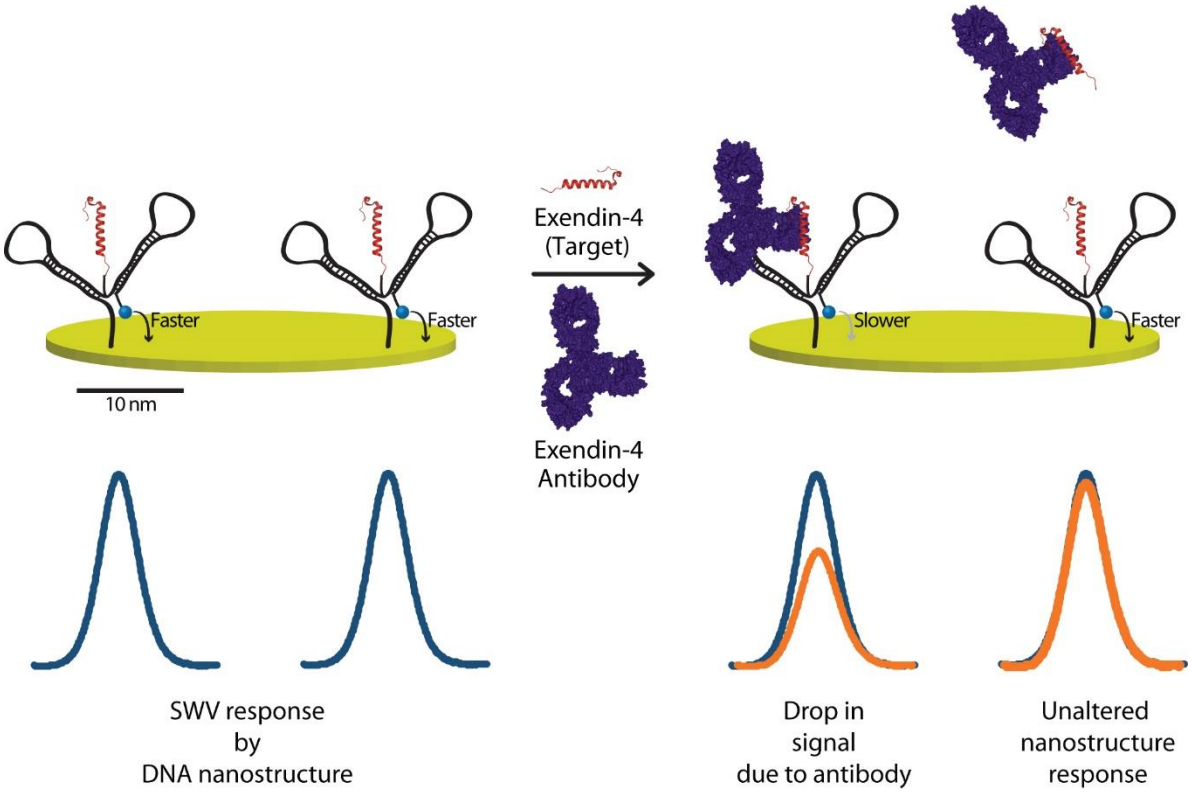

Figure 3.3. Faster diffusion of exendin-4-nanostructure conjugates is hindered by exendin-4 antibodies, and the SWV current change is proportional to antibody concentration. For the peptide assay format, this effect can be blocked using a competitive assay workflow, resulting in SWV current change that proportional to exendin-4 concentration.

3.4.1 Surface Bioconjugation

Commercial solid-phase synthesis, the conventional method to achieve various oligonucleotide bioconjugates, is expensive and can result in very low yields. For instance, in our prior work the cost for tacrolimus-modified DNA anchor was 4,950 USD for 10.29 nmol, which was 481 USD $nmol^{-1}$.[20] As an alternative, there are commercial kits for protein-oligo or peptide-oligo conjugations. In this work, exendin-4 was attached to an amine-modified anchor-DNA using a SoluLink protein-DNA conjugation kit through three easy-to-perform steps (**Figure 3.4A**). Initially, exendin-4 was modified with S-HyNic to incorporate HyNic groups, and anchor-DNA was modified with 4FB cross linker to activate the amine for bioconjugation. Reaction of the two modified biomolecules resulted in the formation of a conjugate bond which is stable to 92 °C and over a range of pH from 2.0-10.0. One major advantage of this method is the mild reaction conditions that do not require metals or oxidation or reducing reagents, thus bioconjugation should not result in loss of binding to the antibody used for EC detection. Furthermore, this technology can feasibly be employed to append a variety of peptides or antibody binding epitopes of any protein with the anchor DNA to allow quantification of the relevant analyte or to promote assay multiplexing.

We initially performed bioconjugation directly on the electrode surface onto already-formed nanostructures, which allows washing away of unused reagents and helps avoid affinity purification steps. The DNA nanostructure was first constructed on the electrode surface using our previous on-electrode ligation method[20], followed by conjugation of exendin-4 to the amine-modified anchor-DNA to create exendin-4 modified nanostructures. First, for building the nanostructure, thio-DNA was immobilized on the gold electrode in a self-assembled monolayer. Later, the anchor-DNA and MB-DNA were introduced into the electrochemical cell and

enzymatically ligated on the electrode. After construction, unreacted strands and enzymes were washed away from surface-immobilized nanostructure on the electrode. First, the nanostructure's current was measured as a blank; then, 20 µL of exendin-4 conjugation solution was incubated on the electrode. The electrode was rinsed to remove unreacted exendin-4, and current was measured again. **Figure 3.4B** depicts the signal response of exendin-4 modified and unmodified nanostructure.

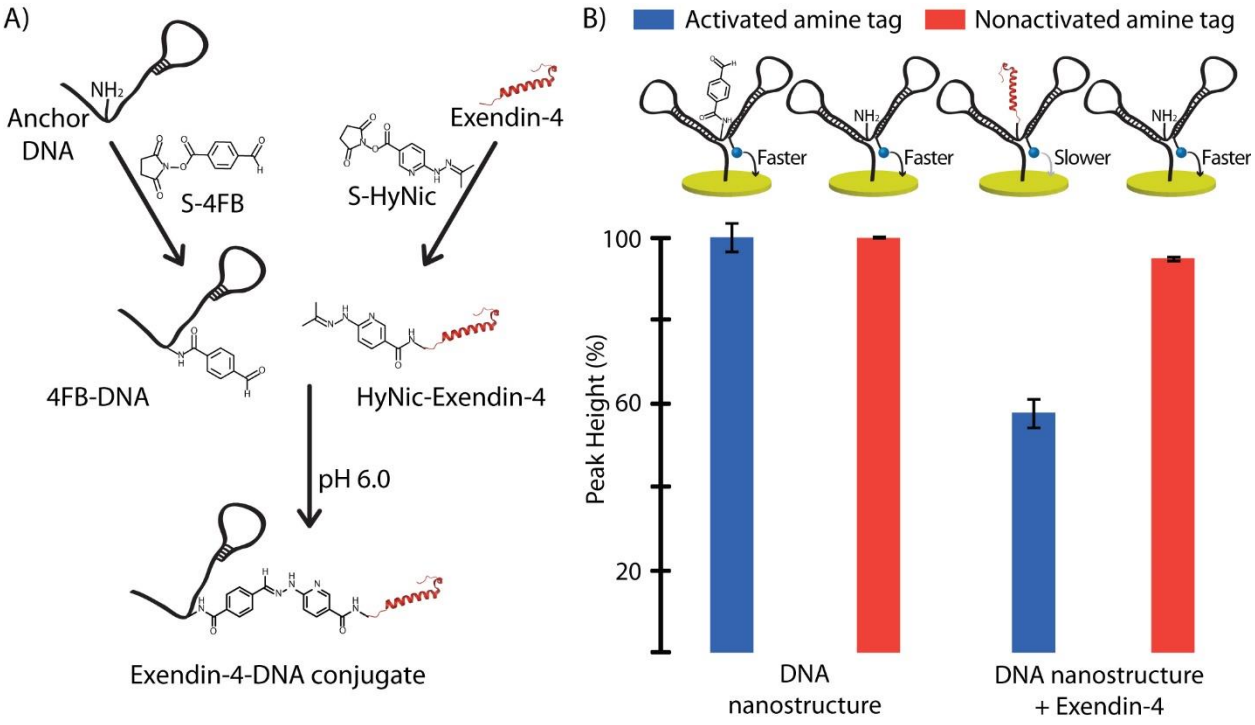

Figure 3.4. A) Oligomer-exendin-4 bioconjugation. Amine tagged DNA was attached to the N-terminus of the peptide through a conjugation reaction. **B)** Activated amine tagged nanostructure showed higher drop in signal (blue bars) compared to nonactivated nanostructure (red bars), confirming bioconjugation.

In the absence of activated amine, formation of a conjugate bond between the anchor-DNA and exendin-4 could not take place, and only a 6% suppression of the initial signal was observed (red bars). In contrast, we observed a 42% drop in the peak height after conjugation (blue bars), indicating that the tethered diffusion of the redox molecule is slowed by exendin-4 attachment, suggesting successful bioconjugation on the electrode surface. However, follow-up studies showed that these exendin-4 modified nanostructures –made by surface conjugation—exhibited only a slight change in response to exendin-4 antibody addition. Our hypothesis for this lack of signal change is based on the multivalency of the surface (**Figure 3.5**), which we discuss in further detail below.

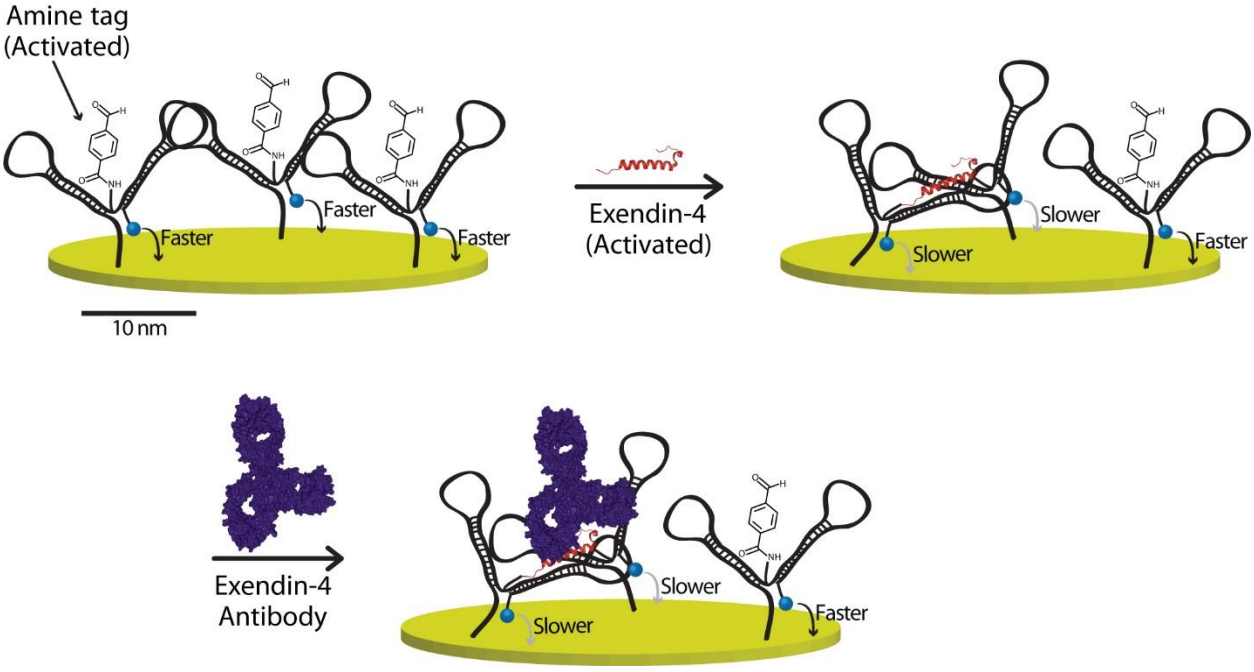

Figure 3.5. Multivalent surface conjugation could result from multiple lysine or arginine residues in the peptide sequence, which would blunt antibody induced changes in signal.

Ideally, the bioconjugation takes place at the N-terminal residues on the peptide, making 1:1 peptide-nanostructure conjugates at electrode surfaces that have predictable surface structures. However, when peptides comprise lysine or arginine residues which incorporate amine groups, it is possible that on-electrode conjugation will result in multivalent conjugates, where the peptide is attached to multiple DNA nanostructures (**Figure 3.5**). Multivalency of surface conjugation would result in large decrease in current after conjugation, but it would blunt antibody-induced changes in signal during sensor tests. Indeed, exendin-4 has two lysine residues (positions 12 and 27 of 39-AA peptide) and one arginine residue (position 20). Therefore, multivalency of surface conjugation could result in restricted nanostructures (**Figure 3.5**, right side), which would give exendin-4 modified nanostructures that exhibit a large decrease in current after conjugation but that were nonresponsive to antibody addition. Our data collected using the surface conjugation approach agrees with this hypothesis.

It should also be noted that the nanostructure distribution represented in **Figure 3.5** was intentionally depicted to-scale, to our best approximation, which is why a scale bar is included. Molecular sizes and lengths for DNA, peptides, and antibodies were based on structural data from The Protein Data Bank (https://www.rcsb.org/), and nanostructure density on the electrode surface was based on our measurement of the number of moles of nanostructure, N_{tot}, using methodology described previously.[21-22] In particular, the average distance between nanostructures was measured to be 27 nm (see Section 3.3.11), and of course a range of distances around this value would be expected. These structural data prove the feasibility of our hypothesis as shown in **Figure 3.5**. Further, because multivalency could significantly enhance the reaction rate of the bioconjugation, it is likely that these multivalent conjugates would be more prevalent than the monovalent

counterparts. Lastly, this hypothesis is further confirmed by the fact that solution-phase bioconjugation was able to resolve the issue of multivalency.

3.4.2 Solution Bioconjugation

To minimize the effect of multivalency, we modified the protocol to a free solution conjugation followed by surface ligation; details are included in Sections 3.3.4 and 3.3.5. After this change, the final sensor was functional, exhibiting a 54.5% reduction in the SWV current when the exendin-4 antibody (100 nM) was added to the electrode. This result provides confirmation that there was a problem with the on-electrode peptide-oligo conjugation. Ultimately, we show here that exendin-4-anchor-DNA conjugates should be synthesized in free solution first then enzymatically ligated into the nanostructure on the electrode surface. If sensor fabrication is carried out this way, the antibody can bind to the exendin-4 modified nanostructure and reduce current in SWV measurements as intended.

After confirming antibody-induced decreases in tethered diffusion of the nanostructure, we hypothesized that this effect could be blocked by preincubating the antibodies with exendin-4 (analyte) followed by adding the mixture onto the electrode surface. In other words, we hypothesized that our nanostructure could be used for a competitive electrochemical immunoassay for exendin-4 quantification. The applicability of this sensing system will be limited by the preincubation antibody concentration, therefore this value should be optimized. Since antibodies has two binding sites, at high antibody concentration one of the binding sites may remain available for the surface, leading to saturation of the surface and complete signal loss. On the contrary, low antibody concentration would result in minimum signal drop even in the absence of target exendin-

4, which would be detrimental to the sensitivity of the assay. To obtain the optimal concentration, we titrated the nanostructure-modified electrode surface with the exendin-4 antibody (i.e. anti-exendin-4).

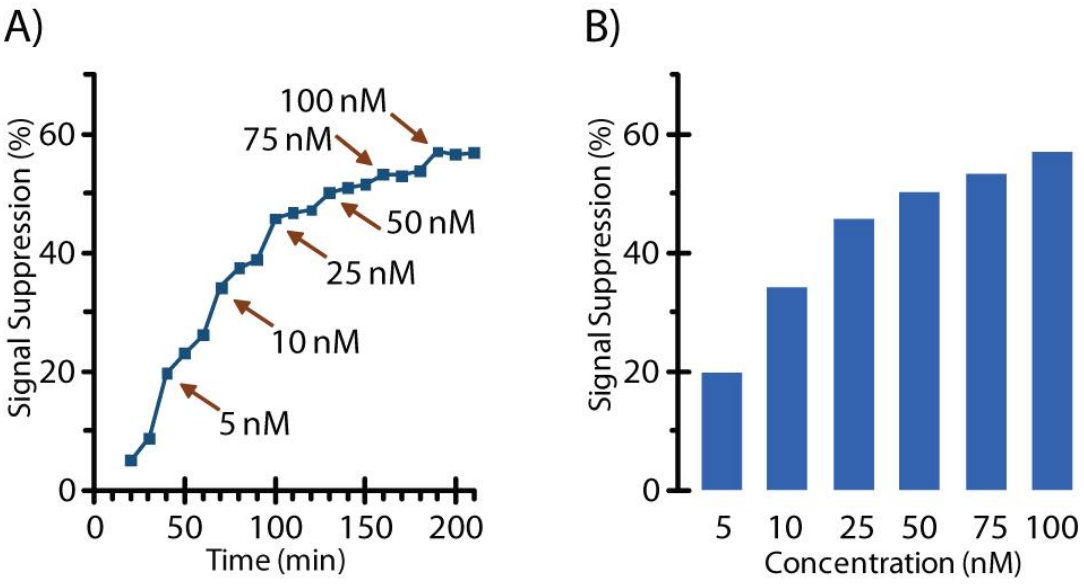

Figure 3.6. Titration of the nanostructure sensor with exendin-4 antibody. **A)** Signal suppression increases with increasing antibody concentration. **B)** Calculated signal suppression by the antibody after 10 min incubation at each concentration.

Figure 3.6A shows that titration with increasing concentrations of exendin-4 antibody results in signal suppression that rises monotonically, with effective saturation of the surface at 100 nM antibody concentration. Evidently, a higher concentration of exendin-4 antibody resulted a sensor surface with highly dense antibody-nanostructure complexes that would produce indiscernible signal change in response to target. Therefore, 10 nM was selected as the optimal concentration of exendin-4 antibody, which resulted an appreciable drop in signal (34.19%) within 10 min of incubation (**Figure 3.6B**).

3.4.3 Exendin-4 Quantification

As noted earlier, because exendin-4 has a narrow therapeutic range (0.1 to 24 nM), monitoring of blood concentrations of the peptide drug is crucial for formulation optimization and optimal suppression of diabetes symptoms in patients. To show proof-of-concept that our nanostructure sensor could be used for exendin-4 quantification, varied concentrations of exendin-4 was preincubated with antibody followed by dropping the mixture onto the sensor surface. Once the mixture was introduced, a measurement was done every 3 min to understand the binding kinetics. **Figure 3.7A** compares the relative differences in signal suppression by 0 and 70 nM exendin-4, where signal was suppressed faster in the absence of analyte and slower when exendin-4 competed with antibody binding to the DNA nanostructure. **Figure 3.7B** compares the calibration curves measured at 3 and 60 min after various concentrations were added. These results are consistent with a functional competitive immunoassay, as expected.

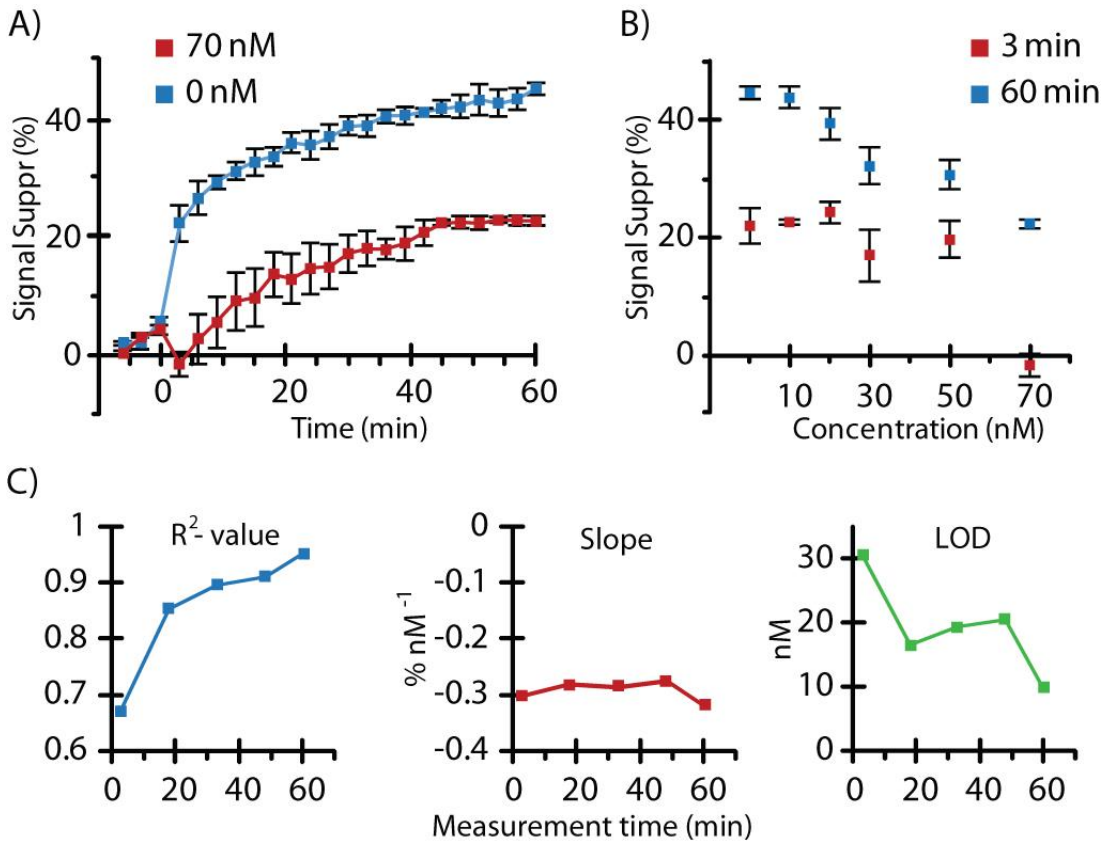

Figure 3.7. A) Comparison of binding kinetics between 70 and 0 nM exendin-4, where the rate of signal suppression was slowed by target. **B)** Calibration curves at 3 and 60 min. **C)** Evaluation of the sensors response at five measurement times.

Figure 3.7C shows plots of R^2 value (blue), magnitude of slope (red) of the linear calibration curve, and limit of detection, LOD (green) as a function of measurement time. These results indicate that with increasing measurement time, R^2 and LOD values both improve, while sensitivity of the assay remains relatively constant. Considering ease of use of the final sensor, we chose 1 hour as an acceptable incubation time for the assay, and this system was capable of exendin-4 quantification in the range of 10 to 70 nM, with 3σ LOD of 5.7 nM (**Figure 3.8A**). To our knowledge, this is the first example where exendin-4 was quantified with a direct EC approach,

utilizing our DNA nanostructure with a three electrode system and without using any correction factor. While the calibration curve does have some overlap with the therapeutic range of 0.1 to 24 nM, future work should focus on methods to improve the sensitivity and extend the dynamic range lower.

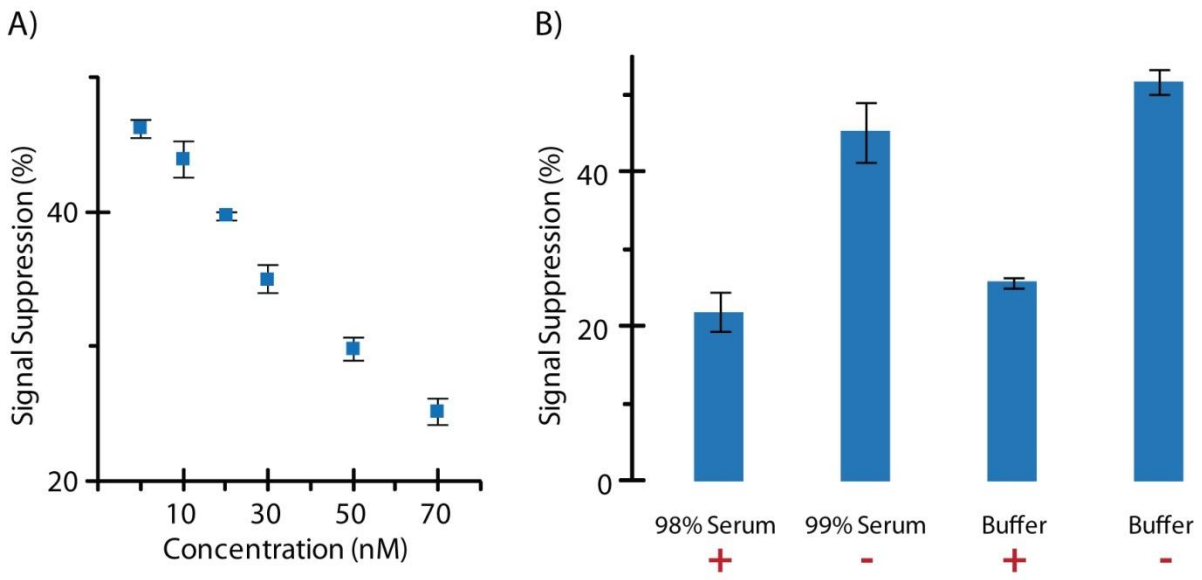

Figure 3.8. A) Exendin-4 calibration curve shows good sensitivity in a range that overlaps with the therapeutic window. **B)** 70 nM exendin-4 (+) mixed with 10 nM antibody was spiked into undiluted serum and in buffer and compared to controls with only antibody (−). Expected trends for the competitive assay were observed. Three different electrodes were used for each of three differently spiked serum samples in part B.

We then investigated the stability of the sensor in undiluted human serum. **Figure 3.8B** demonstrates the signal suppression observed in spiked serum samples (n = 3). With exendin-4 (+), the percentage of signal suppression was blunted compared to controls with only antibody (–

), which agrees with the results in buffer. These results provide an important proof-of-concept that suggests our nanostructure sensor could be function as a sensor of the drug directly in human blood.

3.5 Conclusions

In this work, we describe the development of an electrochemical biosensor system for the quantification of a novel analyte for electrochemistry, exendin-4, which is a widely prescribed diabetic drug. We demonstrated that exendin-4 can be conjugated to the DNA nanostructure, and consecutively antibodies can bind to exendin-4-nanostructure conjugates. Even without using any correction factor, the sensing platform showed limit of detection of 5.7 nM with a dynamic range of 10-70 nM, and the sensor was functional in 98% human serum.

Our DNA nanostructure is an electrode-bound, stable, single molecule on which the redox moiety is covalently linked, therefore the sensor provides direct readout without the needed for multiple washing step. The method also exhibits a reagentless workflow, where no reagents or enzymes are used for signal generation or amplification. We found the sensor to be sensitive to exendin-4 even in a high concentration of serum sample. We therefore believe that our assay could be a simple and inexpensive alternative to current standard methods. In addition, a variety of assays can be targeted by changing the specific peptide or peptide epitope in the bioconjugation step. Thus, the approach offers a simple route for the detection of a wide range of biomarkers in clinical samples. Moreover, compared with ELISA, DNA nanostructure-based peptide quantitative research is worthy of further exploration, as our system provides simple workflow and with optimization should be able to quantify peptide concentration over a wide dynamic range.

Therefore, when the research purpose is to quantify upper pM to nM concentrations of peptides, utilization of our assay should be more practical and cost effective compared to the more highly sensitive yet expensive ELISA method.

3.6 References

1. Wu, F.; Song, G.; de Graaf, C.; Stevens, R. C., Structure and Function of Peptide-Binding G Protein-Coupled Receptors. *Journal of molecular biology* **2017,** *429* (17), 2726-2745.

2. Lau, J. L.; Dunn, M. K., Therapeutic peptides: Historical perspectives, current development trends, and future directions. *Bioorganic & Medicinal Chemistry* **2018,** *26* (10), 2700-2707.

3. Zorzi, A.; Deyle, K.; Heinis, C., Cyclic peptide therapeutics: past, present and future. *Current Opinion in Chemical Biology* **2017,** *38*, 24-29.

4. Sawyer, T. K., CHAPTER 1 Renaissance in Peptide Drug Discovery: The Third Wave. In *Peptide-based Drug Discovery: Challenges and New Therapeutics*, The Royal Society of Chemistry: 2017; pp 1-34.

5. Zong, J.; Cobb, S. L.; Cameron, N. R., Peptide-functionalized gold nanoparticles: versatile biomaterials for diagnostic and therapeutic applications. *Biomaterials science* **2017,** *5* (5), 872-886.

6. Sun, X.; Li, Y.; Liu, T.; Li, Z.; Zhang, X.; Chen, X., Peptide-based imaging agents for cancer detection. *Advanced Drug Delivery Reviews* **2017,** *110-111*, 38-51.

7. Rana, N. K.; Phillips, M.; Carrion, E.; Luisi, G.; Sabatino, D., CHAPTER 3 Peptide Biomarkers and Assay Development. In *Peptide-based Drug Discovery: Challenges and New Therapeutics*, The Royal Society of Chemistry: 2017; pp 76-115.

8. Esposito, S.; de Leonibus, M. L.; Ingenito, R.; Bianchi, E.; Orsatti, L.; Monteagudo, E., A liquid chromatography high-resolution mass spectrometry in vitro assay to assess metabolism at the injection site of subcutaneously administered therapeutic peptides. *Journal of pharmaceutical and biomedical analysis* **2018,** *159*, 449-458.

9. Guillo, C.; Roper, M. G., Simultaneous capillary electrophoresis competitive immunoassay for insulin, glucagon, and islet amyloid polypeptide secretion from mouse islets of Langerhans. *Journal of Chromatography A* **2011,** *1218* (26), 4059-4064.

10. Searle, B. C.; Pino, L. K.; Egertson, J. D.; Ting, Y. S.; Lawrence, R. T.; MacLean, B. X.; Villén, J.; MacCoss, M. J., Chromatogram libraries improve peptide detection and quantification by data independent acquisition mass spectrometry. *Nature Communications* **2018,** *9* (1), 5128.

11. Ai, G.; Chen, Z.; Shan, C.; Che, J.; Hou, Y.; Cheng, Y., Single- and multiple-dose pharmacokinetics of exendin-4 in rhesus monkeys. *International journal of pharmaceutics* **2008,** *353* (1-2), 56-64.

12. Aydin, S., A short history, principles, and types of ELISA, and our laboratory experience with peptide/protein analyses using ELISA. *Peptides* **2015,** *72*, 4-15.

13. Pinho, A. R.; Fortuna, A.; Falcão, A.; Santos, A. C.; Seiça, R.; Estevens, C.; Veiga, F.; Ribeiro, A. J., Comparison of ELISA and HPLC-MS methods for the determination of exenatide in biological and biotechnology-based formulation matrices. *Journal of Pharmaceutical Analysis* **2019,** *9* (3), 143-155.

14. Hu, J.; Easley, C. J., Homogeneous Assays of Second Messenger Signaling and Hormone Secretion Using Thermofluorimetric Methods That Minimize Calibration Burden. *Analytical Chemistry* **2017,** *89* (16), 8517-8523.

15. Zimmet, P. Z., Diabetes and its drivers: the largest epidemic in human history? *Clinical Diabetes and Endocrinology* **2017,** *3* (1), 1.

16. Gepts, W.; Lecompte, P. M., The pancreatic islets in diabetes. *The American Journal of Medicine* **1981,** *70* (1), 105-115.

17. Eng, J.; Kleinman, W. A.; Singh, L.; Singh, G.; Raufman, J. P., Isolation and characterization of exendin-4, an exendin-3 analogue, from Heloderma suspectum venom. Further evidence for an exendin receptor on dispersed acini from guinea pig pancreas. *Journal of Biological Chemistry* **1992,** *267* (11), 7402-7405.

18. Gao, W.; Jusko, W. J., Pharmacokinetic and pharmacodynamic modeling of exendin-4 in type 2 diabetic Goto-Kakizaki rats. *The Journal of pharmacology and experimental therapeutics* **2011,** *336* (3), 881-90.

19. Bradley, D. P.; Kulstad, R.; Schoeller, D. A., Exenatide and weight loss. *Nutrition* **2010,** *26* (3), 243-249.

20. Somasundaram, S.; Easley, C. J., A Nucleic Acid Nanostructure Built through On-Electrode Ligation for Electrochemical Detection of a Broad Range of Analytes. *Journal of the American Chemical Society* **2019,** *141* (29), 11721-11726.

21. O'Connor, S. D.; Olsen, G. T.; Creager, S. E., A Nernstian electron source model for the ac voltammetric response of a reversible surface redox reaction using large-amplitude ac voltages. *Journal of Electroanalytical Chemistry* **1999,** *466* (2), 197-202.

22. Mahshid, S. S.; Camiré, S.; Ricci, F.; Vallée-Bélisle, A., A Highly Selective Electrochemical DNA-Based Sensor That Employs Steric Hindrance Effects to Detect Proteins Directly in Whole Blood. *Journal of the American Chemical Society* **2015,** *137* (50), 15596-15599.

23. Huang, K.-C.; White, R. J., Random Walk on a Leash: A Simple Single-Molecule Diffusion Model for Surface-Tethered Redox Molecules with Flexible Linkers. *Journal of the American Chemical Society* **2013,** *135* (34), 12808-12817.

Chapter 4

Evaluating Strategies for Electrochemical Signal Enhancement in DNA Nanostructure Sensors

4.1 Introduction

Electrochemical sensors have emerged as a promising new platform for the detection of a range of analytes owing to their reliability, rapid response, low cost and portability, low sample consumption, ability to work in complex multicomponent samples, and high sensitivity.[1-2] In recent years, numerous research groups have demonstrated simple variations in sensor fabrication and operational parameters to significantly improve sensitivity of their assays.[3-13] For example, molecular crowding on the sensor surface can affect the signal and sensor equilibration time by altering the efficiency with which the redox reporter approaches the electrode surface.[14] The electron transfer rate of the redox molecule can also be altered by varying the distance between the redox tag and the surface, which could change the redox reporter from effective diffusion-limited to adsorbed behavior, or vice-versa.[15] Similarly, as electrochemical signal depends on changes in the electron transfer rate, precise control of temperature in electrochemical DNA assays can provide simultaneous signal amplification and background signal reduction.[16]

White et al. showed that the geometry of the aptamer can be altered by changing the length of the probe, which can improve the performance of a cocaine-detecting electrochemical sensor.[17] The effects of probe architecture on signal gain was compared by utilizing the standard cocaine aptamer, a "concaptamer" which contains three consecutive cocaine aptamers, and a "pseudosandwich" in which pieces of cocaine aptamer were connected by an unstructured 60-

thymine linker. Both of the new aptamer architectures holds the reporting redox tag further from the electrode in the target-free unfolded conformation, leading to low background current. In the presence of target, the cocaine binding structure reforms, resulting in high signal gain compared to the original aptamer. Silva et al. altered the mobility of the DNA duplex by varying the viscosity of the electrolyte via addition of glycerol, and they observed an increase in faradaic current from the distal redox label with this increase in viscosity of the electrolyte solution.[18] They hypothesized that under these experimental conditions, the mobility of the DNA decreases and the redox moiety spends more time near the surface of the electrode, thus higher signal is observed. Wu et al. compared the performances of sensors fabricated with varying probe packing density on the electrode surface and observed target concentration-dependent decreases in signal for high-coverage sensors due to rigidification of the probe.[19] However, the sensing mechanism could be tuned to achieve higher sensitivity and faster response time by using low-coverage sensors, which show target-dependent increases in signal due to bending of the probe.

In our previous work, we reported a novel DNA nanostructure-based electrochemical sensor for the quantification of a broad range of analytes.[20] From the knowledge we gained in the development of the nanostructure system and other parallel works in our lab and other research groups, we hypothesized that the sensitivity of the assay could be tuned and further improved. In this work, we evaluated two strategies that reduce the molecular weight of the DNA nanostructure, which we hypothesized would enhance the electrochemical signal and sensitivity of the sensors. Specifically, we rationally modified the DNA nanostructure by incorporating polyethylene glycol (PEG) and uracil (U) into selected probe strands to support molecular weight reduction. While large signal enhancements were not observed, these studies nonetheless provide improved

understanding of the sensor response, highlighting parameters that should be considered when designing such systems in the future.

4.2 Reagents and Materials

All solutions were prepared with deionized, ultra-filtered water (Fisher Scientific). The following reagents were used as received: 4-(2-hydroxyethyl)-1-piperazineethanesulfonic acid (HEPES), magnesium chloride hexahydrate from OmniPur, sodium chloride from BDH. Tris-(2-carboxyethyl) phosphine hydrochloride (TCEP), mercapto hexanol (MCH), gold etchant, chromium etchant, and Anti-digoxigenin from Sigma-Aldrich. Gold-sputtered on glass (GoG) (Au 100 nm with Cr adhesion layer 5 nm) from Deposition Research Lab, Inc (St. Charles, MO) with dimension 1" x 3" x 1.1 mm. AZ 40XT (positive thick photoresist) and AZ 300 MIF developer from Microchemicals, polydimethylsiloxane(PDMS) from Dow Corning Corp., and dimethyl sulfoxide (DMSO) from anachemia. Methylene blue-conjugated DNA was purchased from Biosearch Technologies (Novato, CA), purified by RP-HPLC. Thiolated DNA was obtained from Integrated DNA Technologies (IDT; Coralville, Iowa), with purity confirmed by mass spectroscopy. T4 DNA ligase (400,000 units), Uracil-DNA Glycosylase, UDG (5,000 units) and adenosine triphosphate (ATP, 10 mM) are from New England Bio. DNAs are listed in **Table 4.1**.

Table 4.1: Single-Stranded DNA Sequences Used in Nanostructure Construction

Sequence Name	Abbreviation	DNA sequence, listed 5′ to 3′
Thiolated DNA	thio-DNA	**/5Phos/** CTG TGC AAG AAC TCA CAG CCT CAC CTC TTC CTA AAA A **/3ThioMC3-D/**
PEG-Uracil-modified thiolated DNA	P-thio-DNA	**/5Phos/** CUA UG **/iSp18//iSp18/** CAU AGU CUC GCU CUC UCG GAA AA **/3ThioMC3-D/**
Uracil-modified thiolated DNA	U-thio-DNA	**/5Phos/** CUA UGU UUU UUU UCA UAG UCU CGC UCU CUC GGA AAA **/3ThioMC3-D/**
Anchor connector DNA	anchor-DNA	**/5Phos/** GGG CGA CTG TGT CCG CCC CGG TTG AAG TGG AGA **/iDigN/** TAG GAA GAG GTG AGG
PEG-Uracil-modified anchor connector DNA	P-anchor-DNA	**/5Phos/** AA GAC **/iSp18//iSp18/** GUC UUC CAU CAA GUG GCG A **/ iDigN /** CCG AGA GAG CGA GA
Uracil-modified anchor connector DNA	U-anchor-DNA	**/5Phos/** AAG ACU UUU UUU UGU CUU CCA UCA AGU GGC GA **/ iDigN /** CCG AGA GAG CGA GA
Methylene Blue DNA	MB-DNA	**/dT MB/** CTC CAC TTC AAC CG
Uracil modified methylene Blue DNA	U-MB-DNA	**/dT MB/** CGC CAC UUG AUG G

Abbreviations: /5phos/ = Phosphorylation (IDT), /3ThioMC3-D/ = Dithiol attachment (IDT), /iDigN/ = Intermediate Digoxigenin (IDT), /dT MB/ = Methylene Blue modification (Biosearch).

4.3 Experimental Methods

4.3.1 Preparation of Gold Electrodes and DNA Nanostructure Construction

The same photolithographic procedures explained in Chapter 3, Section 3.3.1 were followed to make the photoresist pattern on the gold on glass slides (GoG). As explained in Section 3.3.2, the PDMS electrochemical cell was prepared with the 3D-CAD design and PLA mold shown

in **Figure 3.1C**. Following this, DNA monolayer assembly was prepared following the protocol in Section 3.3.3, and the DNA nanostructure was finally constructed following the protocol in Section 3.3.5.

4.3.2 Electrochemical Measurements

Electrochemical measurements were performed using a Gamry Reference 600 potentiostat. Once the working electrode was ready for measurements, the silver/silver chloride (3 M KCl) reference (BASi) and platinum counter (CH instruments) were introduced into the electrochemical cell. Square-wave voltammetry was carried out from -0.425 to -0.075 V (vs reference electrode) with step size 1 mV, pulse height 25 mV, and SWV frequency of 100 Hz.

4.3.3 DNA Melting Analysis

A Bio-Rad CFX96 real-time quantitative PCR instrument (qPCR) was used. Assay mixtures containing 100 nM of thio-DNA, anchor-DNA, MB-DNA, and 1.0 mM ATP were prepared in HEPES buffer (10 mM HEPES with 0.1 M NaCl at pH 7). The mixture was divided into four batches, in which 0.1 µL of 400 000 U T4 DNA ligase was added to two batches and incubated in room temperature for 1 hour. Later, 0.1 µL of 5 000 U Uracil-DNA Glycosylase (UDG) was added to two batches, one with and another without T4 DNA ligase. Following this, 1x SYBR Green was added to four batches and incubated for 15 minutes. Later, the components were transferred to qPCR tubes and placed in the instrument. The temperature was scanned from 4 °C to 90 °C at 0.5 °C min^{-1}. Fluorescence was measured at each set temperature after a 10 s equilibration, with 470 ± 20 nm excitation and 520 ± 10 nm emission filters.

4.3.4 Anti- digoxigenin Detection

Once the DNA nanostructure was constructed, the electrode was ready for initial SWV measurement in 100 µL volume. After measurement, 20 µL of UDG (in 10 mM HEPES with 0.15 M NaCl, 20 mM Tris-HCl, 1 mM DTT, and 1 mM EDTA at pH 7) was introduced into the cell and incubated at 37 ℃ for 10 min. Later the enzyme solution was removed, and measurement was done in HEPES buffer in 100 µL volume. 100 nM of anti-digoxigenin antibody was prepared in buffer. The electrochemical cell was emptied, and 20 µL of sample was introduced into the cell and incubated at room temperature for 1 hour. Then the sample was removed, and a 100 µL final measurement was done in the same buffer.

4.3.5 Data Analyses

Peak Height

The procedure followed in Section 3.3.11 was used for subtraction of baseline and peak height measurement.

Signal Suppression

The following equations were used to calculate signal suppression, where i_p *(initial)* is the peak height of the initial current measurement (before target incubation) and i_p *(final)* is the peak height of the final current measurement (after target incubation).

$$\boldsymbol{Signal\ Suppression}\ (\%) = -\mathbf{100} \times \frac{\boldsymbol{i_p\ (final)} - \boldsymbol{i_p\ (initial)}}{\boldsymbol{i_p\ (initial)}}$$

4.4 Results and Discussion

4.4.1 Construction of the DNA Nanostructure

In our previous work, a DNA nanostructure system was developed that underwent a change in tethered diffusion[15], which was reported as an analyte responsive electrochemical signal change.[20] Through either attachment or displacement of an anchor molecule to the anchor recognition unit, this sensor presumably experiences a change in mass—possibly with some steric hindrance—that affects its movement, thereby changing the SWV current. Our novel strategy to construct the DNA nanostructure was to use on-electrode enzymatic ligation of three rationally designed DNA segments (**Figure 4.1**). The anchor-DNA (red) binds with both thio-DNA (blue) and the MB-DNA (brown) with 15 base-pairs each. These two hybridization events place the 5' terminal phosphate group and 3' terminal in adjacent positions, assisted by intra-strand hairpin loops (5-bp hairpins). Upon the introduction of T4 DNA ligase, the enzyme ligates the three single-strand DNA sequences, resulting in the formation of a single stable DNA (black) on the surface, which is the intact DNA nanostructure (two 20-bp intramolecular hairpins). Not only does this strategy provide a simple route to changing targets, by changing the anchor-DNA strand, but it also gives significant cost savings compared to solid-phase synthesis of the entire nanostructure.[20]

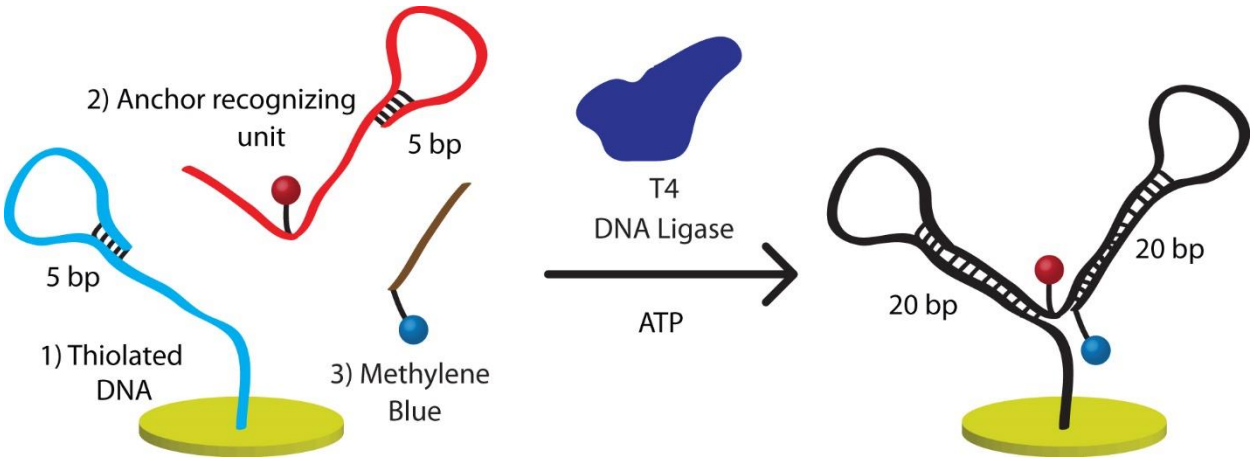

Figure 4.1. Three DNA segments, thiolated-DNA (blue), anchor-DNA (red), and MB-DNA (brown), are ligated on the electrode surface by T4 DNA ligase.

The signaling mechanism of the proposed assay mainly depends on the tethered diffusion of the nanostructure, in which molecular weight of the DNA nanostructure plays a crucial role. Higher DNA nanostructure signal should increase sensitivity of the system and widen the dynamic range of measurement for quantification of both large protein and small molecule analytes. We hypothesized that a decrease in nanostructure molecular weight should result in faster tethered diffusion and reasonably higher signal, i.e. the absolute value of current response of the nanostructure should become larger. In this way, signal loss due to attachment of a large anchor (analyte) would be easier to observe, even if the percentage signal change is not large. Similarly, sensitivity of small molecule detection would be improved if removal of the anchor from the nanostructure results higher electrochemical signal. Here, we test this hypothesis by using several strategies to reduce the molecular weight of the DNA nanostructure.

4.4.2 Polyethylene glycol (PEG)- and Uracil (U)-Modified Nanostructure

To reduce the molecular weight of the DNA nanostructure, we conceived of a new DNA nanostructure sequence where we made three modifications.

1. Replacement of the DNA hairpin loops by polyethylene glycol (PEG) spacers
2. Reduction of binding energy in the helical regions
3. Utilization of uracil in the helical region, which will be enzymatically cleaved

Modification 1: Substitution of the DNA hairpin loops by PEG spacers

The hairpin loop portions of the DNA nanostructure, which are eight nucleotide (8 nt) single stranded DNA, contributes 8% of the total molecular weight of the nanostructure and can be replaced by polyethylene glycol (PEG). PEG is a very flexible and uncharged molecule which makes surfaces more biocompatible and does not interact significantly with the DNA.[21-22] The diameter of the DNA helix is 2 nm, and the estimated contour length of an 8 nt long single stranded DNA is 5.67 nm.[15] Therefore two PEG spacer-18 groups (hexa-ethyleneglycol spacer), which would be flexible 4.8 nm long central loops, should retain proximity of the 5-base pair self-complementary DNA to form a stable DNA hairpin structure. A depiction of these PEG spacers are shown in **Figure 4.2** (orange regions).

Modification 2: Reduction of base pairing in the helical region

The DNA nanostructure is a single stranded DNA containing two intramolecular, 20 bp double helix regions. Reduction of base pairing in the helix region can also aid in decreasing

molecular weight. Reduction of 15 base pair binding between anchor-DNA – thio-DNA and MB-DNA – anchor-DNA to 14 base pair should not adversely affect the DNA nanostructure formation, as 14 base pairs still exhibits a strong binding energy at room temperature.

Modification 3: Utilization of uracil

The new DNA nanostructure sequence contains uracil (U). It is possible to use Uracil DNA-Glycosylase (UDG) to cleave the uracil base from a uracil-deoxynucleotide in any DNA, leaving behind an abasic site at every U.[23] This cleavage will reduce the molecular weight of the nanostructure. Since the nanostructure is composed of stable hairpin-loop structures, it should be able to hold the native structure with the remaining 22 GC base pairs, 11 on each stem (**Figure 4.2**).

The above described modifications would result in a 24% decrease in molecular weight of the nanostructure as well as an increase in the flexibility. Of course, it is also possible that structural changes to DNA helical regions could occur due to the flexibility increase and the lack of continuous double-strand regions. The experiments below were carried out to evaluate these modifications for sensor improvement.

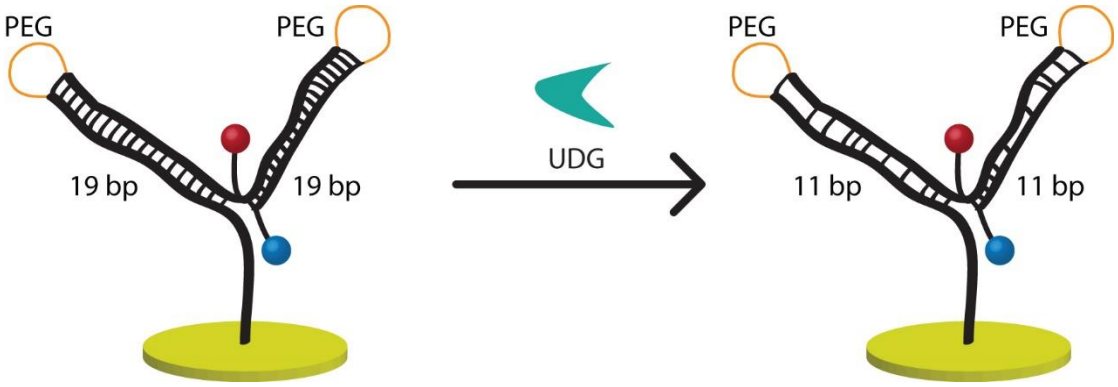

Figure 4.2. Reduced molecular weight of the nanostructure was achieved through addition of PEG loops (orange) and through enzymatic formation of abasic sites on the modified nanostructure by Uracil DNA-Glycosylase (UDG).

To study the effect of UDG, a DNA nanostructure (control) and a PEG- and uracil-modified nanostructure were separately constructed on the surface of different electrodes. the current from the nanostructure (control)was measured as a blank; then, 20 μL of UDG solution was incubated on the electrode at 37 °C for 10 min. The enzyme solution was removed, and current was measured again with each measurement done in triplicate (3 electrodes). **Figure 4.3A** depicts signal response of PEG-U-modified and unmodified nanostructure. The original DNA nanostructure (control) that does not contain uracil resulted in ~18% suppression compared to the initial signal (red bars), which could be due to weakened DNA binding caused by the enzyme buffer, as it does not contain a significant concentration of cations. In contrast, we observed an ~80% drop in the peak height for the PEG-U nanostructure (blue bars), indicating successful enzymatic cleavage of uracil. However, this result suggests that contrary to our original hypothesis, removal of uracil did not enhance the nanostructure signal. In fact, the opposite effect was observed, warranting further study.

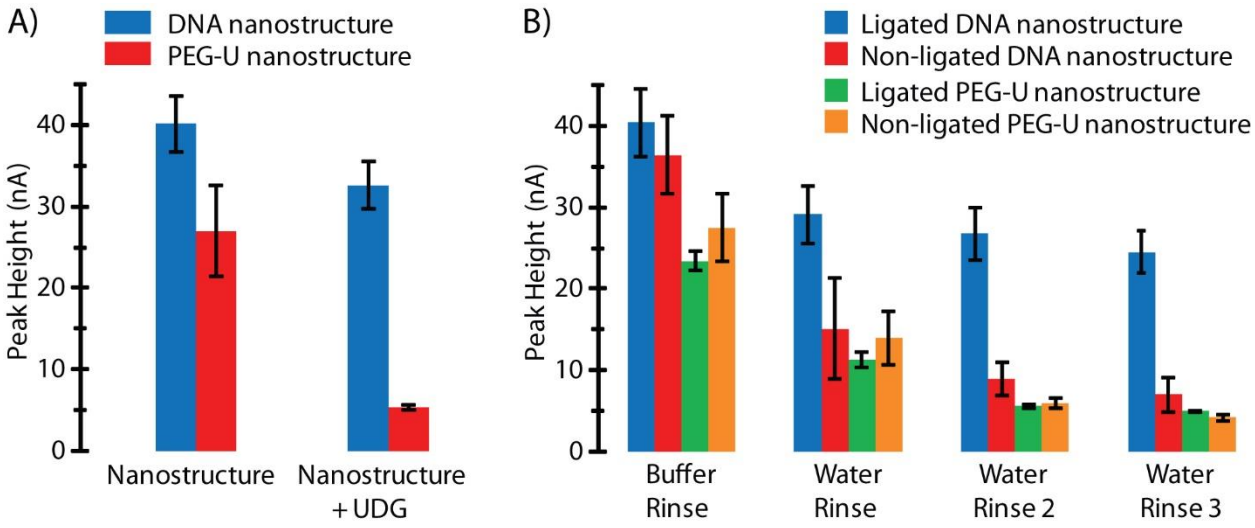

Figure 4.3. A) Enzymatic cleavage of uracil from the PEG-U nanostructure resulted in signal loss (red bars), whereas the DNA nanostructure control signal remained relatively stable (blue bars). **B)** Ligated DNA nanostructure was stable on electrodes even after four rinses (blue bars), while ligated PEG-U nanostructure (green bars) and non-ligated structures were removed easily via water rinses (red and orange bars).

Since we observed almost complete loss of signal, we hypothesized that perhaps the ligation reaction during nanostructure construction was somehow inhibited by the PEG or uracil modifications. To test this, we chose to compare the stabilities of the DNA nanostructure and the PEG-U nanostructure on the electrode surface (**Figure 4.3B**). In the absence of ligase, the nanostructure is bound by noncovalent hybridization, but when exposed to water, the non-ligated components dissociate (red and orange bars), as we demonstrated in our previous work.[20] As expected, the ligated DNA nanostructure (control) was stable on the surface even after three water rinses (blue bars). However, even after treating with ligase, the PEG-U nanostructure (green bars)

gave a similar response to the non-ligated complexes (red and orange bars). These results indicated that the PEG-U nanostructure was either not forming on the electrode surface or that these modifications somehow inhibited the ligase enzyme.

To confirm these findings, we conducted a free solution DNA melting study on the various nanostructures and labeled them with a DNA-intercalating fluorescence dye, SYBR green. **Figure 4.4A** shows that the ligated DNA nanostructure melts at a higher temperature (blue and yellow curves) than the non-ligated complex (orange and red curves), while as expected, the presence of UDG in the solution had no influence on the melting temperature. On the other hand, **Figure 4.4B** shows that in the case of the PEG-U nanostructure, both the ligated and non-ligated complexes gave a similar melt profile (black and gray curves), and enzymatic removal of uracil resulted in further destabilization and thermal degradation of the complexes (green and purple curves). These data confirm that the modification with PEG and uracil results in the formation of an unstable nanostructure on the electrode surface due to unsuccessful DNA ligation. A major contrast between the standard DNA nanostructure and the modified nanostructure is the intra-strand PEG loop. Therefore, our hypothesis was that either the hairpin loop structure was not forming, or PEG was hindering the ligation process. To investigate the formation of stable hairpin loop structure, we compared the melt profile of thio-DNA and anchor-DNA used for the nanostructure construction. **Figure 4.4C** shows a similar melting temperature for PEG-U-modified and unmodified thio-DNA (cyan and brown curves), and anchor-DNA (pink and lime curves), indicating successful formation and stability of the hairpin loop structure.

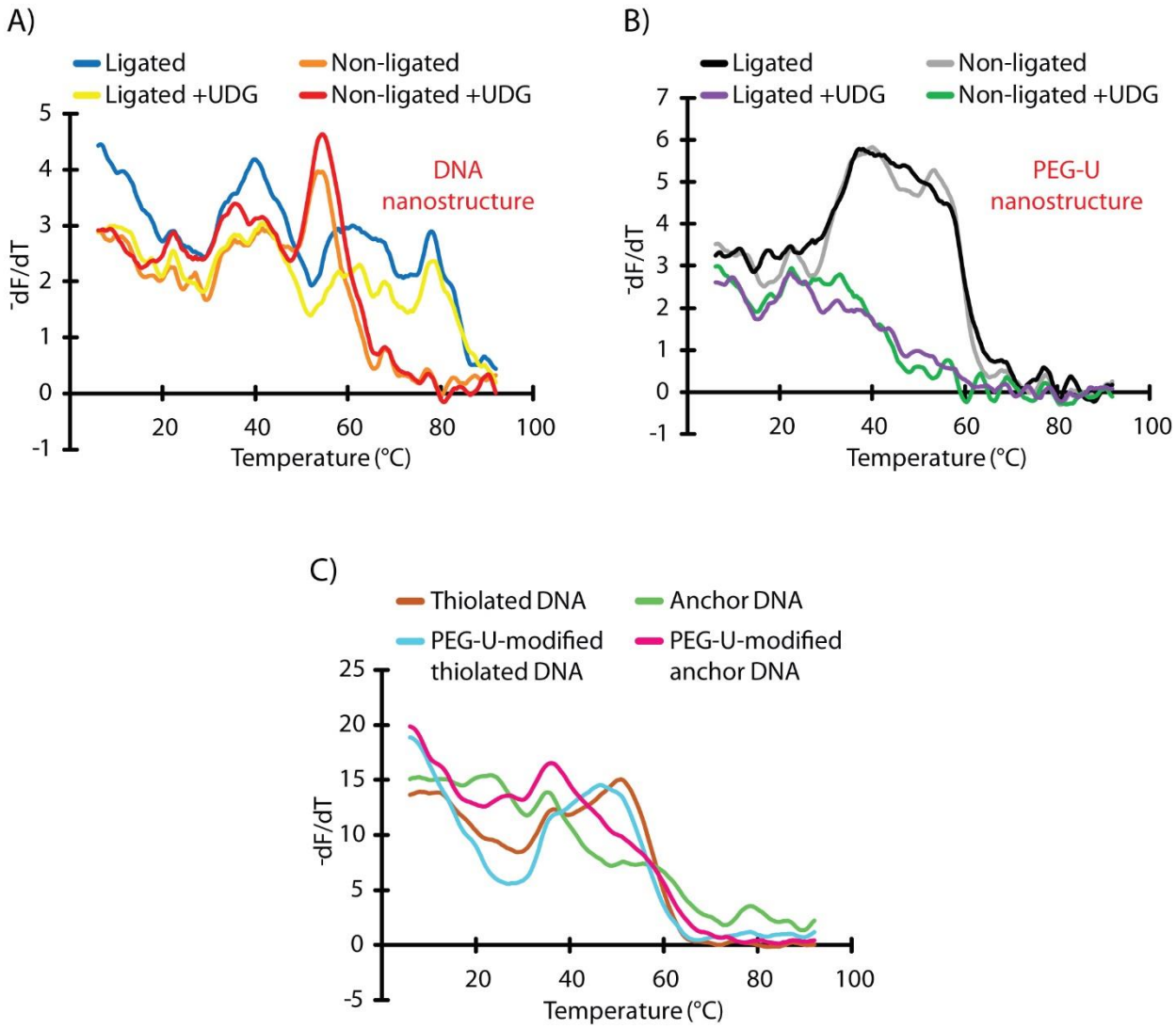

Figure 4.4. DNA melting analysis. **A)** ligated DNA nanostructure was stable (blue and yellow curves) compared to non-ligated DNA (orange and red curves). **B)** Ligated and non-ligated PEG-U nanostructure exhibited similar melt profile, confirming unsuccessful ligation. **C)** Comparable melt profile of thiolated-DNAs (cyan and brown curves) and anchor-DNAs (pink and lime curves) confirmed stability of the hairpin loop structure.

Further research into this issues suggested that one possibility is that molecular crowding was inhibiting ligation. PEG is often used as a molecular crowding agent, increasing the effective local concentrations of reactants in aqueous solution. For efficient catalytic reaction, there is an optimal balance of concentrations of enzyme and molecular crowding agents.[24-25] This optimal concentration of PEG indicates that molecular crowding can actually enhance DNA ligation, but in the PEG dense environment, the effect that triggers enhanced ligation gradually decreases. In the overcrowded solution, molecular crowding instigates attractive but nonspecific interactions between ligase protein and DNA[26], which reduces the effective concentration of ligase, and the DNA entrapped enzymes no longer exhibit catalytic activity. Based on these studies, we think one possibility is that incorporation of the PEG loops very close (1.36 nm) to the nicks—breaks in single strands in the stem region—hindered the ligase from binding to the 5' terminal phosphate groups and inhibited the enzyme activity. Therefore, ligation of the three DNA segments could not take place, resulting in non-ligated nanostructure complex on the electrode surface and likely complete dissociation of the structure upon addition of the uracil cleaving enzyme, UDG.

4.4.3 Uracil-Modified Nanostructure

The second architecture we designed was comprised of an 8-nt uracil loop instead of the PEG loop to avoid unsuccessful ligation (**Figure 4.5A**). Enzymatic cleavage of uracil from the loop and helical region would result in a 16% reduction of the molecular weight of the nanostructure. To confirm the ligation, we first investigated the stability of the uracil-modified nanostructure on the electrode surface (**Figure 4.5B**).

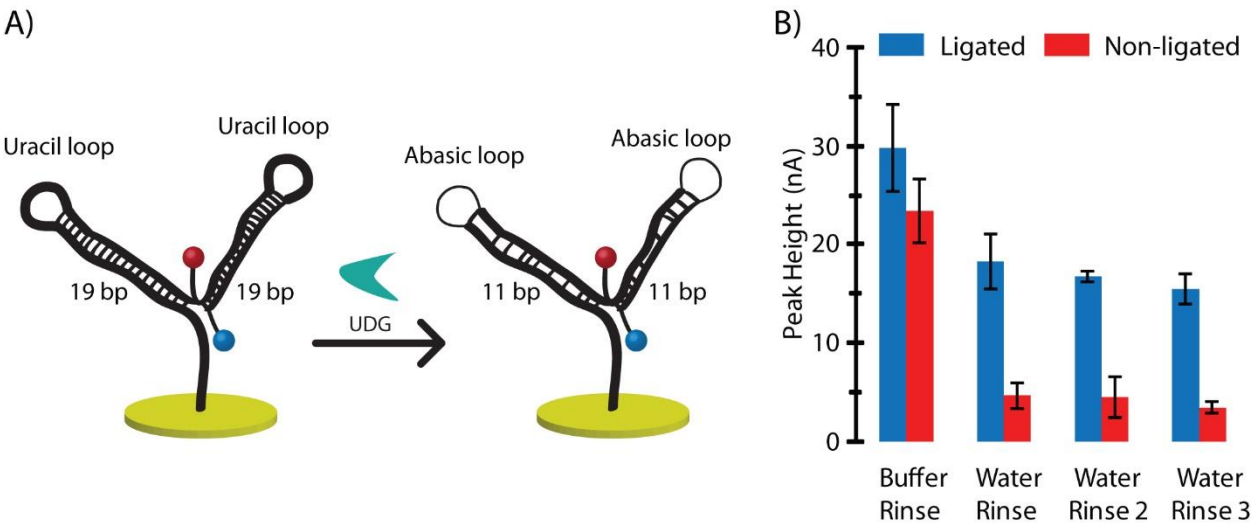

Figure 4.5. A) Formation of abasic sites on uracil modified nanostructure by Uracil DNA-Glycosylase (UDG). **B)** Ligated nanostructure was stable on electrodes (blue bars) while non-ligated structures were removed even with a single water rinse (red bars).

Without treating with ligase, the nanostructure is bound only by noncovalent hybridization exhibiting ~23 nA of SWV current in buffer, however when exposed to water, the non-ligated components easily dissociated (red bars) even after just one rinse step. On the contrary, the ligated nanostructure was stable on the surface after four rinses (blue bars), with a surface yield of ~52%. These data confirm successful construction and stability of the uracil-modified nanostructure on the electrode surface. The results also provide evidence to support our earlier hypothesis that the PEG modification inhibits DNA ligation (perhaps through crowding effects).

Next, to study the hydrolysis and removal of uracils from DNA by UDG, ligated and non-ligated nanostructures were incubated with the enzyme. **Figure 4.6** shows that the non-ligated complex lost ~94% of the initial signal (red bars), indicating destabilization of the double-stranded DNA segments due to formation of the abasic sites. We observed ~43% drop in the peak height

for the ligated nanostructure (blue bars), hence even after enzymatic cleavage of uracil, many of the nanostructures can hold their structure intact enough for electron transfer between the electrode and MB-DNA. However, the reduction of molecular weight by removal of uracils still did not enhance the signal, meaning that our earlier hypothesis was rejected. Nonetheless, the sensor could still be useful for antibody detection.

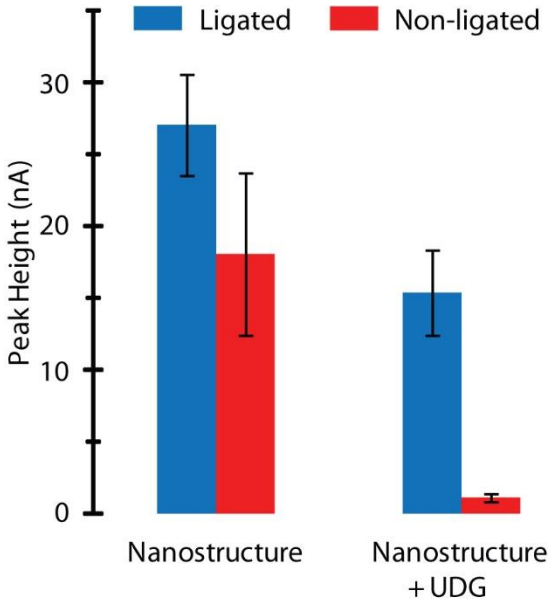

Figure 4.6. Ligated, uracil-modified nanostructure (blue bars) maintained ~15 nA of SWV current after removal of uracils by UDG, while non-ligated structures (red bars) were destabilized and lost from the surface after enzymatic cleavage of uracils.

To test the sensing capability of this modified structure, we compared the DNA nanostructure and uracil-modified nanostructure when used for the quantification of anti-digoxigenin antibody. First, the nanostructure's current was measured as a blank; another

measurement was done followed by incubation with UDG enzyme at 37 °C for 10 min; then, 20 µL of 100 nM antibody solution was incubated on the electrode. The electrode was rinsed, and current was measured again.

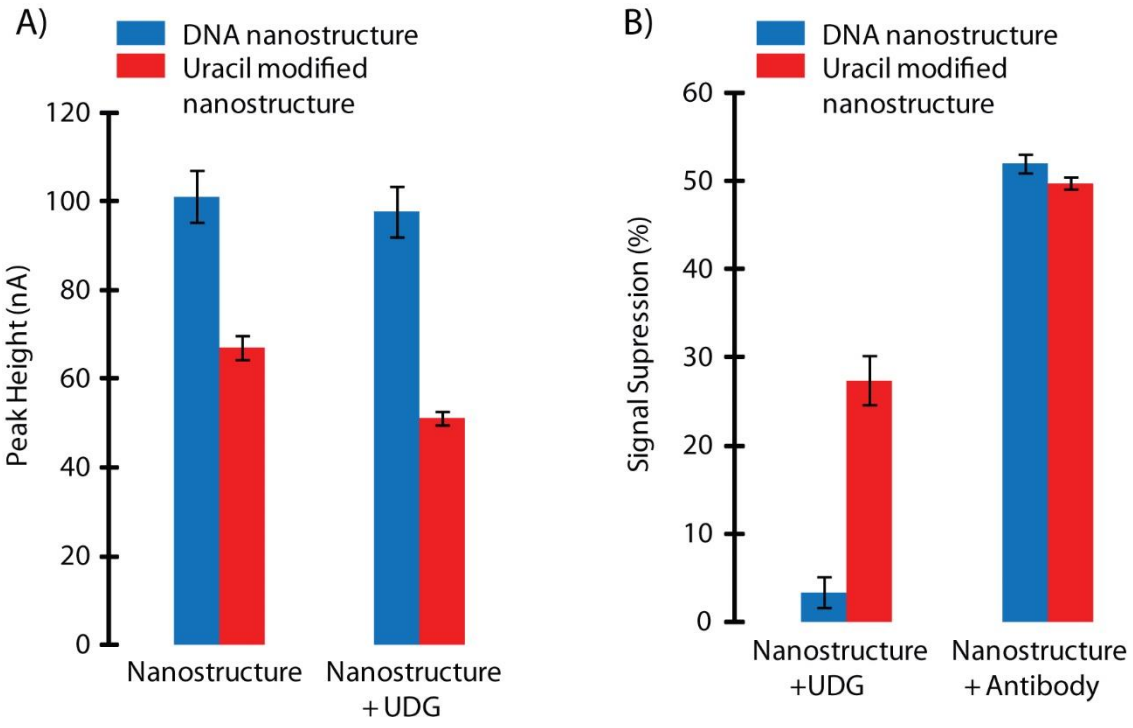

Figure 4.7. A) DNA nanostructure signal remains stable (blue bar) compared to uracil modified nanostructure (red bar) after cleavage reaction. **B)** Enzymatic cleavage of uracil resulted 3% and 27% signal suppression for DNA nanostructure (blue bar) and uracil modified nanostructure (red bar), respectively. Both sensors displayed good response to the target antibody with ~50% signal suppression.

Figure 4.7A shows that the standard DNA nanostructure resulted in higher signal compared to the uracil-modified nanostructure on multiple electrodes, disproving our hypothesis

that reduction of base pairs and abasic site creation on the nanostructure would generate more signal by permitting faster tethered diffusion. As expected, successful enzymatic cleavage of uracil resulted in 27% signal loss for the uracil-modified nanostructure (red bars), whereas the DNA nanostructure response remained unaltered with only 3% signal suppression (blue bars) as shown by **Figure 4.7A** and **Figure 4.7B** (left data). This result also indicated exceptional stability of the DNA nanostructure when challenged with a cleaving enzyme. Upon addition of antibody to these sensors (**Figure 4.7B**, right data), we observed a noticeable drop in the peak height—i.e. an increase in signal suppression—confirming slower tethered diffusion of the redox molecule by anti-digoxigenin antibody binding. In terms of signal suppression percentage, both versions of the nanostructure gave comparable results.

4.5 Conclusions

The performance of our DNA nanostructure sensor depends on the extent to which the tethered diffusion is altered upon a change in mass by target binding. In this work, we described our efforts to achieve faster initial tethered diffusion in order to enhance electrochemical signal, which we hypothesized could be done by reduction of the molecular weight of the nanostructure. Two new nanostructures were designed by incorporating PEG loops and uracil substitutions, and the effects of these modifications on the sensor performance were evaluated. Interestingly, we observed that incorporation of PEG loops in the probe DNA hindered the ligation reaction, which prevented complete construction and resulted in an unstable nanostructure complex on the surface. Although the uracil-modified nanostructure was successful in detecting the target antibody, even after removal of uracils, the nanostructure exhibited somewhat poorer stability, and lower initial signal was observed.

This study suggested that there is either a limited effect of molecular weight on signal enhancement in DNA nanostructure sensors, or that the abasic sites left behind by UDG had some detrimental effect on the overall structure. Of course, the results also demonstrate that the performance of our original nanostructure sensor is thus far unmatched by alternatives, owing to its outstanding stability and robust architecture. The results reported in this chapter should help inform future researchers to 1) avoid using PEG modifications within the DNA nanostructure sensors, and 2) maintain the double-stranded DNA structure within the stems of the DNA nanostructure.

4.6 References

1. Turner, A. P. F., Biosensors: sense and sensibility. *Chemical Society Reviews* **2013,** *42* (8), 3184-3196.

2. Tibor, H.; Joseph, W., Electrochemical Aptasensors – Recent Achievements and Perspectives. *Electroanalysis* **2009,** *21* (11), 1223-1235.

3. Goud, K. Y.; Moonla, C.; Mishra, R. K.; Yu, C.; Narayan, R.; Litvan, I.; Wang, J., Wearable Electrochemical Microneedle Sensor for Continuous Monitoring of Levodopa: Toward Parkinson Management. *ACS Sensors* **2019,** *4* (8), 2196-2204.

4. Clay, M.; Monbouquette, H. G., A Detailed Model of Electroenzymatic Glutamate Biosensors To Aid in Sensor Optimization and in Applications in Vivo. *ACS chemical neuroscience* **2018,** *9* (2), 241-251.

5. Matharu, Z.; Daggumati, P.; Wang, L.; Dorofeeva, T. S.; Li, Z.; Seker, E., Nanoporous-Gold-Based Electrode Morphology Libraries for Investigating Structure-Property Relationships in

Nucleic Acid Based Electrochemical Biosensors. *ACS applied materials & interfaces* **2017,** *9* (15), 12959-12966.

6. Dauphin-Ducharme, P.; Plaxco, K. W., Maximizing the Signal Gain of Electrochemical-DNA Sensors. *Analytical Chemistry* **2016,** *88* (23), 11654-11662.

7. Kang, D.; Ricci, F.; White, R. J.; Plaxco, K. W., Survey of Redox-Active Moieties for Application in Multiplexed Electrochemical Biosensors. *Analytical Chemistry* **2016,** *88* (21), 10452-10458.

8. Schoukroun-Barnes, L. R.; Wagan, S.; White, R. J., Enhancing the Analytical Performance of Electrochemical RNA Aptamer-Based Sensors for Sensitive Detection of Aminoglycoside Antibiotics. *Analytical Chemistry* **2014,** *86* (2), 1131-1137.

9. Zhou, Y.-G.; Wan, Y.; Sage, A. T.; Poudineh, M.; Kelley, S. O., Effect of Microelectrode Structure on Electrocatalysis at Nucleic Acid-Modified Sensors. *Langmuir* **2014,** *30* (47), 14322-14328.

10. White, R. J.; Plaxco, K. W., Exploiting Binding-Induced Changes in Probe Flexibility for the Optimization of Electrochemical Biosensors. *Analytical Chemistry* **2010,** *82* (1), 73-76.

11. Lubin, A. A.; Vander Stoep Hunt, B.; White, R. J.; Plaxco, K. W., Effects of Probe Length, Probe Geometry, and Redox-Tag Placement on the Performance of the Electrochemical E-DNA Sensor. *Analytical Chemistry* **2009,** *81* (6), 2150-2158.

12. Ricci, F.; Zari, N.; Caprio, F.; Recine, S.; Amine, A.; Moscone, D.; Palleschi, G.; Plaxco, K. W., Surface chemistry effects on the performance of an electrochemical DNA sensor. *Bioelectrochemistry (Amsterdam, Netherlands)* **2009,** *76* (0), 10.1016/j.bioelechem.2009.03.007.

13. White, R. J.; Phares, N.; Lubin, A. A.; Xiao, Y.; Plaxco, K. W., Optimization of Electrochemical Aptamer-Based Sensors via Optimization of Probe Packing Density and Surface Chemistry. *Langmuir : the ACS journal of surfaces and colloids* **2008,** *24* (18), 10513-10518.

14. Ricci, F.; Lai, R. Y.; Heeger, A. J.; Plaxco, K. W.; Sumner, J. J., Effect of Molecular Crowding on the Response of an Electrochemical DNA Sensor. *Langmuir : the ACS journal of surfaces and colloids* **2007,** *23* (12), 6827-6834.

15. Huang, K.-C.; White, R. J., Random Walk on a Leash: A Simple Single-Molecule Diffusion Model for Surface-Tethered Redox Molecules with Flexible Linkers. *Journal of the American Chemical Society* **2013,** *135* (34), 12808-12817.

16. Somasundaram, S.; Holtan, M. D.; Easley, C. J., Understanding Signal and Background in a Thermally Resolved, Single-Branched DNA Assay Using Square Wave Voltammetry. *Analytical Chemistry* **2018,** *90* (5), 3584-3591.

17. White, R. J.; Plaxco, K. W., Engineering New Aptamer Geometries for Electrochemical Aptamer-Based Sensors. *Proceedings of SPIE--the International Society for Optical Engineering* **2009,** *7321*, 732105.

18. Silva, S. M.; Tavallaie, R.; Gonçales, V. R.; Utama, R. H.; Kashi, M. B.; Hibbert, D. B.; Tilley, R. D.; Gooding, J. J., Dual Signaling DNA Electrochemistry: An Approach To Understand DNA Interfaces. *Langmuir* **2018,** *34* (4), 1249-1255.

19. Wu, Y.; Lai, R. Y., Tunable Signal-Off and Signal-On Electrochemical Cisplatin Sensor. *Analytical Chemistry* **2017,** *89* (18), 9984-9989.

20. Somasundaram, S.; Easley, C. J., A Nucleic Acid Nanostructure Built through On-Electrode Ligation for Electrochemical Detection of a Broad Range of Analytes. *Journal of the American Chemical Society* **2019,** *141* (29), 11721-11726.

21. Immoos, C. E.; Lee, S. J.; Grinstaff, M. W., DNA-PEG-DNA Triblock Macromolecules for Reagentless DNA Detection. *Journal of the American Chemical Society* **2004,** *126* (35), 10814-10815.

22. Chapman, R. G.; Ostuni, E.; Yan, L.; Whitesides, G. M., Preparation of Mixed Self-Assembled Monolayers (SAMs) That Resist Adsorption of Proteins Using the Reaction of Amines with a SAM That Presents Interchain Carboxylic Anhydride Groups. *Langmuir* **2000,** *16* (17), 6927-6936.

23. Hölz, K.; Pavlic, A.; Lietard, J.; Somoza, M. M., Specificity and Efficiency of the Uracil DNA Glycosylase-Mediated Strand Cleavage Surveyed on Large Sequence Libraries. *Scientific Reports* **2019,** *9* (1), 17822.

24. Shiraki, T. Y.; Kamei, K.-i.; Maeda, Y. T., Randomness and optimality in enhanced DNA ligation with crowding effects. *Physical Review Research* **2020,** *2* (1), 013360.

25. Sasaki, Y.; Miyoshi, D.; Sugimoto, N., Effect of molecular crowding on DNA polymerase activity. *Biotechnology journal* **2006,** *1* (4), 440-6.

26. Marenduzzo, D.; Finan, K.; Cook, P. R., The depletion attraction: an underappreciated force driving cellular organization. *J Cell Biol* **2006,** *175* (5), 681-686.

Chapter 5

Automated Microfluidic Device For Electrode Preparation and Nucleic Acid Detection

5.1 Introduction

Microfluidic and electrochemical technologies have a symbiotic association, bolstering inherent features of each other and opening new doors for the development of point-of-care (POC) analysis.[1] Microfluidics allows miniaturization of device, integration of several functional compartments in a single device, precise control and low consumption of expensive samples and reagents (nL), detection of multiple sample in parallel, portability, and overall low-cost operations.[2-3] However, for POC application, miniaturization of the detection system is required in order to incorporate into microfluidic device. Electrochemical detection methods are ideal for POC setups and can be easily coupled with microfluidics, owing to their compatibility with microfabrication technologies.[4-5] Microfluidic technologies enable better control of fluids through electrode, decreasing sample and reagents consumption. The small size of microchannels allow faster reaction by reducing the diffusion time and automated operation minimized local variations which aid in reproducibility of the sensor. In recent years, integrated microfluidic devices with electrochemical detection method have been utilized to monitor blood metabolites, quantify disease biomarkers, and study cell culture.[6-12] This integrated technology has also shown promising results in other fields of research, particularly in domains such as pharmaceutical, environmental, and food analysis. [13-18] Microfluidics enable high-throughput analysis by driving sample to different electrochemical cells, allowing multiplexing and simultaneous detection of multiple target molecules in a single device.[19-20] For instance, Lee et al. coupled electrochemical

detection system with a digital microfluidic platform for the simultaneous detection of multiple biomarkers of pulmonary hypertension.[21] The device comprises five fluidic chambers, each of which is controlled by pneumatic microvalves and connected to an electrochemical sensor designed to detect four biomarkers and control. Panini et al. developed a sensitive and selective method for the quantification of prostate specific antigen (PSA) in human serum samples by utilizing continuous flow microfluidics.[22] Carbon nanotubes/horseradish peroxidase/anti-tPSA immobilized glassy carbon electrodes were used as working electrode in microfluidic Plexiglas biochip to generate electrochemical readout. Their microfluidic immunosensor resulted in a detection limit of 0.08 µg/L which was 6 times lower than the conventional ELISA. Uliana et al. described the construction of a fully disposable, low-cost microfluidic electrochemical array device (µFED) for detection of biomarker estrogen receptor alpha.[23] The device comprises estrogen response element modified carbon-based working electrodes, which captures nanoparticles that are loaded with estrogen receptor alpha and horseradish peroxidase. The system resulted electrochemical readout when H_2O_2 and hydroquinone were injected into the microfluidic device. These are only a few of many unique studies which demonstrates microfluidic platforms integrated with electrochemical detection hold great promise for a wide range of biomolecule detection.

Herein, we describe the integration of electrochemical sensor with an automated microfluidic device. This microdevice, pictured in **Figure 5.3**, consists of a gold working electrode integrated with microfluidics, where three input channels are controlled by active microvalves to achieve generalizable dynamic control over fluids. We have shown that our automated, valve-controlled microfluidics is useful for electrode preparation and analyte detection in a DNA-based

surface assay platform using square wave voltammetry (SWV). In future we aim to utilize this automated microfluidic biosensor for the detection of secretions from cells and tissues in real time.

5.2 Reagents and Materials

All solutions were prepared with deionized water filtered with a Barnstead MicroPure Water Purification system (Thermo Fisher Scientific, Waltham, MA, USA) with the resistance value as 18.2 MΩ·cm at 23.5 °C and particles less than 0.2 µm. The following reagents were used as received: 4-(2-hydroxyethyl)-1-piperazineethanesulfonic acid (HEPES), sodium chloride from BDH. Tris-(2-carboxyethyl) phosphine hydrochloride (TCEP), mercapto hexanol (MCH), gold etchant, and chromium etchant from Sigma-Aldrich. Gold-sputtered on glass (GoG) (Au 100 nm with Cr adhesion layer 5 nm) from Deposition Research Lab, Inc (St. Charles, MO) with dimension 1" x 3" x 1.1 mm. The silicon wafers were acquired from the Polishing Corporation of America (Santa Clara, CA, USA). Negative photoresists (SU-8 2015) and SU-8 developer were purchased from MicroChem (Westborough, MA, USA). AZ 40XT (positive thick photoresist) and AZ 300 MIF developer from AZ Electronic Materials USA (Somerville, NJ, USA), polydimethylsiloxane (PDMS) precursors, SYLGARD 184 silicone elastomer base, and curing agent from Dow Corning Corp. (Midland, MI, USA), and dimethyl sulfoxide (DMSO) from anachemia. Bovine serum albumin (BSA) from VWR (West Chester, PA). Fluorescein was purchased from Alfa Aesar (Ward Hill, MA, USA). Fluorescence excitation and emission were accomplished using a Nikon Ti-E inverted fluorescence microscope (40X objective, 0.75 NA; Nikon Instruments Inc., Melville, NY, USA) interfaced to a CCD camera (CoolSnap HQ2; Photometrics Scientific, Tucson, AZ, USA). Fluorescence images were acquired by focusing on a chosen region of interest (**Figure 5.5**) and collected through the green fluorescence filter cube (λ_{ex} = 470 ± 20 nm, λ_{em} = 525 ± 25 nm).

Methylene blue-conjugated DNA was purchased from Biosearch Technologies (Novato, CA), purified by RP-HPLC. Thiolated DNA was obtained from Integrated DNA Technologies (IDT; Coralville, Iowa), with purity confirmed by mass spectroscopy. DNAs are listed in Table: 5.1.

Table 5.1: Single-Stranded DNA Sequences Used in Oligonucleotide Quantification

Sequence Name	Abbreviation	DNA sequence, listed 5′ to 3′
Thiolated DNA	thio-DNA	/**5ThioMC6-D**/AAA AGC ATG GTG ACG TGT GAG AGA TAG GAA AAG GAC AAT AAC AA
Methylene Blue DNA	MB-DNA	TTG UTA TTG UCC TTU TCC UAT CTC TCA CAC GUC ACC AUG C/**MB-C7**/

Abbreviations: /5ThioMC6-D/ = disulfide bond flanked by two six-carbon spacers (IDT), /MB-C7/ = methylene blue modification (Biosearch).

5.3 Experimental Methods

5.3.1 Preparation of Gold Electrodes

The photomask of electrode design used in the experiment was designed in Adobe Illustrator, and files were sent to Fineline Imaging (Colorado Springs, Colorado) for printing positive photomask. **Figure 5.1A** shows the mask design. Same photolithographic procedure explained in Chapter 3, Section 3.3.1 was followed to make the photoresist pattern on the gold on glass slide (GoG).

5.3.2 3D-printed Template For The Fabrication of Electrochemical Cell

A 3D computer-aided design (CAD) file was designed in Sketchup© (Trimble Navigation Limited), and Makerbot Replicator 2 (200 µm layer resolution in the z-direction) with Hatchbox's

polylactic acid filament (PLA, 1.75 mm diameter) was used to print the 3D mold. The 3D CAD depiction and an example of a printed template is shown **in Figure 5.1B & 5.1C**.

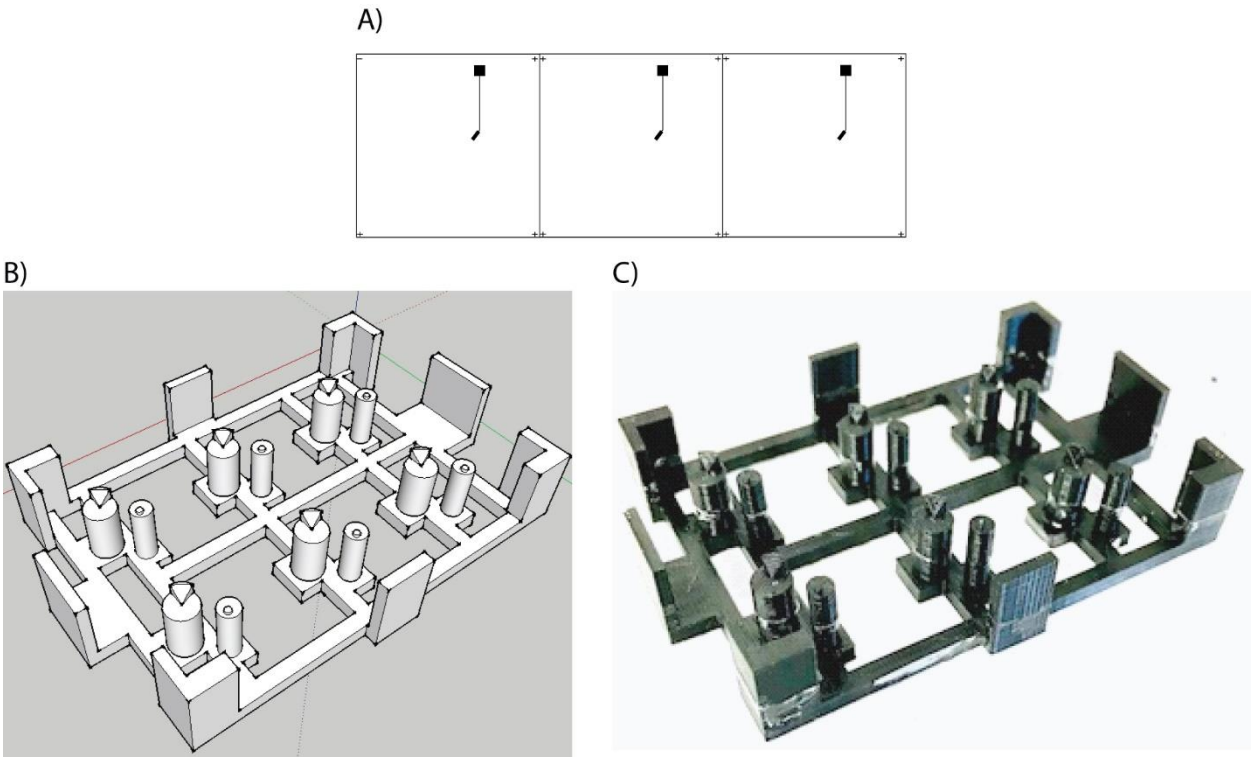

Figure 5.1. A) Photomask design used for gold-on-glass (GoG) preparation. **B)** 3D CAD of the master to prepare electrochemical cell. **C)** 3D printed PLA used for molding PDMS electrochemical cells.

5.3.3 Master Wafer Fabrication

Two master wafers for templating liquid channels and pneumatic control channels were fabricated using standard photolithography. Channel layouts were designed in Adobe Illustrator software, and plastic film photomasks were printed at Fineline Imaging (Colorado Springs, CO, USA) at a 50,800 dpi resolution. The silicon wafers were ready to use after shaken in 1.0 M H_2SO_4 at 300 rpm speed for 30 min, washed and shaken in D.I. water for 30 min and dried by air. For the pneumatic control channel layer, a ~30 µm layer of SU-8 2015 was spin-coated on the silicon wafer at 2000 rpm for 45 seconds. Later, the wafer was soft-baked at 95 ℃ for 5 min, and passively cooled down to room temperature. The photomask was aligned on the photoresist coated wafer and UV exposed for 2 min by an in-house built UV lithography light exposure unit. Finally, the wafer was developed for 5 min in SU-8 developer solution after a 5-min hard bake on a hot plate at 95 ℃. The fluidic layer wafer was fabricated with positive photoresist. The AZ40 XT photoresist was warmed to room temperature. Next, a ~40 µm layer of AZ 40 XT was spin-coated on the silicon wafer at 2000 rpm for 45 seconds and soft-baked at 65 ℃ for 5 min, at 95 ℃ for 5 min, and at 115 ℃ for 5 min. Then slowly it was cooled down to room temperature. The photomask was aligned on the AZ photoresist coated wafer and exposed under UV for 120 seconds and hard-baked at 65 ℃ for 1.5 min, at 95 ℃ for 1.5 min, and at 105 ℃ for 1.5 min, cooled to room temperature passively. The wafer was developed in AZ developer for 5 min. Finally, the AZ portion of the wafer was annealed to allow templating of rounded channel cross-sections by baking at 120 ℃ for 10 min.

5.3.4 Microchip Fabrication

The 3D template was aligned on the flow channel wafer. After degassing under vacuum, 45 g of well-mixed PDMS precursor mixture (5:1 ratio, monomer: curing agent) was poured onto the flow channel patterned silicon wafer in an aluminum foil boat. The fluid layer was baked at 65 °C for 1 hour in an oven. At the time when the fluid layer was halfway baked, 10.5 g of PDMS precursor mixture (20:1 ratio, monomer: curing agent) was degassed and spin-coated onto the control layer at 2100 rpm for 45 s, creating a layer of ~30 µm thickness. The control layer was baked at 60 °C for 30 min. After the bulk PDMS was peeled off from the 3D template and wafer, the electrochemical cell reservoir was formed. The flow channel layer was then cut to shape, inlets were punched by Miltex disposable biopsy punches, and aligned to the valve channel layer under 3X microscopy. The two mated layers were baked in an oven at 65 °C overnight to facilitate permanent bonding. The PDMS was peeled from the wafer, diced into individual devices, control valve inlets were punched, fluidic channel and via channel connection was made using 0.35-mm ID punch, and the surfaces were washed with methanol and dried with N_2 gas. Electrodes were cleaned with piranha solution prior to plasma oxidation of the PDMS device. The piranha solution (H_2SO_4:H_2O_2, 3:1) was freshly prepared and dropped onto the surface of the electrode for 1 minute, later the electrodes was rinsed with deionized water. Each device was then irreversibly bonded to GOG by plasma oxidization (Harrick Plasma; Ithaca, NY, USA) and these devices were then ready to use.

5.3.5 Automated Flow Control System of Microchip

The 7 pneumatic push-up control valves on the microfluidic chip were programmatically controlled by an in-house written LabVIEW application which was interfaced to a custom manifold of solenoid switches (LHDA0533115H; the Lee Company, Westbrook, CT, USA) using a multifunction data acquisition system (PCI-6259, National Instruments). A house nitrogen gas source was used to actuate these pneumatic solenoid valves by 20-psi pressure adjusted by a pressure regulator. The control valves on microchip were connected to the corresponding solenoid valve with 90-degree angled 22-gauge blunt 304 stainless steel needles (Jensen Global JG22-0.5HPX-90, Santa Barbara, CA) through Tygon microbore tubing (0.02" I.D. X 0.06" O.D., Cole-Parmer, Vernon Hills, IL). The valve inlet interfaced with the control system were punched by 0.75-mm ID punch (69039-07, electron Microscopy Sciences, Hatfield, PA). An in-house written LabVIEW application was used to control the open/close of the valves. When the valve is set in close status, the solenoid switch will be activated to pressure the nitrogen gas into the dead-end channel of the control layer, filled with deionized water to avoid the air permitting into the channels, to deflect the PDMS membrane up to close the flow channel in the upper layer, which are push-up valve.

5.3.6 Mixer Performance Evaluation

The microfluidic chip was set up on the stage of the fluorescence microscope mounted with a Tokai Hit microscope stage top incubator, with D.I. water back-filled into the microchip valve inlets. 100 nM of 20 μL fluorescein was loaded into the probe inlet and 20 μL of D.I. water was added into the sample and reference inlet. The device was then set for fully automated operation

by the 6 or 5-step peristaltic pumping with 600 ms pumping time and 50 pump cycles. The fluorescence imaging in the region of interest (**Figure 5.5A**) were operated continuously in 150 ms interval in FITC filter cube ($\lambda_{ex} = 470 \pm 20$ nm, $\lambda_{em} = 525 \pm 25$ nm) by CCD camera (CoolSnap HQ2; Photometrics Scientific) interfaced with Nikon inverted Ti-E fluorescence microscope (40X, 0.75 NA). The fluorescence intensity data from the images were analyzed by ImageJ software and data analysis was processed in Excel.

5.3.7 Custom Reference Electrode

A custom L-shaped reference electrode was used in the experiments, as showed in **Figure 5.2A**. L-shaped reference electrode is made from 2 mm OD glass tubing, one CoralPor glass frit (BASi West Lafayette, IN), and 0.5 mm silver wire (Alfa Aesar), and it was filled with 3 M KCl. A 60-mm length of silver wire was cut from stock, and a 2-mm diameter rubber plug was cut from a rubber stopper with a 2-mm biopsy punch. The plug was fitted onto the silver wire ~30 mm from the end. The lower 15 mm was chlorinated by immersion in 3 M KCl solution with application of 9 V (dc) for ~10 seconds, where the wire was positive with respect to ground, and the return electrode was a platinum electrode. This procedure produced a gray/white AgCl coating on the wire. The chlorinated silver wire was threaded into the L-shaped glass, the rubber plug was seated 5 mm below the end of the glass tube, epoxy (Loctite, D¨usseldorf, Germany) was applied to the end. After curing, 3 M KCl was injected into the glass tubing and the frit was affixed to the end of glass tubing, held in place by transparent heat shrink tubing. The reference electrode was equilibrated 24 hours, before use. Another 3D CAD templet was designed and printed for positioning the counter electrode on the electrochemical cell, as shown in **Figure 5.2B & 5.2C**.

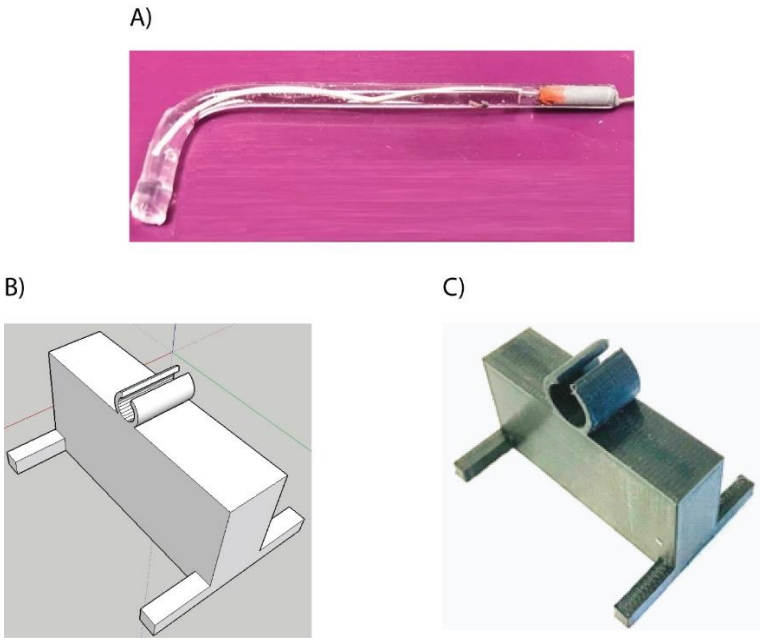

Figure 5.2. A) Assembled Ag/AgCl L-shaped reference electrode, filled with 3M KCl and closed by porous frits. **B)** 3D CAD of the reference electrode holder. **C)** 3D printed PLA used as a reference electrode holder.

5.3.8 Electrochemical Measurements

Electrochemical measurements were performed using in-house built potentiostat. The custom silver/silver chloride (3 M KCl) reference and platinum counter (CH instruments) were introduced into the electrochemical cell, which was previously filled with 0.1 M potassium chloride buffer solution. 20 µL equimolar concentration of potassium ferricyanide and potassium ferrocyanide was loaded into the sample inlet and 0.1 M of 20 µL potassium chloride buffer was added into the probe and reference inlet. The device was then set for fully automated operation by the peristaltic pumping with 600 ms pumping time and ran for 50 or 400 pump cycles for each sample concentration. Current generated by varying concentrations (0, 1, 5, 10 nM) of

ferri/ferrocyanide redox couple in 0.1 M potassium chloride buffer was measured every minute using square-wave voltammetry (SWV), performed from -0.2 to +0.6 V (vs reference electrode) with step size 1 mV, pulse height 25 mV, and SWV frequency of 100 Hz.

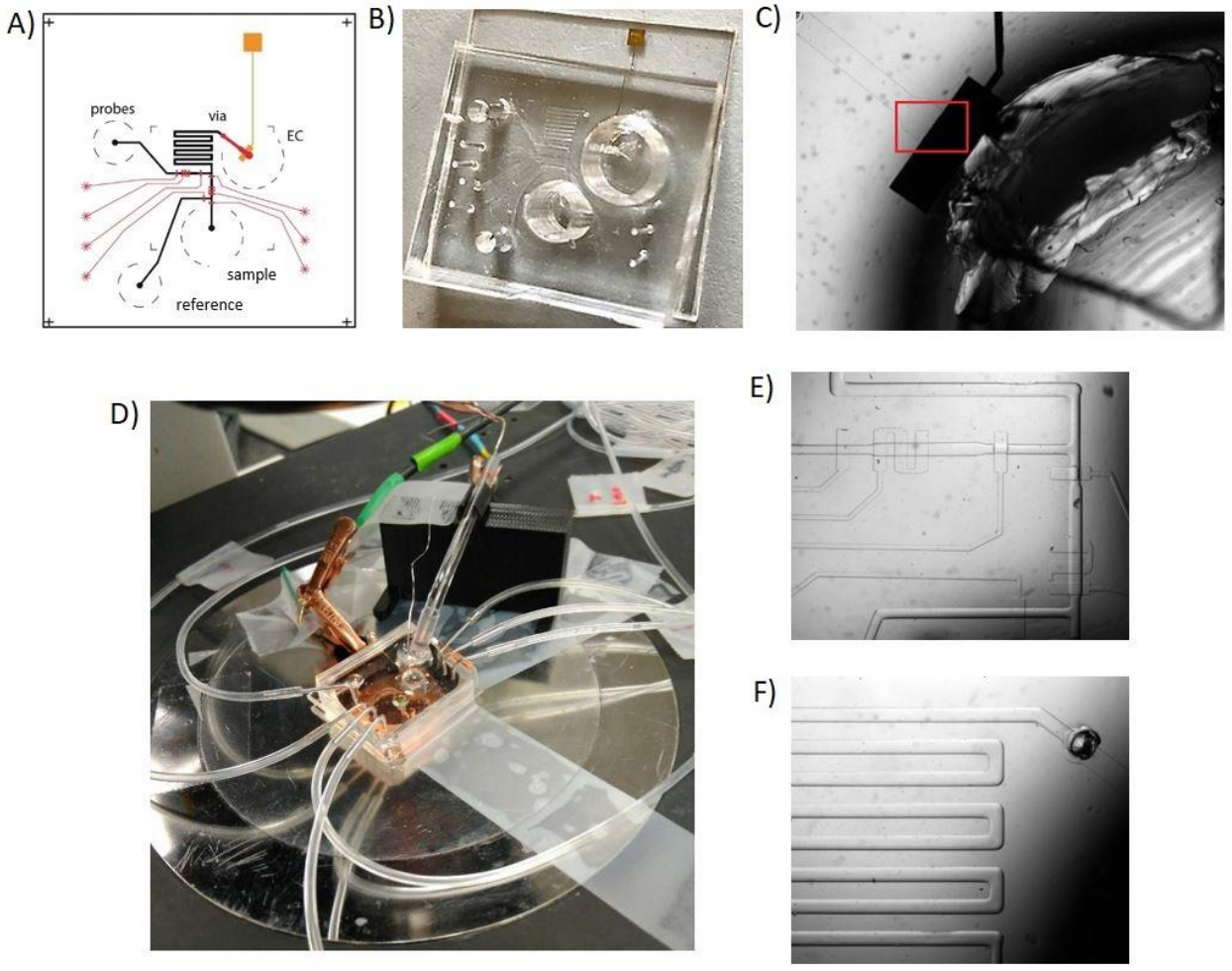

Figure 5.3. A) Schematic of the channel layouts, with fluidic channels shown in black and pneumatic control channels and detection channel in red. **B)** Photo of assembled device. **C)** Gold electrode placed inside the detection channel. **D)** Photo of working device in the microscope stage. Tubing was connected to control channels. Reference and counter electrodes were positioned on top of the 3D-templated reservoir to serve as the full sensor. **E)** Microvalves controlling the fluid flow. **F)** Serpentine-shaped incubation channel for homogenization of fluids.

5.3.9 Electrode Preparation and Detection of Nucleic Acid

Once the device was ready to use, 20 µL of HEPES 10 mM with NaCl 0.5 M pH 7 buffer was loaded into all the 3 inlets and flowed through the channel using valve-based peristaltic pumps. Custom silver/silver chloride (3 M KCl) reference and platinum counter (CH instruments) were introduced into the electrochemical cell, which was previously filled with the same HEPES buffer solution and initial SWV measurement was performed from -0.45 to 0 V (vs reference electrode) with step size 1 mV, pulse height 25 mV, and SWV frequency of 100 Hz. The thio-DNA was reduced by reducing agent TCEP. To reduce 1 µL of 200 µM thio-DNA, 3 µL of 10 mM TCEP was mixed and incubated at room temperature in dark for 1 hour. The solution was then diluted to final thio-DNA concentration of 1.25 µM with HEPES 10 mM with NaCl 0.5 M pH 7 buffer. The electrochemical cell was emptied, and 50 µL of thio-DNA was introduced into the cell and incubated at room temperature for 1 hour. Later, thio-DNA was removed, buffer was introduced, and another measurement was done. In the next step, 20 µL of 3 mM mercaptohexanol (MCH) in HEPES 10 mM with NaCl 0.5 M pH 7 buffer was loaded into the inlets and flowed through the channel for 1 hour, while SWV measurement was performed every 10 min. Followed by MCH passivation, 20 µL of 1% BSA HEPES buffer was flowed through the channel for 30 min and SWV measurement was performed every 10 min. For the electrochemical detection of MB-labeled complementary DNA, sample inlet was loaded with 20 µL of 100 nM sample and injected into the microfluidic biosensor at a flow rate of 4.35 nL/min and subsequently measured by SWV. For the kinetics experiment 20 µL of 50 nM sample was used.

5.3.10 Data Analyses

Peak Height

The procedure followed in Section: 3.3.11 was used for subtraction of baseline and peak height measurement.

5.4 Results and Discussion

5.4.1 Microchip Design and Operation

The microchip design consist of two layers of PDMS, as shown in **Figure 5.4**. The bottom control layer contains 7 pneumatic channels (red) for fully automated chip operation and a detection channel. The top layer is designed for fluidic channel (black), which has a T-junction channel for reagent and sample mixing, a serpentine-shaped long incubation channel for homogenization of the two components, and a connection point (via) between the two layers. The sample will flow through the serpentine-shaped channel to the detection channel, where the downstream profile of sample solution will allow its direct contact with the electrode and will reduce diffusion of the sample in bulk solution. At the end of the detection channel the electrode is placed, and a 3D-templated reservoir is located on top of the electrode to hold the supporting electrolyte, reference and counter electrodes for electrochemical measurement.

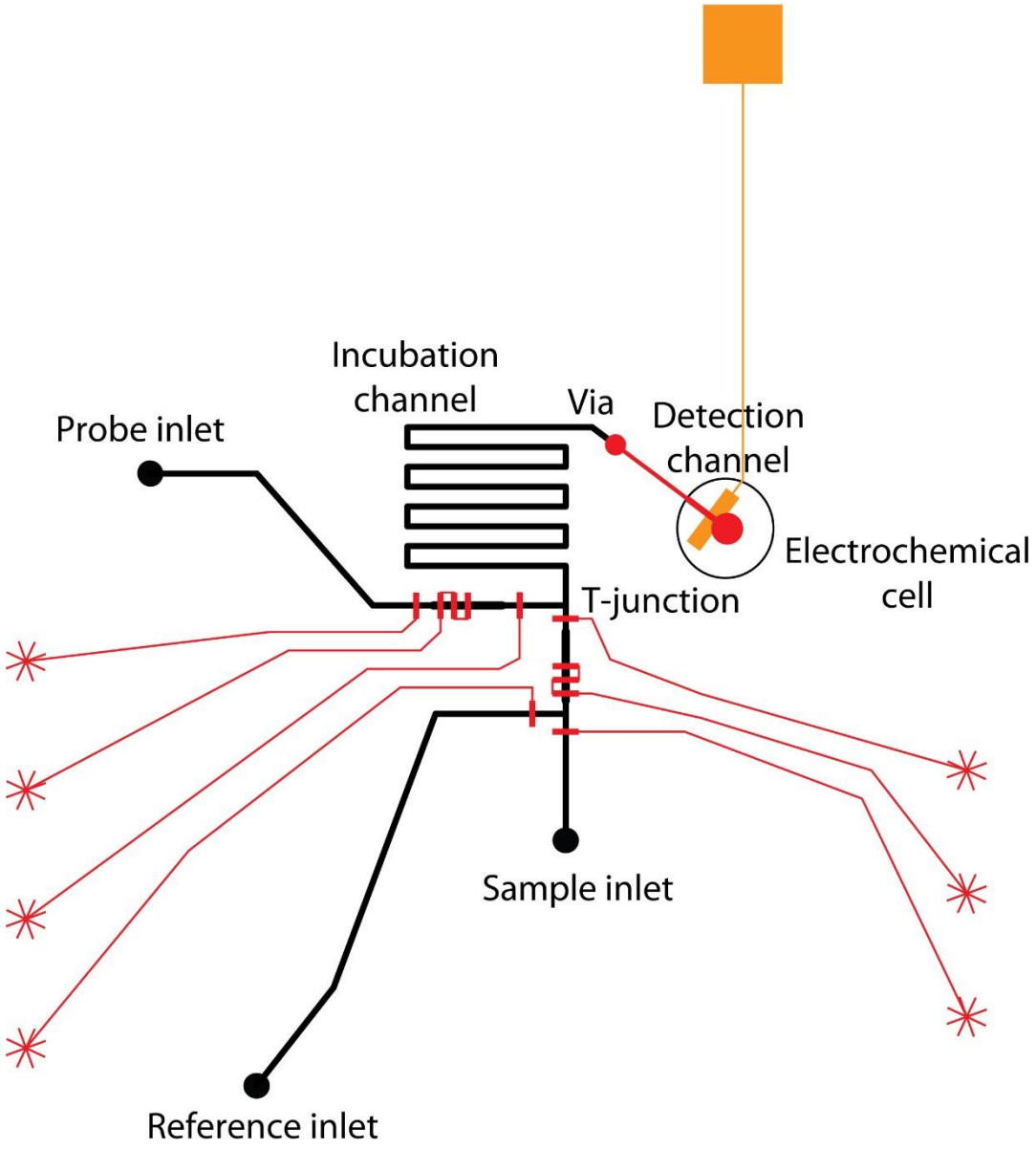

Figure 5.4. Schematic of the channel design at higher resolution. Two-layer microfluidic chip design: the short red lines, representing the microvalves, is the bottom layer for controlling. Via is the connection point between the two layers, which connects the fluidic channel and detection channel. The inlets and incubation channel are in the top layer for fluid flow.

In this device fluids moved through channels by valve-based peristaltic pumps. One key feature of the device is that fluids from probe inlet and sample or reference inlet orthogonally meet at the T junction since valves in the respective channels programmed to pump simultaneously. Both channels include three valves arranged in a single channel. Peristaltic pumping occurs when actuated in the 6 step pattern (101, 100, 110, 010, 011, 001), or the 5 step pattern (100, 110, 011, 001, 101), where 0 and 1 represent open and closed valves, respectively. In each pumping cycle, the net volume dispensed downstream equals the volume occupied by the center valve membrane upon closing, thus the sample volume can be accurately controlled by pumping a specified number of cycles. The peristaltic pumps provide much higher precision over the volume metered compared to more passively controlled microfluidic systems which are driven by syringe pump, pressure, or vacuum, rely on laminar flow to control the ratio of mixed components, and suffer from fluctuation over long periods of time.

5.4.2 Evaluation of Mixer Performance

The microchip contains a serpentine shaped long incubation channel to ensure complete mixing of two assay solutions at a designed flow rate. A solution containing 100 nM fluorescein and water was pumped in via the probe and sample/reference inlet, respectively, at 4.35 nL/min. Fluorescein sample solution flowed through the long channel and mixed with water, where the fluorescence intensity was measured at different region of interest (ROI). As shown in **Figure 5.5**, the sample and water homogenize after 8 turns and results a steady fluorescence signal at ROI#11, which is the detection channel. As the two fluids ran across the serpentine channel, the center of each fluid flows faster than the edges, resulting stretching of the interface between the two fluids,

which allows the diffusion to occur quickly across the interface and results in fast mixing and equilibration of the solution.

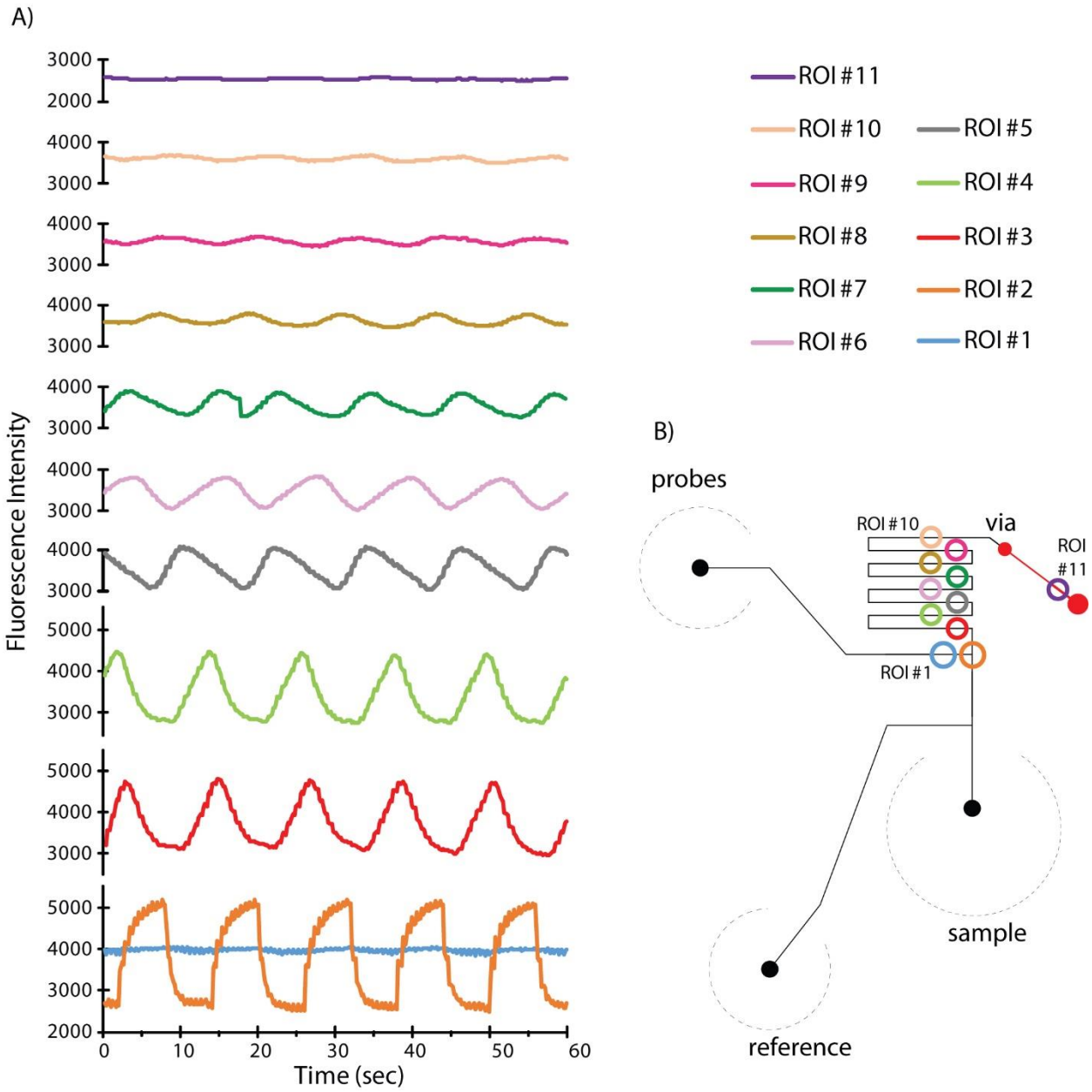

Figure 5.5. A) Fluorescence intensity measured at different region of interest (ROI) to evaluate the extent of mixing. Steady fluorescence signal at ROI#11 indicates homogenization of two fluids. **B)** Channel layout with color coded circles to represent ROI.

5.4.3 Dynamic Electrochemical Measurement

To verify simultaneous fluidic and electrical operation of the device, an experiment involving concurrent sample flow and electrochemical detection was performed. The microfluidic system was used as a flow injection device in which the sample potassium ferri/ferrocyanide was injected into a continuous buffer stream. The microchannel had a constant flow of 0.1 M potassium chloride supporting electrolyte through the probe inlet. A sample solution containing varying concentration of potassium ferri/ferrocyanide was pumped in via the sample inlet, ran across the incubation channel, mixed with the buffer, and the diluted sample then flowed through the detection channel. The gold electrode placed at the end of the microfluidic detection channel was used to electrochemically verify that system response. As expected, a sharp and well-defined SWV peak of $[Fe(CN)_6]^{-3/-4}$ redox couple was obtained, shown by example for the 10 nM concentration in **Figure 5.6A**. The system was also successful in distinguishing four different concentrations of sample. We observed decrease in the signal when lower concentration of sample was injected in the channel (**Figure 5.6B**). However, the signal was detected 3 minutes after injection of the sample, which was presumably due to placement of the electrode outside the detection channel.

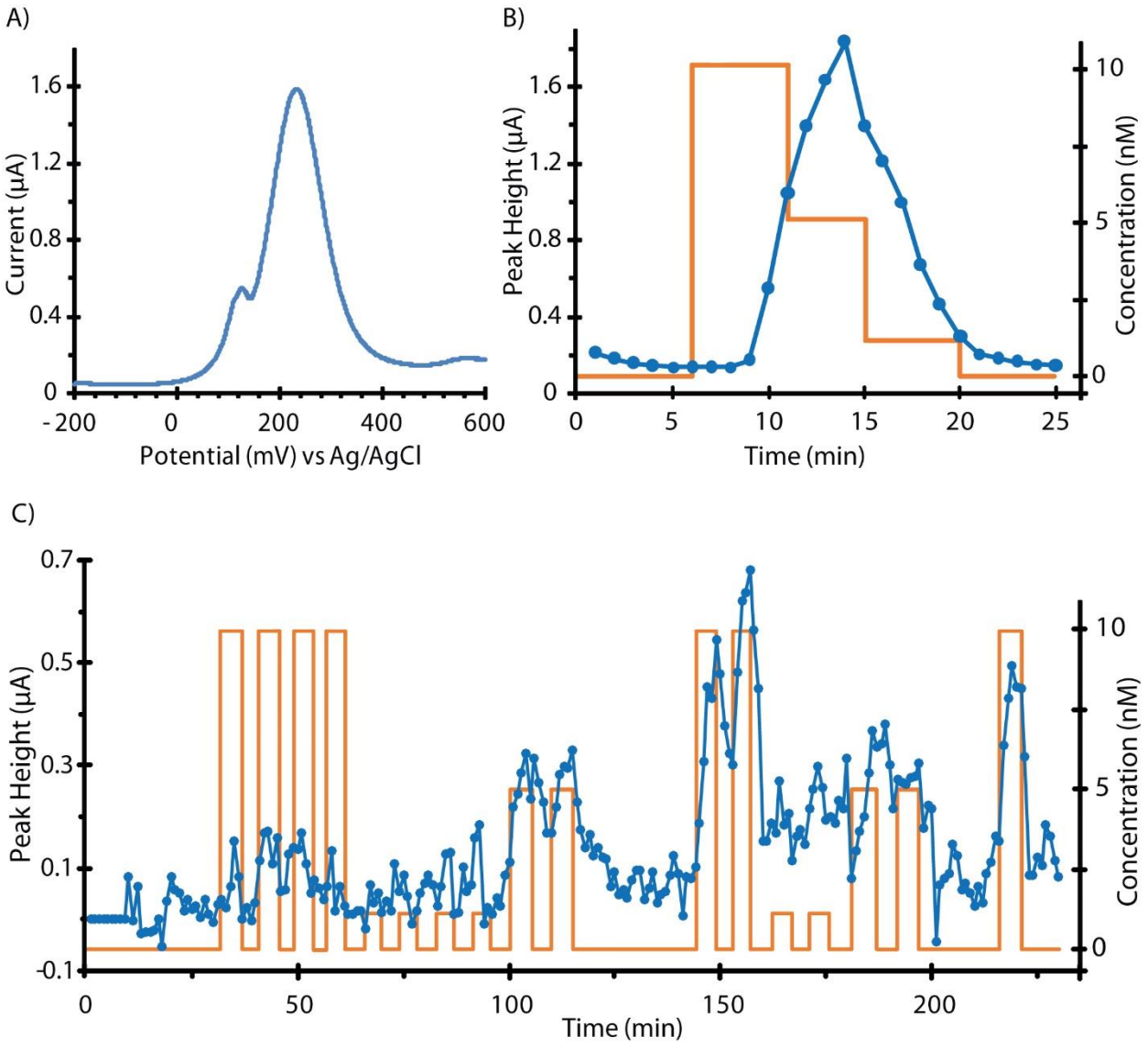

Figure 5.6. A) SWV peak of $[Fe(CN)_6]^{-3/-4}$ redox couple obtained by simultaneous sample flow and electrochemical measurement. **B)** Profile of the sensor current signal in response to three concentrations of $[Fe(CN)_6]^{-3/-4}$ injected into a stream of buffer flowing through the electrode. **C)** Profile of the sensor current signal in response to programmed square wave of buffer and sample at different concentrations.

We conducted another experiment with the electrode placed inside the detection channel and the device was operated under a square wave of buffer and sample at different concentrations, in an automated fashion to demonstrate the temporal sampling mode. In this instance, buffer solution was injected in the channel through the reference inlet. As shown in **Figure 5.6C**, The microfluidic flow-injection system resulted increase in the peak current with sample injection into the channel and then decrease with buffer injection. These electrochemical measurements within integrated microfluidics verified functional operation of the electrochemical system and fluidic mixer, as well as confirmed the devices flexibility in temporal sampling mode. However, the device was non-responsive for the first 100 minutes which we assume due to clog on the channel or valve sticking to flow channel resulting slow or no movement of the fluid.

5.4.4 Automated Microfluidic Electrode Preparation

After initial verification of the device functionality, our automated, valve-controlled microfluidics was adapted for electrode preparation. Gold electrodes were taken through the standard preparation steps, all on-chip: 1) bare gold, 2) DNA monolayer formation, 3) mercaptohexanol (MCH) passivation, and 4) bovine serum albumin (BSA) based passivation in buffer. As shown in **Figure 5.7**, higher capacitive current (1.6 µA) was observed after formation of DNA monolayer, due to negative charge on the phosphate backbone of the nucleic acid. With injection of MCH through the channel, capacitive current gradually decreased, which indicates blocking of the surface by MCH and removal of weak, nonspecifically adsorbed nucleic acids by formation of a dense MCH sublayer. Finally, with introduction of BSA, capacitive current was further decreased to 74 nA. These results demonstrated electrodes can be prepared with low volume of reagents (Dead volume: 20 µL) utilizing automated microfluidic.

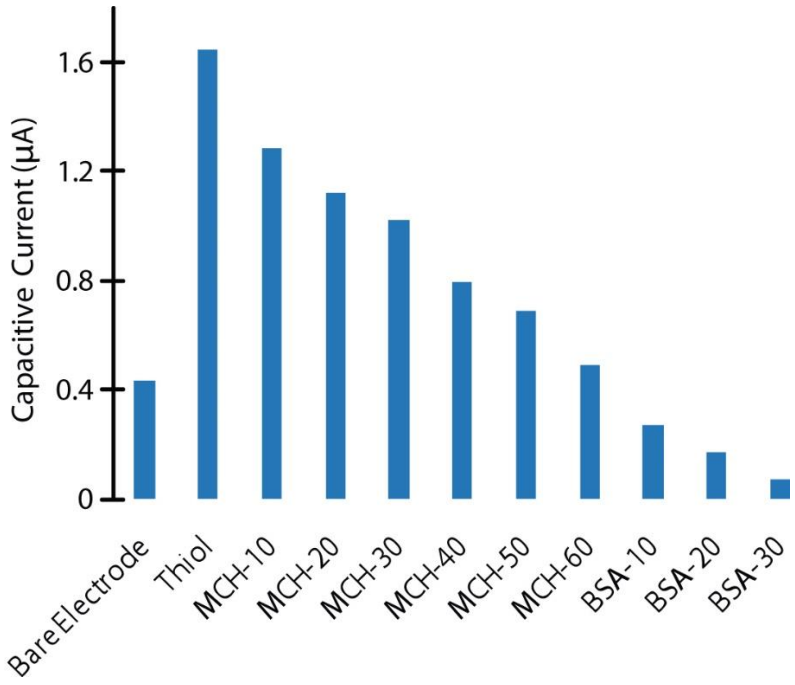

Figure 5.7. Multiple, automated electrode preparation steps conducted on-chip. DNA monolayer formation resulted high capacitive current, which was gradually decreased by MCH and BSA passivation.

5.4.5 Detection of Nucleic Acid

For the detection of complementary DNA, the redox tag labeled sample solution was injected into a continuous buffer stream via sample inlet which was captured by the thiolated-DNA on the electrode surface resulting electrochemical signal. As shown in **Figure 5.8A**, MB-labeled DNA was detected in real-time within 1 minute after introduction into the channel (red arrow) by pumping using valve-based peristaltic pumps on-chip. The signal stabilized after 20 minutes. The device was then operated under a square wave of buffer and sample by injecting buffer through the reference inlet. **Figure 5.8B** depicts, signal appeared with sample injection into the well, whereas stable signal was observed in the buffer stream, and then signal continued to increase with

second cycle of sample injection. These results again confirmed the devices flexibility in temporal sampling mode.

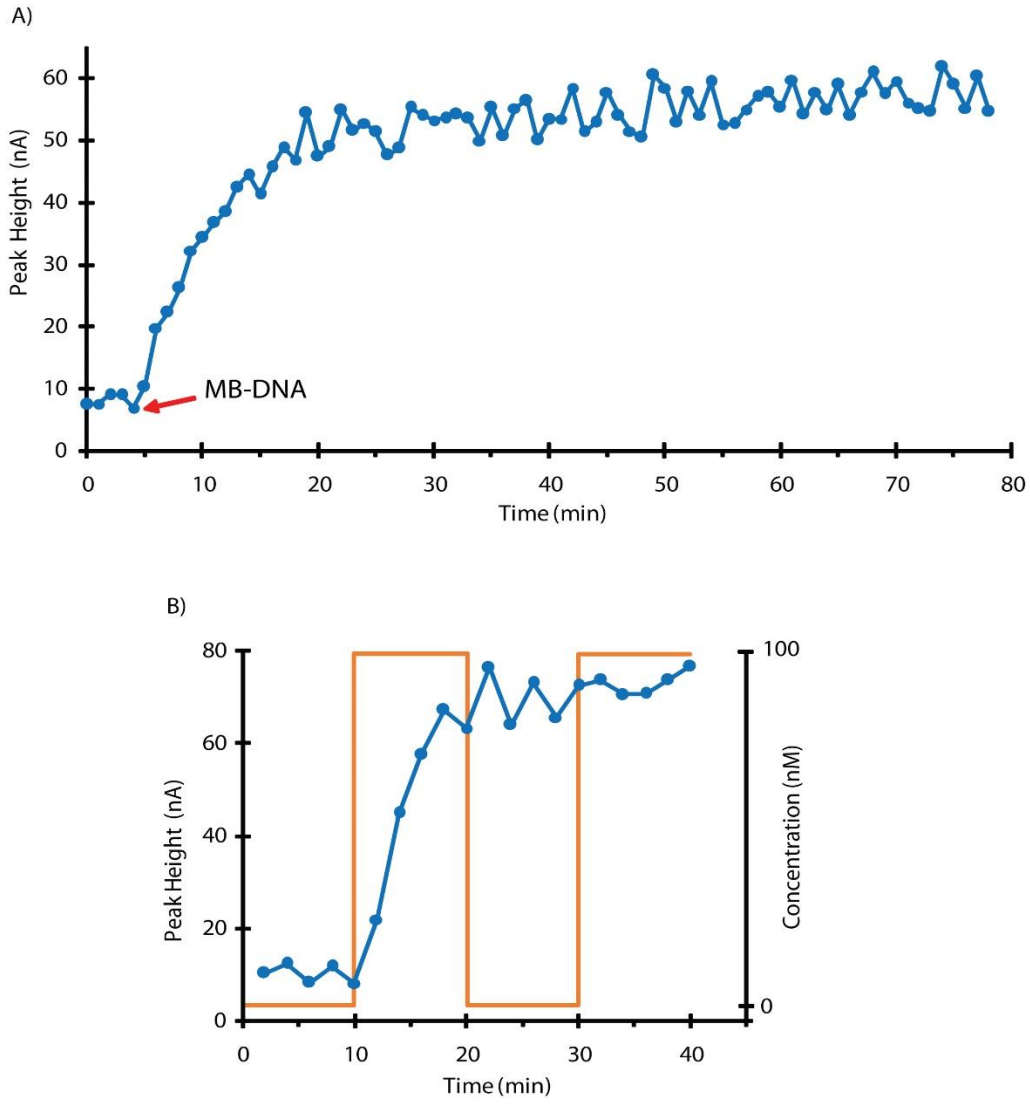

Figure 5.8. A) Real-time detection of 50 nM MB-DNA strand. **B)** Sensor response to programmed square wave of buffer and 100 nM MB-DNA strand.

5.5 Conclusions

The integration of electrochemical detection system with automated microfluidics for electrode preparation and detection of nucleic acid has been successfully demonstrated. The use of automated, valve-controlled microfluidics allowed minimization of reagent consumption during the multi-step electrode fabrication process, as well as detection of target DNA in real time within 1 minute after injection into the microchannel. Our system has shown efficient mixing of fluids in the microchannel system, suggesting biochemical assays that require premixing of sample and reagents can be conducted on the chip. While more development is needed, this automated microfluidics coupled electrochemical detection system sets the platform for cell secretion study in real time. For instance, electrochemical proximity assay (ECPA)[24-25] can be performed on this device to monitor insulin secretion from living murine pancreatic islets over time in response to stimulatory agents such as glucose. The simultaneous injection of secreted insulin and antibody-oligo probes into the microchannel will enable their mixing and subsequent capture of the complex on the thiolated-DNA modified electrode surface resulting electrochemical signal. Therefore, a better understanding of the dynamic function of endocrine tissues can be obtained with the aid of this integrated device.

5.6 References

1. Rackus, D. G.; Shamsi, M. H.; Wheeler, A. R., Electrochemistry, biosensors and microfluidics: a convergence of fields. *Chemical Society Reviews* **2015,** *44* (15), 5320-5340.

2. Chiu, D. T.; deMello, A. J.; Di Carlo, D.; Doyle, P. S.; Hansen, C.; Maceiczyk, R. M.; Wootton, R. C. R., Small but Perfectly Formed? Successes, Challenges, and Opportunities for Microfluidics in the Chemical and Biological Sciences. *Chem* **2017,** *2* (2), 201-223.

3. Nikoleli, G.-P.; Siontorou, C. G.; Nikolelis, D. P.; Bratakou, S.; Karapetis, S.; Tzamtzis, N., Chapter 13 - Biosensors Based on Microfluidic Devices Lab-on-a-Chip and Microfluidic Technology. In *Nanotechnology and Biosensors*, Nikolelis, D. P.; Nikoleli, G.-P., Eds. Elsevier: 2018; pp 375-394.

4. Abdulbari, H. A.; Basheer, E. A. M., Electrochemical Biosensors: Electrode Development, Materials, Design, and Fabrication. *ChemBioEng Reviews* **2017,** *4* (2), 92-105.

5. da Silva, E. T. S. G.; Souto, D. E. P.; Barragan, J. T. C.; de F. Giarola, J.; de Moraes, A. C. M.; Kubota, L. T., Electrochemical Biosensors in Point-of-Care Devices: Recent Advances and Future Trends. *ChemElectroChem* **2017,** *4* (4), 778-794.

6. Evans, D.; Papadimitriou, K. I.; Vasilakis, N.; Pantelidis, P.; Kelleher, P.; Morgan, H.; Prodromakis, T., A Novel Microfluidic Point-of-Care Biosensor System on Printed Circuit Board for Cytokine Detection. *Sensors (Basel)* **2018,** *18* (11), 4011.

7. Kaur, G.; Tomar, M.; Gupta, V., Development of a microfluidic electrochemical biosensor: Prospect for point-of-care cholesterol monitoring. *Sensors and Actuators B: Chemical* **2018,** *261*, 460-466.

8. Shin, S. R.; Kilic, T.; Zhang, Y. S.; Avci, H.; Hu, N.; Kim, D.; Branco, C.; Aleman, J.; Massa, S.; Silvestri, A.; Kang, J.; Desalvo, A.; Hussaini, M. A.; Chae, S. K.; Polini, A.; Bhise, N.;

Hussain, M. A.; Lee, H.; Dokmeci, M. R.; Khademhosseini, A., Label-Free and Regenerative Electrochemical Microfluidic Biosensors for Continual Monitoring of Cell Secretomes. *Advanced science (Weinheim, Baden-Wurttemberg, Germany)* **2017,** *4* (5), 1600522.

9. Wang, R.; Xu, Y.; Sors, T.; Irudayaraj, J.; Ren, W.; Wang, R., Impedimetric detection of bacteria by using a microfluidic chip and silver nanoparticle based signal enhancement. *Microchimica Acta* **2018,** *185* (3), 184.

10. Li, Y.; Sella, C.; Lemaître, F.; Guille-Collignon, M.; Amatore, C.; Thouin, L., Downstream Simultaneous Electrochemical Detection of Primary Reactive Oxygen and Nitrogen Species Released by Cell Populations in an Integrated Microfluidic Device. *Analytical chemistry* **2018,** *90* (15), 9386-9394.

11. Liu, Z.; Jin, M.; Cao, J.; Niu, R.; Li, P.; Zhou, G.; Yu, Y.; van den Berg, A.; Shui, L., Electrochemical sensor integrated microfluidic device for sensitive and simultaneous quantification of dopamine and 5-hydroxytryptamine. *Sensors and Actuators B: Chemical* **2018,** *273*, 873-883.

12. Lakey, A.; Ali, Z.; Scott, S. M.; Chebil, S.; Korri-Youssoufi, H.; Hunor, S.; Ohlander, A.; Kuphal, M.; Marti, J. S., Impedimetric array in polymer microfluidic cartridge for low cost point-of-care diagnostics. *Biosensors and Bioelectronics* **2019,** *129*, 147-154.

13. Li, S.; Zhang, C.; Wang, S.; Liu, Q.; Feng, H.; Ma, X.; Guo, J., Electrochemical microfluidics techniques for heavy metal ion detection. *The Analyst* **2018,** *143* (18), 4230-4246.

14. Kudr, J.; Zitka, O.; Klimanek, M.; Vrba, R.; Adam, V., Microfluidic electrochemical devices for pollution analysis–A review. *Sensors and Actuators B: Chemical* **2017,** *246*, 578-590.

15. Holmes, J.; Pathirathna, P.; Hashemi, P., Novel frontiers in voltammetric trace metal analysis: Towards real time, on-site, in situ measurements. *TrAC Trends in Analytical Chemistry* **2019,** *111*, 206-219.

16. Gallardo-Gonzalez, J.; Baraket, A.; Boudjaoui, S.; Metzner, T.; Hauser, F.; Rößler, T.; Krause, S.; Zine, N.; Streklas, A.; Alcácer, A.; Bausells, J.; Errachid, A., A fully integrated passive microfluidic Lab-on-a-Chip for real-time electrochemical detection of ammonium: Sewage applications. *Science of The Total Environment* **2019,** *653*, 1223-1230.

17. Lu, L.; Gunasekaran, S., Dual-channel ITO-microfluidic electrochemical immunosensor for simultaneous detection of two mycotoxins. *Talanta* **2019,** *194*, 709-716.

18. Pol, R.; Céspedes, F.; Gabriel, D.; Baeza, M., Microfluidic lab-on-a-chip platforms for environmental monitoring. *TrAC Trends in Analytical Chemistry* **2017,** *95*, 62-68.

19. Liao, Z.; Wang, J.; Zhang, P.; Zhang, Y.; Miao, Y.; Gao, S.; Deng, Y.; Geng, L., Recent advances in microfluidic chip integrated electronic biosensors for multiplexed detection. *Biosensors and Bioelectronics* **2018,** *121*, 272-280.

20. Cincotto, F. H.; Fava, E. L.; Moraes, F. C.; Fatibello-Filho, O.; Faria, R. C., A new disposable microfluidic electrochemical paper-based device for the simultaneous determination of clinical biomarkers. *Talanta* **2019,** *195*, 62-68.

21. Lee, G.; Lee, J.; Kim, J.; Choi, H. S.; Kim, J.; Lee, S.; Lee, H., Single Microfluidic Electrochemical Sensor System for Simultaneous Multi-Pulmonary Hypertension Biomarker Analyses. *Scientific Reports* **2017,** *7* (1), 7545.

22. Panini, N. V.; Messina, G. A.; Salinas, E.; Fernández, H.; Raba, J., Integrated microfluidic systems with an immunosensor modified with carbon nanotubes for detection of prostate specific antigen (PSA) in human serum samples. *Biosensors & bioelectronics* **2008,** *23* (7), 1145-51.

23. Uliana, C. V.; Peverari, C. R.; Afonso, A. S.; Cominetti, M. R.; Faria, R. C., Fully disposable microfluidic electrochemical device for detection of estrogen receptor alpha breast cancer biomarker. *Biosensors & bioelectronics* **2018,** *99,* 156-162.

24. Hu, J.; Wang, T.; Kim, J.; Shannon, C.; Easley, C. J., Quantitation of Femtomolar Protein Levels via Direct Readout with the Electrochemical Proximity Assay. *Journal of the American Chemical Society* **2012,** *134* (16), 7066-7072.

25. Hu, J.; Yu, Y.; Brooks, J. C.; Godwin, L. A.; Somasundaram, S.; Torabinejad, F.; Kim, J.; Shannon, C.; Easley, C. J., A Reusable Electrochemical Proximity Assay for Highly Selective, Real-Time Protein Quantitation in Biological Matrices. *Journal of the American Chemical Society* **2014,** *136* (23), 8467-8474.

Chapter 6

Conclusions and Future Directions

6.1 Conclusions

This dissertation set out to develop and optimize DNA-based electrochemical assays, and integrate automated microfluidics with electrochemical sensors. In this closing chapter, the major accomplishments and their impact are summarized, followed by a discussion of possible future experiments, that build upon these works.

6.1.1 Electrochemical Sensor Development

For improved understanding of solution-to-surface hybridization we studied the kinetics of DNA hybridization at the electrode surface. We found surface kinetics depend strongly on the distance between the electrode and the binding site, and the ionic strength dependence suggests that this effect is driven by the electric double-layer. This work signify that the positions of nucleic acid hybridization sites and the salt concentration should be carefully chosen in DNA-based biosensors, which in turn helped us select the conditions needed for the DNA nanostructure construction.

A peptide sensor for diabetic drug, exendin-4 was developed for direct quantification with electrochemistry for the first time. This work showcases our ability to conjugate novel targets to the nanostructure and successfully quantify in DNA nanostructure platform.

To enhance the electrochemical signal, we rationally modified the DNA nanostructure by incorporating polyethylene glycol (PEG) loops and uracils into selected probe strands. Interestingly, incorporation of PEG loops in the probe DNA hindered the ligation reaction, which prevented complete construction and hence resulted in an ineffectual sensor, whereas removal of uracils had detrimental effect on the stability of the nanostructure. This work improved our understanding on surface ligation and highlighted parameter that should be considered when designing nucleic acid-based sensors.

6.1.2 Automated Microfluidic Assisted Electrochemical Sensor

We have developed an electrochemical detection system integrated into microfluidic to be deployed for automated electrode preparation and analyte detection. The device was fabricated with multilayer PDMS technology and was digitally controlled by in-house written LabVIEW applications. The device integrated precise peristaltic pumping to control fluid flow form three individually addressable input channels, a long incubation channel for homogenization of fluids, and an embedded electrode within the channel for analyte detection. The automated, valve-controlled device was proven to be useful for multi-step electrode fabrication and rapid detection of target DNA employing low volumes of reagent and sample solution. This work sets the stage for future real-time cell secretion study and DNA nanostructure construction with minimal reagent consumption.

We believe that the findings presented in this dissertation will be of interest to a broad scientific community and help them engineer better biosensors.

6.2 Future Directions

6.2.1 High-throughput Cell Secretion Study

The integration of automated microfluidic and electrochemical biosensing onto a single device paves the way for high temporal resolution insulin secretion dynamics analysis from pancreatic islets employing highly sensitive electrochemical proximity assay (ECPA). Briefly, the probe, sample, and reference inlets can be loaded with ECPA probes, islets, and standard insulin solution, respectively. The simultaneous fluid flow from sample and probe inlets would allow secreted insulin to mix with ECPA probes, homogenize the mixture on the serpentine channel, and capture by the electrode-bound thiolated-DNA, resulting target dependent electrochemical signal. Intermediate measurement of the standard insulin will allow calibration of the system and quantification of the secretion sample. This study will give us better understanding of the cell function and biological processes.

6.2.2 Automated Fabrication of DNA Nanostructures

The microfluidic device can be employed to develop an automated, on-chip protocol for electrode preparation in the DNA nanostructure format, which will start with DNA monolayer formation, mercaptohexanol (MCH) passivation, anchor-DNA addition, MB-DNA addition, and enzymatic ligation. This automated microdevice should minimize reagent consumption when assembling nanostructures compared to conventional pipette-based preparation. To determine the suitability of the platform, desthiobiotin-labeled DNA nanostructures will be fabricated, streptavidin detection will be performed, and the amount of consumed reagents will be evaluated.

6.2.3 Real-time Measurement on Nanostructure Platform

It is possible to use the DNA nanostructure for real-time secretion quantification by introducing built-in assay reversibility. As shown in **Figure 6.1**, Antibody-DNA conjugates will tether anchor molecules to electrodes, along with DNA nanostructures. In this case, surface bound DNA nanostructure-antibody complex will be disrupted upon introduction of small-molecule/peptide target, resulting displacement of antibody and increased DNA nanostructure signal. If there is a drop in target concentration in bulk solution, the native DNA nanostructure-antibody complex will be restored as the target will be lost by the antibody due to the equilibrium nature of the binding, resulting in decrease in the signal. In this case, tether lengths should be studied carefully to elucidate optimal length, since short tethers will hinder competitive assays and longer tethers will prevent antibody binding.

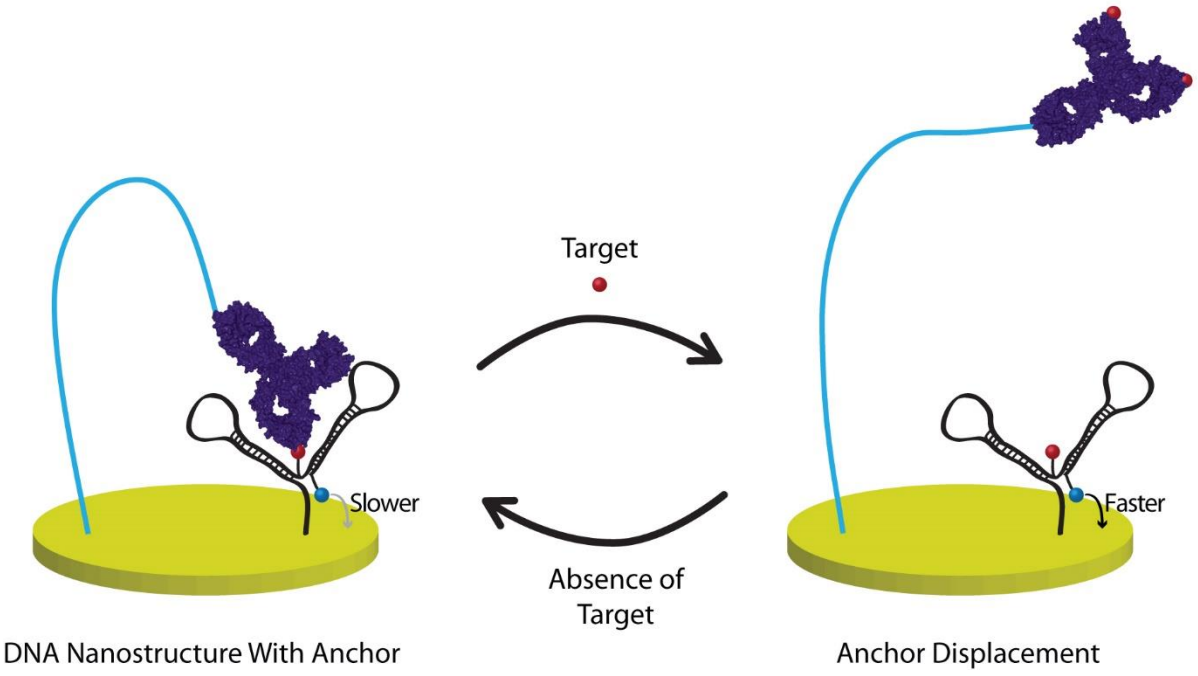

Figure 6.1. Real time measurement of small molecules using DNA nanostructure.

6.2.4 Electrochemical Nucleic Acid Switch for Bioanalysis

With the knowledge we gained in the development of the nanostructure system, we can develop a novel and versatile quantification method using a single stranded DNA probe. **Figure 6.2** shows a conceptual illustration of the electrochemical nucleic acid switch for quantification which is interchangeable between protein and small-molecule/peptide. A single stranded DNA will be modified with a thiol linker at one end to anchor the DNA to the electrode surface. The other end will consist a signaling molecule and an amine tag which will be modified with 4FB cross linker to activate for bioconjugation. Conjugation of anchor recognizing unit to the amine-modified DNA will prepare the sensor. As shown in **Figure 6.2**, for protein quantification, initial faster diffusion of the redox tag is hindered by the antibody binding, reducing electrochemical signal (upper data). For the small-molecule/peptide quantification, this effect can be blocked using a competitive assay workflow by preincubating target with its large binding partner (lower data). The sensor will be independent of solution equilibrium, provide direct readout upon target addition, and will be generalizable to a broad range of analyte.

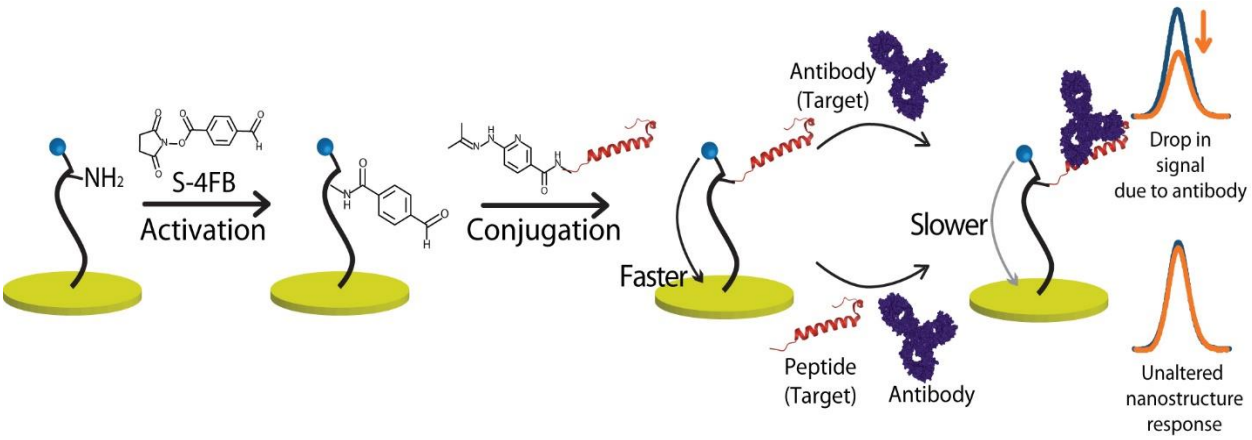

Figure 6.2. Electrochemical nucleic acid switch for quantification of antibodies and peptides.

Antibodies reduced current (upper data), and this effect can be blocked by peptides (lower data).

6.2.5 Comparative Study on the Hybridization of Peptide Nucleic Acid (PNA) and DNA Probes

PNA has demonstrated extraordinary binding affinity over DNA for complementary nucleic acid.[1] At low ionic strength environment, DNA-DNA hybridization suffers from charge repulsion due to the abundant negative charges on the sugar phosphate backbone.[2-3]While, Neutral PNA can hybridization with DNA at lower salt concentrations.[4-5] As our studies on surface hybridization kinetics suggest that electric double-layer hinders hybridization of short DNA sequences at locations very close to the electrode, thus we can conduct a comparative study on the hybridization of PNA and DNA probes on the surface and assess whether PNA probes exhibits higher sensitivity over DNA for complementary DNA detection.

6.2.6 Novel Signaling Probe

To achieve high electrochemical signal from nucleic acid base sensors we can strategically design a novel signaling probe which will comprise multiple redox label on the same probe. Higher signal would increase sensitivity and widen the dynamic range of the system.

6.3 References

1. Mach, K. E.; Kaushik, A. M.; Hsieh, K.; Wong, P. K.; Wang, T.-H.; Liao, J. C., Optimizing peptide nucleic acid probes for hybridization-based detection and identification of bacterial pathogens. *Analyst* **2019,** *144* (5), 1565-1574.

2. Wong, I. Y. H.; Melosh, N. A., An electrostatic model for DNA surface hybridization. *Biophysical journal* **2010,** *98 12*, 2954-63.

3. Ravan, H.; Kashanian, S.; Sanadgol, N.; Badoei-Dalfard, A.; Karami, Z., Strategies for optimizing DNA hybridization on surfaces. *Analytical Biochemistry* **2014,** *444*, 41-46.

4. Keighley, S. D.; Estrela, P.; Li, P.; Migliorato, P., Optimization of label-free DNA detection with electrochemical impedance spectroscopy using PNA probes. *Biosensors and Bioelectronics* **2008,** *24* (4), 906-911.

5. Ali, M.; Neumann, R.; Ensinger, W., Sequence-Specific Recognition of DNA Oligomer Using Peptide Nucleic Acid (PNA)-Modified Synthetic Ion Channels: PNA/DNA Hybridization in Nanoconfined Environment. *ACS Nano* **2010,** *4* (12), 7267-7274.